Secondary instability of Mack mode disturbances in hypersonic boundary layers over micro-porous surface

Jiakuan Xu,[1, 2] Jianxin Liu,[3, a)] Shahid Mughal,[2] Peixun Yu,[4] and Junqiang Bai[4]

[1)]*Center for Applied Mathematics, Tianjin University, 300072, Tianjin, P.R. China*

[2)]*Department of Mathematics, Imperial College London, SW7 2AZ, London, UK*

[3)]*Laboratory of High-speed Aerodynamics, School of Mechanical Engineering, Tianjin University, 300072, Tianjin, P.R. China*

[4)]*School of Aeronautics, Northwestern Polytechnical University, 710072, Xi'an, P.R. China*

(Dated: 4 March 2020)

In laminar hypersonic boundary layers, it is known that secondary instability plays a crucial role in transition to turbulence. The secondary instability usually includes fundamental mode, subharmonic mode and the detuned mode. Considerable research exists on the secondary instability mechanism in hypersonic boundary layers with the smooth wall condition. The topic of using micro-porous surfaces for disturbance stabilization has recently drawn interest. The stabilization and thus a possible delay in transition, arises due to a reduction in the growth rate of the primary Mack mode by the porous surface. The paper focuses on investigating whether the secondary instability mechanism of Mack modes can also be affected by a surface porosity condition. It is known that the primary Mack mode linear disturbances are changed significantly on the porous surface, how it subsequently influences the secondary instability of the modified time varying basic flow is our concern. The analysis demonstrates that on the porous surface, as the amplitude of the primary Mack mode increases, the fundamental mode is not stable. Instead, the fundamental mode amplifies rapidly with increasing primary amplitudes. At larger secondary instability spanwise wavenumbers, when the primary amplitude exceeds a certain threshold value, the fundamental modes surpass the subharmonic modes and dominate the secondary instability. However, when the spanwise wavenumber is relatively small, especially at the spanwise wavenumber corresponding to the maximum growth rate of the subharmonic mode, the fundamental modes are weakened and lose their dominant position. We find that corresponding to different amplitudes of primary Mack mode disturbances affected by the porosity parameters, there are no strongly preferred interaction modes that dominate the secondary instability; this contrasts with smooth wall findings. We further find that the larger the pore size or porosity, the more severe is the suppression of the fundamental mode.

[a)]Electronic mail: shookware@tju.edu.cn

I. INTRODUCTION

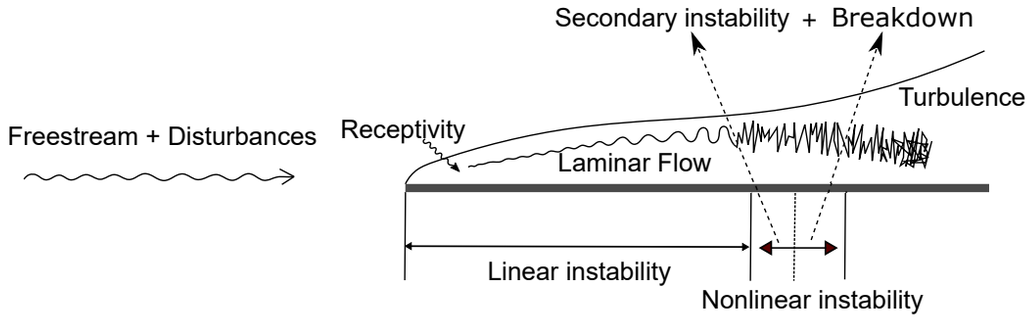

FIG. 1. Diagram for flow instability during laminar-turbulent transition in a boundary layer.

Understanding laminar to turbulence tripping mechanisms in boundary layer transition has seen significant research activity over the past few decades, leading to significant insights into the many fluid processes at play. In civilian transonic speed regimes, delaying transition to turbulence has an importance in drag reduction and thus promise of fuel efficiency in air transport. At the other extreme of very high speed hypersonic flight, the significant temperature differences arising in laminar and turbulent boundary layers is of crucial concern in the design of aero-thermal protection systems. Generally with the birth of disturbances, through receptivity processes in the boundary layer, any unstable waves excited amplify linearly and lead onto nonlinear processes, as shown in Fig. 1 – generally referred to as the primary instability route. At some point in space, dependent upon the disturbance environment, the breakdown to turbulence then is assumed to arise through a secondary instability mechanism. In lower Mach number supersonic boundary layers, the first mode oblique breakdown route proposed by Fasel, Thumm, and Bestek [1] plays a crucial role in the secondary instability. With increasing Mach number, the second mode two-dimensional (2D) wave, i.e. the so-called Mack mode becomes the dominant unstable disturbance while the importance of the first mode is reduced. Different from the first mode, the Mack mode is produced by acoustic modes trapped in the relative supersonic region having acoustic-wavelike behavior[2] and is associated with an inviscid instability. The wavelength of the most unstable Mack-mode is nearly twice the hypersonic boundary layer thickness[2]. Beginning with the purely 2D Mack mode disturbances, there may will arise at some stages of the breakdown process, the development of secondary unstable structures playing a crucial role in the development of three-dimensional(3D) structures leading to turbulence. Therefore, it is of significant interest to clarify the existence of and role of secondary instability in the flow destabilisation. In 1988, based on the

Floquet expansion, Herbert[3] proposed secondary instability theory, identifying three types of secondary instability modes: fundamental, subharmonic and the detuned modes[4]. The fundamental mode having the same streamwise wavelength and frequency as the primary 2D disturbance, often leads to the weakly-nonlinear so-called K-type resonance interaction[5]. The subharmonic mode with twice the streamwise wavelength and one half the frequency of the primary mode results in staggered Λ-structures (i.e., the so-called H/N-type weakly-nonlinear interaction[6–8]). The detuned mode lies in between the fundamental and subharmonic modes[7–10]. It is worth mentioning that in 1977, Kachanov, Kozlov, and Levchenko[6] first observed the N-type subharmonic resonance in experiment and was confirmed by Saric and Thomas[11], Kachanov and Levchenko[7] and Corke and Mangano[8]; see also a summary by Kachanov[12]. Nevertheless, in high-speed flows there are more complex routes of breakdown to turbulence and subharmonic resonance also plays a very crucial role in secondary instability. Kosinov and co-workers[13–17] conducted lots of measurements on the subharmonic resonance mechanism in 2D supersonic boundary layers and further investigations were performed by Ermolaev, Kosinov, and Semionov[18] and Kolosov *et al.*[19] for 3D boundary layers. The corresponding theoretical analysis and numerical simulations were carried out by Kosinov and Tumin[20], Mayer and Fasel[21] and Fezer and Kloker[22] – verifying the existence and feasibility of subharmonic resonances arising.

Concerning presence of more complex resonances, triadic resonance theory was firstly proposed by Craik[23] in incompressible flows which was subsequently enhanced by Volodin and Zelman[24] and Volodin and Zelman[25]. The theory was extended to explore nonlinear resonant interactions by Smith and Stewart[26], Zelman and Maslennikova[27], Goldstein and Lee[28]. Presently, as a result of the significant research effort in hypersonic laminar flow instability, the subharmonic mode is identified as the most unstable type and found to play a significant role in flow destabilisation. In 1990, Masad and Nayfeh[29] investigated subharmonic instability of compressible boundary layers with Floquet theory – a comprehensive parametric study involving Mach number, spanwise wave number, primary disturbance amplitude, Reynolds number and frequencies of primary modes was undertaken. Subsequently, Masad and Nayfeh[30] and El-Hady[31] calculated the effects of suction, wall shaping and wall cooling on secondary instability in incompressible and compressible boundary layers. It was found that suction stabilizes the primary, fundamental and subharmonic waves, while cooling of the wall destabilizes the secondary subharmonic of a Mack mode primary disturbance. It also confirmed the conclusion by Masad and Nayfeh[29] that higher Mach numbers stabilize the subharmonic mode when the primary mode is the first mode;

while destabilization occurs when the primary mode is the Mack mode. Ng and Erlebacher[32] also investigated the secondary instability in compressible boundary layers through Floquet theory and found that at a high Mach number of 4.5, the secondary instability due to a primary Mack mode is stronger than that of the primary first mode, with the subharmonic mode instability being prominent.

Experiments by Bountin, Shiplyuk, and Maslov[33] on a sharp smooth surfaced cone at Mach 5.95 show that subharmonic resonance is the basic mechanism of nonlinear interaction for the primary Mack mode disturbances. However, Schneider's group undertaking series of experiments in 2009[34] on a flared cone in the Boeing/AFOSR Mach 6 Quiet Tunnel (BAM6QT) at Purdue University found that fundamental modes appeared in earlier stage of transition. Later, a second and comprehensive experimental study was performed and revealed very similar conclusions[35,36], which contradicted the earlier previous opinions. Furthermore, results replicating quiet background noise through direct numerical simulation (DNS) corroborated the hypersonic experimental deductions. In 2012, Sivasubramanian and Fasel[37] simulated the fundamental breakdown of the Purdue flared cone through DNS and found the typical "hot" streak pattern similar to the experimental observations. In addition to the stationary mode produced by self-interactions of the Mack mode, very low-frequency waves were observed in the process of breakdown at Mach 6 boundary layers[38]. Recently, the non-linear mechanism of the interactions between the low-frequency waves and the Mack mode has been explored by Chen et al.[39,40]. Hader and Fasel[41–44] have demonstrated through their DNS simulations that the fundamental breakdown is initiated by the non-linear resonance of a high amplitude 2D primary wave. Consistent with the measured data, the DNS indicates a symmetric pair of low amplitude 3D secondary waves at the same frequency, but the stationary mode exhibits the strongest secondary instability growth. Li et al.[9] conducted research about fundamental resonances using non-linear parabolized stability equations (NPSE) and secondary instability theory (SIT). They found that a strong fundamental secondary instability can exist for a range of initial amplitudes of the most amplified Mack mode disturbance at the Purdue Mach 6 flared cone conditions. It was also determined that for the straight cone, the subharmonic mode dominates the secondary instability within a certain range of azimuthal wavenumbers. Liu and Zhang[45] also investigated the fundamental resonance at Mach 6 over a zero pressure gradient flat plate with Floquet theory. They found that when the amplitude of the primary mode reaches a threshold value, the fundamental resonances (relative to subharmonic and detuned types) were the most unstable from the secondary instability viewpoint. In this paper, we focus on the secondary

instability analysis at Mach 4.5 used by Ng & Erlebacher[32] and analyze the missing solutions of secondary instability in this case.

Controlling flow transition at hypersonic conditions is a topic of considerable interest presently. Porous surfaces even of small size can substantially influence the primary Mack mode instability and thus ultimately influence transition in hypersonic boundary layers. Disturbance sensitivity due to micro-porous surfaces has been demonstrated by a series of linear stability analyses, DNS simulations and experiments. In 2001, Fedorov et al.[2] developed the linear instability porous coating mathematical model (key parameters are the diameter and depth of the holes and the distance between the holes). This was subsequently validated by the CalTech (T5) flight experiment. After the establishment of this classic model, many researchers[46–48] have studied the primary linear instability of high speed boundary layers porous surface phenomenon. In 2009, Wartemann et al.[49] employed DNS and concluded that Fedorov's model for porous surface in the linear stability regime is reasonable and correct. They further performed analysis that included not only the growth rate but also the corresponding eigenfunctions of the primary Mack mode on the porous surface. Recently, Zhao et al.[50,51] through detailed DNS analysis revealed that the out-of-phase behavior between the incident and reflected waves at the resonant frequency minimizes the near-surface acoustic pressure, largely inhibiting the growth of the Mack mode. Moreover, Wang[52] undertook DNS modeling to investigate the performance of porous coatings for flow stabilization at hypersonic thermo-chemical non-equilibrium gas conditions.

It is now accepted that the mechanism for suppression of the primary Mack modes by the porous surface arises through changing the eigenfunction shapes of the primary Mack modes, thus delaying transition. Hence, for porous surface the interesting and meaningful research objective is that of enquiring, since the eigenfunction shapes are modified by the porosity in what manner does the porosity impact upon the secondary instability? In 2005, Chokani *et al.* [53] studied experimentally the nonlinear stabilization aspects of the second-mode disturbance using a passive, ultrasonically absorptive coating of regular micro-structures. They found that the subharmonic and fundamental resonances (i.e., the harmonic resonances) of the second mode observed on solid surface are significantly modified by the porous surface. Moreover, the quite pronounced fundamental resonance on the smooth wall is completely absent with the porous surface. Furthermore, unlike the solid surface, there are no strongly preferred interaction modes. The objective of the investigation undertaken herein is to improve our insight and to clarify the mechanism of second-mode stabilization in the presence of micro-porous surface coatings. In this paper, through a theoreti-

cal analysis method we attempt to analyze and determine the explicit rules between the primary amplitude and secondary instability at Mach 4.5 on a smooth wall. We then assess whether the rules determined from the smooth wall analysis operate and remains quantitatively viable over a micro-porous surface.

II. MATHEMATICAL DESCRIPTION

A. Compressible Navier-Stokes equations

The two-dimensional compressible Navier-Stokes equations are the basis for all modeling undertaken in this paper, which take the usual form[54,55]

$$\frac{\partial \rho}{\partial t}+\frac{\partial(\rho v_j)}{\partial x_j} = 0, \tag{1a}$$

$$\rho\left(\frac{\partial v_i}{\partial t}+v_j\frac{\partial v_i}{\partial x_j}\right) = -\frac{\partial p}{\partial x_i}+\frac{1}{Re}\frac{\partial}{\partial x_j}\left[\mu(\frac{\partial v_i}{\partial x_j}+\frac{\partial v_j}{\partial x_i}-\frac{2}{3}\delta_{ij}\frac{\partial v_k}{\partial x_k})\right], \tag{1b}$$

$$\begin{aligned}\rho\left(\frac{\partial T}{\partial t}+v_j\frac{\partial T}{\partial x_j}\right) = & \frac{1}{RePr}\frac{\partial}{\partial x_j}\left(\kappa\frac{\partial T}{\partial x_j}\right)+\frac{\gamma-1}{\gamma}\left(\frac{\partial p}{\partial t}+v_j\frac{\partial p}{\partial x_j}\right)\\ & +\frac{(\gamma-1)M^2}{Re}\left[\mu\frac{\partial v_i}{\partial x_j}\left(\frac{\partial v_i}{\partial x_j}+\frac{\partial v_j}{\partial x_i}-\frac{2}{3}\delta_{ij}\frac{\partial v_k}{\partial x_k}\right)\right],\end{aligned} \tag{1c}$$

where t means the time, x_j indicates the Cartesian coordinate, ρ represents the density, v_j denotes the velocity component. In addition, T is the temperature, μ the dynamic viscosity, κ the heat conductivity, Pr the Prandtl number, δ_{ij} the Kronecker operator and M the Mach number. Equations(1) should be non-dimensionalized in this way: the coordinates are non-dimensionalized by a reference length L_{ref}, velocity by U_∞, density by ρ_∞, pressure by $\rho_\infty U_\infty^2$, temperature by T_∞, viscosity by μ_∞, heat conductivity by κ_∞, and time by L_{ref}/U_∞. Hence, the Reynolds number Re is given by $Re = U_\infty L_{ref}/\nu_\infty$ where ν_∞ is the kinematic viscosity. Note that $\boldsymbol{U_0} = (\rho_0, u_0, v_0, w_0, T_0)$, the primitive variables in laminar flow boundary layers, can be solved by the steady form of Eq. (1) and the displacement thickness $\delta_1 = \int_0^\infty \left(1-\frac{\rho u}{\rho_\infty U_\infty}\right) dy$ is chosen to be the reference length scale for non-dimensionalization, where y is the coordinate in wall-normal direction.

B. Primary linear instability theory

1. *Linear stability theory on smooth wall*

To conduct the linear stability analysis of the primary Mack mode disturbances, linear stability theory is introduced. Assuming that the linear disturbances take the form

$$\phi'_{LST}(x,y,z,t) = \widehat{\phi}(y)e^{i(\alpha x+\beta z-\omega t)} + c.c. \tag{2}$$

where ϕ' represents the five primitive disturbance variables ρ', u', v', w', T' and $\widehat{\phi}$ indicates the disturbance shape function for each disturbance variable, α, β are the wavenumbers in streamwise x and spanwise z directions respectively, and ω represents the angular frequency. Note that in temporal mode ω is a complex variable and the imaginary part ω_i represents the temporal growth rate. In spatial mode, ω the angular frequency non-dimensionalized by $\omega_r = 2\pi f L_{ref}/U_\infty$ where f is the dimensional frequency in Hertz and the imaginary part α_i indicates the spatial growth rate.

Substituting the sum of basic flow variables and disturbances into the non-dimensional compressible Navier-Stokes equations, with the parallel flow approximation which assumes that the mean flow variables are functions of wall-normal coordinate y only so that $\rho_0 = \rho_0(y), u_0 = u_0(y), w_0 = w_0(y), T_0 = T_0(y)$ and the wall-normal velocity $v_0 = 0$, and the disturbance form in equation(2), retaining the derivatives in wall normal direction and removing the non-linear terms, the linear stability theory (LST) equations in temporal mode can be written as

$$\omega \mathscr{M} \widehat{\phi} = \mathscr{N} \widehat{\phi}, \tag{3}$$

where $\mathscr{M}$ and $\mathscr{N}$ are the corresponding large sparse matrices composed of the mean flow variables, frequencies and wavenumbers. This eigenvalue problem with the homogeneous boundary conditions is discretized by the five-point 4^{th}-order central difference scheme in the wall-normal direction. The eigenvalue problem is solved using the Arnoldi method (in the open source library ARPACK[56]). In order to calculate the local eigenvalue, the Rayleigh inverse iteration method[57]

$$(\mathscr{N} - \omega_k \mathscr{M})\widehat{\phi}^{(k+1)} = \mathscr{M}\widehat{\phi}^{(k)}, \tag{4a}$$

$$\widehat{\phi}^{(k+1)} = \widehat{\phi}^{(k+1)}/max(\widehat{\phi}^{(k+1)}), \tag{4b}$$

$$\omega_{k+1} = \frac{(\widehat{\phi}^{(k+1)})^H \mathscr{N} \widehat{\phi}^{(k+1)}}{(\widehat{\phi}^{(k+1)})^H \mathscr{M} \widehat{\phi}^{(k+1)}} \widehat{\phi}^{(k+1)}. \tag{4c}$$

is employed. When $|\omega_{k+1} - \omega_k| < \varepsilon_l$, the local temporal eigenvalue can be assumed to have converged. Note that ε_l is usually prescribed as $1e^{-8}$.

2. *Linear stability theory on porous surface*

In order to simulate the linear stability in the presence of porous walls, the classical boundary conditions modeled by Fedorov et al.[2] have the form

$$\widehat{u}_w = \widehat{w}_w = 0, \widehat{v}_w = \overline{A}\widehat{p}_w, \widehat{T}_w = \overline{B}\widehat{p}_w, \tag{5}$$

where $\overline{A}$ means the admittance and $\overline{B}$ is the thermal admittance. The definition of admittance proposed by Fedorov et al.[2] is used to describe the property of the porous surface. From the DNS research by Wartemann et al.[49], it can be seen that when the the pore depth is larger than about 0.4, the growth rate levels out to a nearly constant value on the porous surface. Hence, in this research, we assume that the pore depth d is relatively thick enough ($\tanh(\Lambda d) \to -1$) for all cases, yielding

$$\overline{A} = \frac{n}{Z_0}\tanh(\Lambda d) = -\frac{n}{Z_0}, \overline{B} = -n(\gamma-1)M^2 T_w J_2(k_t)/J_0(k_t), \tag{6}$$

where Λ is a propagation constant, γ the specific heat ratio, n the porosity coefficient and Z_0 the impedance. The remaining parameters are given by

$$Z_0 = \sqrt{Z_1/Y_1}, \Lambda = \sqrt{Z_1 Y_1}, k_t = k_v\sqrt{\mathrm{Pr}} \tag{7a}$$

$$Z_1 = \frac{i\omega}{T_w}\frac{J_0(k_v)}{J_2(k_v)}, k_v = r\sqrt{\frac{i\omega\rho_w}{\mu_w}\mathrm{Re}}, \tag{7b}$$

$$Y_1 = -i\omega M^2\left[\gamma + (\gamma-1)\frac{J_2(k_v\sqrt{\mathrm{Pr}})}{J_0(k_v\sqrt{\mathrm{Pr}})}\right]. \tag{7c}$$

where M stands for the Mach number at the edge of boundary layer and r indicates the pore radius non-dimensionalized by δ_1. Z_1 means the impedance and Y_1 represents the shunt admittance[2]. The subscript 'w' means the values on the wall. Furthermore, J_0 and J_2 are the Bessel functions. Combining these special boundary conditions with Eq.(3), the eigenvalues and eigenfunctions can be determined.

C. Secondary instability theory

1. *Secondary instability theory on smooth wall*

For the secondary instability analysis, the Floquet-based secondary instability theory (SIT) proposed by Herbert[3], is adopted in this paper; the same approach has been used by a number of

authors [58–60]. This model describes the instability characteristics in the boundary layer when the primary mode disturbance has grown up to a saturated amplitude. Following this a new basic flow can be constructed by the composition of the primary mode and the 2D basic flow solution. In other words, the new flow can be written as $U(x,y,z,t) = \boldsymbol{U_0}(y) + A(\widehat{u}(y)e^{i(\alpha x-\omega t)} + c.c.)$ Here, $\boldsymbol{U_0}$ is the original 2D basic steady boundary-layer flow solution, $\widehat{u}$ is the primary mode, and A is its amplitude. Obviously, the new basic flow is a function of time t. To eliminate the time t, a Galilean transformation with the form of $\widetilde{x} = x - c_r t, \widetilde{y} = y, \widetilde{z} = z$ is introduced; where c_r stands for the phase velocity. It means that the basic flow of the secondary instability moves with the primary mode disturbance. It is obvious that the high order disturbances can be governed by the dynamics system

$$\widetilde{L}\phi'_S = 0 \tag{8}$$

where ϕ'_S is the secondary instability disturbance corresponding to the five primitive variables and $\widetilde{L}$ represents the operator of the new basic flow $\widetilde{U}(\widetilde{x},y)$. Due to the saturated primary mode disturbance, a quasi-parallel assumption can be adopted assuming an insignificant variation of the primary mode amplitude. Moreover, it is imposed that the secondary instability is periodic in the streamwise direction $\widetilde{x}$. As a result, the secondary disturbance is given by

$$\phi'_S(\widetilde{x},\widetilde{y},\widetilde{z},t) = e^{\sigma t}e^{i\beta_2\widetilde{z}}e^{i\varepsilon\widetilde{\alpha}\widetilde{x}}\sum_{j=-\infty}^{\infty}\widetilde{\phi}_{S,j}(\widetilde{y})e^{i(j\widetilde{\alpha}\widetilde{x})}. \tag{9}$$

where ε is the detuning parameter which means the phase difference between the new basic flow $\widetilde{U}(\widetilde{x},y)$ and the secondary disturbance and β_2 stands for the wave number in the $\widetilde{z}$ direction. The parameter ε with values of 0.5 and 0 produce subharmonic modes and fundamental modes, respectively. Obviously, this is a complex eigenvalue problem that reads

$$\sigma\mathscr{M}\widehat{\phi_S} = \mathscr{N}\widehat{\phi_S}. \tag{10}$$

subject to the homogeneous boundary conditions being satisfied.

For a given real wave number β_2, the unknown complex variable σ describes the temporal instability of the secondary disturbance. The real part of σ stands for the growth rate and the imaginary part represents the phase. For the spatial problem, Gaster's transformation can be employed. The 4^{th}-order central difference scheme is adopted in the normal discretization and the Fourier spectral method is used in the streamwise direction. As with the primary instability case, ARPACK[56] is used to solve this 2D eigenvalue problem through the Arnoldi algorithm. The code

for temporal and spatial secondary instability analysis has also been developed and verified by Zhang and Luo[61] and Liu, Zhang, and Fu[62].

2. *Secondary instability theory on porous surface*

Through personal communication with Mujeeb R. Malik from NASA Langley, we consider that the secondary instability equations on porous walls should have the same boundary conditions as that used for linear stability equations on porous walls earlier. Therefore, based on the framework in Eq.(8), the boundary conditions for the secondary instability model over the porous surface satisfy

$$\widehat{u}_{S,w} = \widehat{w}_{S,w} = 0, \widehat{v}_{S,w} = \overline{A}\widehat{p}_{S,w}, \widehat{T}_{S,w} = \overline{B}\widehat{p}_{S,w}; \tag{11}$$

where $\overline{A}$ and $\overline{B}$ are same with those given in Eq. (6).

III. RESULTS AND DISCUSSIONS

In this section, the compressible Navier-Stokes equations are used to solve the mean flow, followed by temporal linear stability theory to compute the primary disturbances and to construct the new modified basic flow for the secondary instability analysis. A brief introduction of the construction method is given herein. According to previous studies, the linear primary disturbance contributes the most in the secondary instability. We assume that including the full effects of nonlinearity and non-parallelism to establish the modified basic flow for the secondary instability analysis, will only give rise to small deviations in the analysis. Therefore, the basic flow variable $U(x,y,z,t)$ for secondary instability can be constructed by the sum of the mean flow variable $\boldsymbol{U}_0(y)$ and the linear theory disturbances of the Mack mode $A\hat{\phi}_1^+(y)e^{i(\alpha x-\omega t)} + \text{c.c.}$ with the Galilean transformation as mentioned in §II C 1. Here, $\hat{\phi}_1^+$ means the primary disturbance $(\rho_1^+, u_1^+, v_1^+, w_1^+, T_1^+)$ and A stands for its amplitude. The subscript '1' represents the primary mode. Note that the amplitude is defined using the maximum value of the temperature disturbance $\max\limits_{0\le y<\infty} |T_1^+(y)|^2 = \frac{1}{2}$ for high Mach number and using the maximum value of the streamwise velocity perturbation $\max\limits_{0\le y<\infty} |u_1^+(y)|^2 = \frac{1}{2}$ for the low Mach number analysis. There are four flow cases used in this paper, and the corresponding flow conditions are listed in Table I.

TABLE I. Flow conditions.

Case	Mach	Re	T_∞ (K)	T_w (K)
Ng and Erlebacher	1.6	1675	288.89	adiabatic
Ng and Erlebacher	4.5	10000	61.11	adiabatic
Fedorov et al.	6.0	3500-5000	243.9	341.46
Wartemann et al.	6.0	20000	216.65	adiabatic

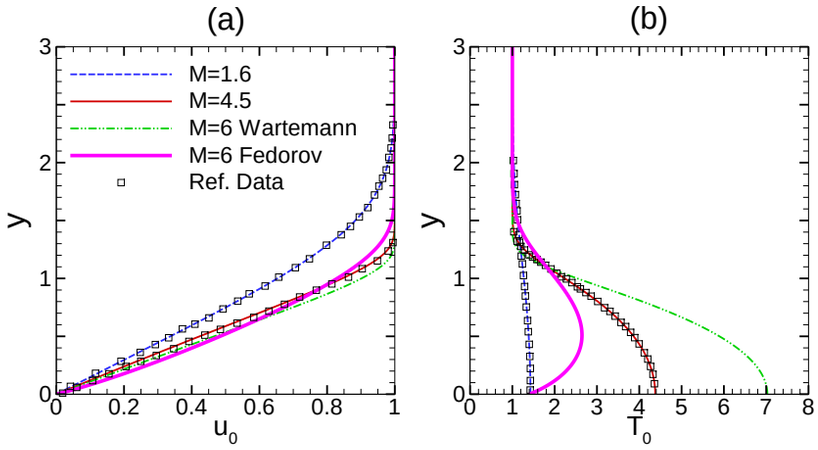

FIG. 2. Comparison of mean flow variables (The reference data extracted from Ng & Erlebacher[32]). (a) streamwise velocity u_0; (b) temperature T_0.

A. Primary instability and secondary instability on smooth wall

In order to investigate the secondary instability over the porous surface, it is necessary to understand the secondary instability mechanism for a smooth wall first. The mean flow variables for a supersonic flat plate at Mach 1.6 and Mach 4.5, are compared with results of[32] in Fig. 2, demonstrating that the present results for mean flow are consistent with the reference results. At Mach 6.0, the flow cases by Fedorov et al.[2] and Wartemann et al.[49] are calculated and Fig.2 displays the distributions of streamwise velocity u_0 and temperature T_0.

The primary Mack modes using linear stability theory are next computed. Fig.3 (a) and (b) depict the primary eigenfunctions of the first modes at Mach=1.6 with $\alpha = 0.24$ and Mach=4.5 with $\alpha = 0.6$. When $Re = 10,000$, $\alpha = 2.25$ and $\alpha = 2.52$, the modulus of the primary eigenfunctions for the 2-D Mack mode disturbances is shown in Fig.4. Compared with the reference data[32], the present calculations for primary instability perform well, thus validating the correctness of the

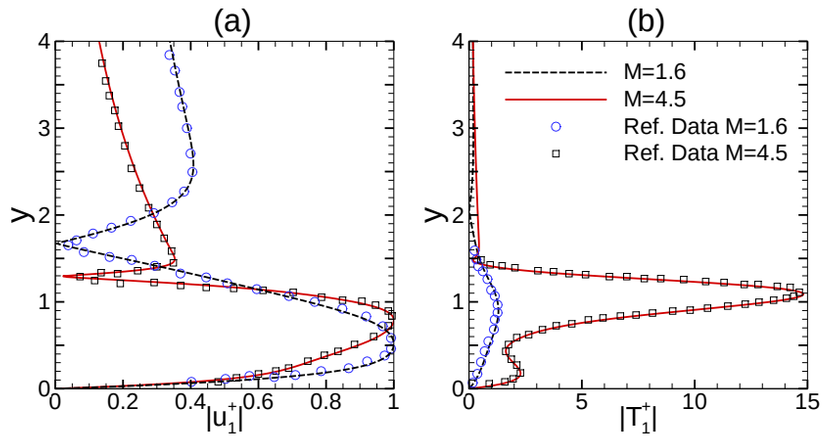

FIG. 3. First mode (2D) primary eigenfunctions at Mach=1.6 with $\alpha = 0.24$ and Mach=4.5 with $\alpha = 0.6$ (The reference data extracted from Ng & Erlebacher[32]). (a) streamwise primary disturbances u_1^+; (b) temperature primary disturbances T_1^+.

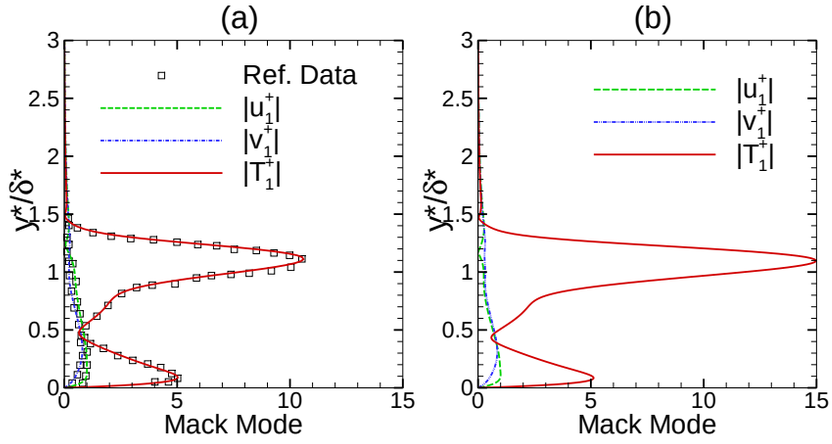

FIG. 4. Mack mode (2D) primary eigenfunctions at Mach=4.5 with (a) $\alpha = 2.25$; (b) $\alpha = 2.52$ (The reference data extracted from Ng & Erlebacher[32]).

LST computation. Note that the distributions of primary eigenfunctions at Mach 6 are similar with these at Mach 4.5, so it is not displayed herein.

With the primary eigenfunctions computed, the basic flows for secondary instability are next constructed. Prescribing various primary amplitudes, the fundamental modes of first mode primary wave at Mach 1.6 as well as the subharmonic modes of Mack mode disturbances at Mach 4.5 are illustrated in Fig. 5(a) and (b), respectively; which are all in a good agreement with published results. Hence, we may conclude the correctness of the secondary instability computations has

been verified too, for confidence in usage with the porous surface investigations undertaken by us.

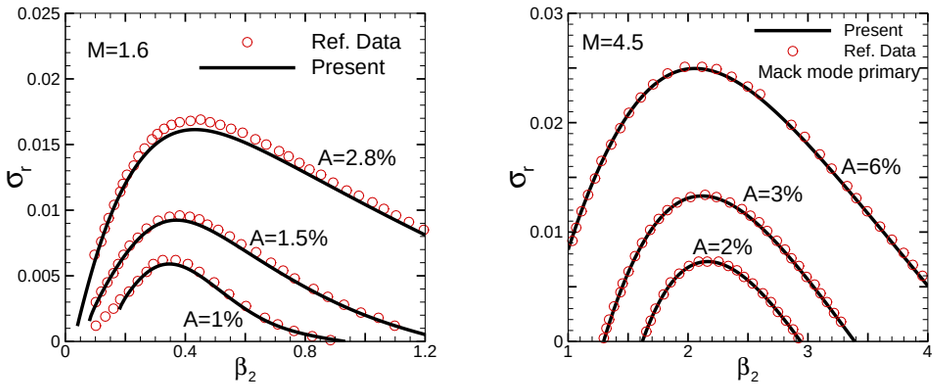

(a) Fundamental (b) Subharmonic

FIG. 5. Comparison of secondary instability temporal growth rates against the spanwise wavenumber β_2 between the present calculations and the reference data at Mach 1.6 and Mach 4.5 (The reference data extracted from Ng & Erlebacher[32]). (a) Fundamental instability for first mode primary at Mach 1.6; (b) Subharmonic instability for Mack mode primary at Mach 4.5.

As mentioned in §I, according to experimental observations and DNS simulations, when the amplitude of the primary Mack mode is large enough the fundamental mode may dominate the secondary instability, rather than the subharmonic mode revealed in Ng and Erlebacher's paper[32]. With further analysis, Fig.6(a) and (b) demonstrate the secondary instabilities of the 2D Mack mode's primary disturbances with various primary amplitudes – this indicates that the fundamental mode gradually dominates as the primary amplitude increases. Extracting the data at spanwise wavenumber $\beta_2 = 2.1$ corresponding to the maximum growth rate of subharmonic mode and a larger spanwise wavenumber $\beta_2 = 3.5$, the explicit rules of fundamental, subharmonic and detuned mode versus primary amplitude A are sketched in Fig. 7(a) and (b) respectively. Obviously, the primary amplitude of Mack mode is the crucial factor in the secondary instability. Ng and Erlebacher omitted the fundamental mode proportional to the primary amplitude in their Mach 4.5 boundary layer analysis. With small and medium primary amplitudes, a subharmonic mode is always dominant. When the primary amplitude exceeds a threshold value, the fundamental mode in the secondary instability has the largest growth rate.

Furthermore, the eigenfunctions of the unstable mode provide a powerful methodology for clarification of the mechanisms involved. Consequently, when the primary amplitude equals 1, the eigenfunctions $|u_2^+|$ for the fundamental mode and subharmonic mode at $\beta_2 = 2.1$ are shown in

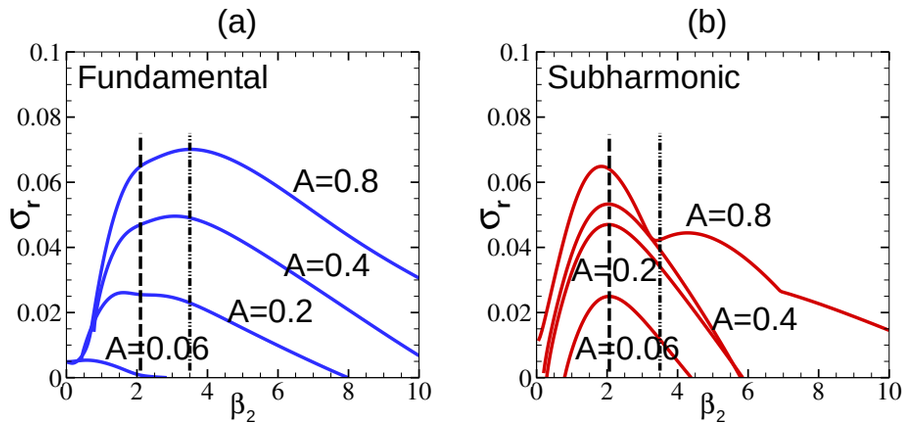

FIG. 6. Secondary instabilities of the 2D Mack mode primary disturbances at Mach 4.5 with various primary amplitudes on smooth wall. (a) fundamental mode; (b) subharmonic mode.

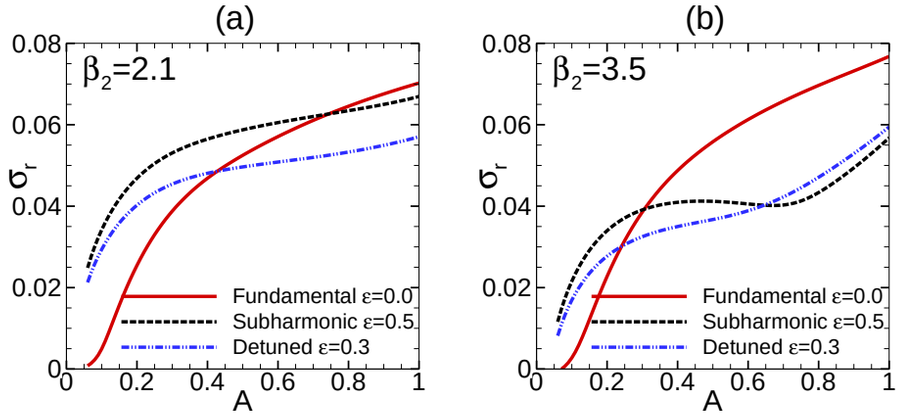

FIG. 7. Secondary instabilities of the 2D Mack mode primary disturbances with various primary amplitudes on smooth wall at (a) $\beta_2 = 2.1$; (b) $\beta_2 = 3.5$.

Fig.8(a) and Fig.8(b), respectively. It can be seen that the disturbance energy of the fundamental mode is concentrated in the near-wall region but the disturbance energy of the subharmonic mode is mainly distributed near the boundary layer edge. Note that the lines plotted in the contours of the fundamental mode represent the derivatives $\partial\widetilde{U}/\partial\widetilde{x}$ of the basic flow for secondary instability and the lines plotted in the contours of subharmonic mode represent the derivatives $\partial\widetilde{U}/\partial y$ of basic flow for secondary instability. The figures indicate that a finite amplitude second mode can create a concentration of strong mean flow shear, which is in agreement with the conclusion in Ref.[9]. Through an energy balance analysis,[63] suggests that the fundamental mode is mainly produced by the energy-conversion mechanism from the near edge of the boundary layer to the near-wall re-

gion via the work done by the Reynolds stresses as the shear strength increases. On the other hand, the outer boundary layer edge region always dominates the production of the subharmonic mode. Therefore, the present results imply that the derivatives $\partial\widetilde{U}/\partial\widetilde{x}$ and $\partial\widetilde{U}/\partial y$ play an important role in the production of secondary instability eigenfunctions. In addition, when the primary amplitude equals 1, the eigenfunctions $|u_2^+|$ for the fundamental mode and subharmonic mode at $\beta_2 = 3.5$ are displayed in Fig.9(a) and Fig.9(b), respectively. It indicates that the disturbance energy of the fundamental mode changes significantly and concentrates towards the edge of boundary layer, implying that the fundamental mode at a larger spanwise wavenumber is no longer simply generated by the mean shear in the near-wall region.

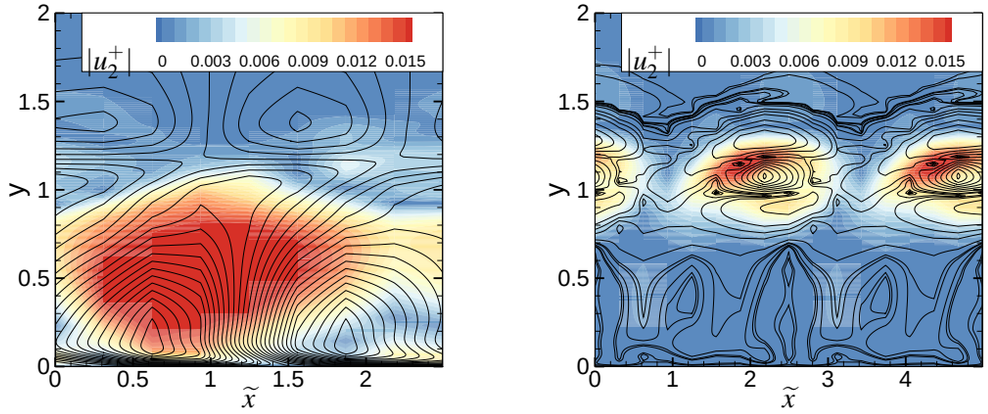

(a) Fundamental mode (b) Subharmonic mode

FIG. 8. Eigenfunctions of the secondary instability modes and the derivatives of the basic flow for secondary instability on smooth wall at Mach 4.5 when the primary amplitude is 1.0 and $\beta_2 = 2.1$. (a) fundamental mode; (b) subharmonic mode.

According to the experimental data from Schneider's group[34] and DNS investigations from Fasel's group[42,43], they make the point that stationary streaky structures dominate the earlier stage of the fundamental breakdown. In order to validate this, Fourier analysis was conducted for the eigenfunctions of fundamental modes. The parameter group (m_f, n_f) is one of the spatial Fourier spectra. Here, m_f stands for the multiple of the frequency and n_f indicates the multiple of the given spanwise wavenumber β_2. Fig.10(a) and (b) depict the Fourier analysis results of the fundamental eigenfunctions at $\beta_2 = 2.1$ and $\beta_2 = 3.5$, respectively. Obviously, the (0, 1) stationary structures mode, has the largest amplitude in the spectrum especially in the near-wall region. It means that the stationary structures dominate the fundamental breakdown process before turbulence, which

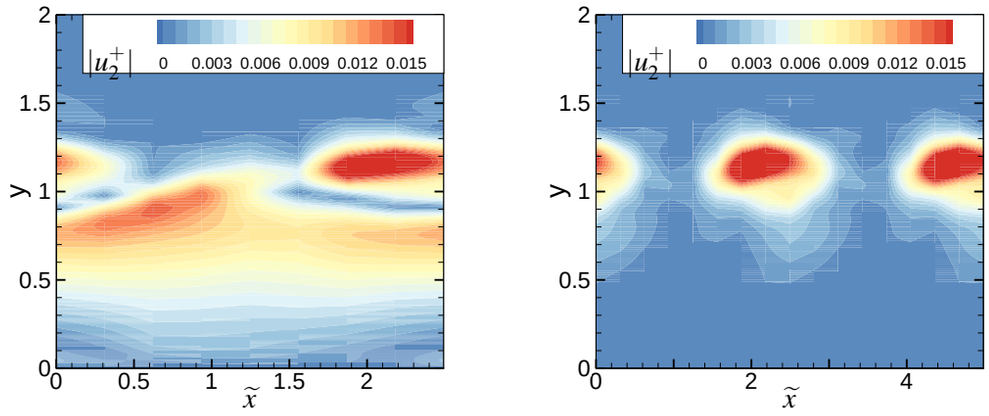

(a) Fundamental mode (b) Subharmonic mode

FIG. 9. Eigenfunctions of the secondary instability modes and the derivatives of the basic flow for secondary instability on smooth wall at Mach 4.5 when the primary amplitude is 1.0 and $\beta_2 = 3.5$.(a) fundamental mode; (b) subharmonic mode.

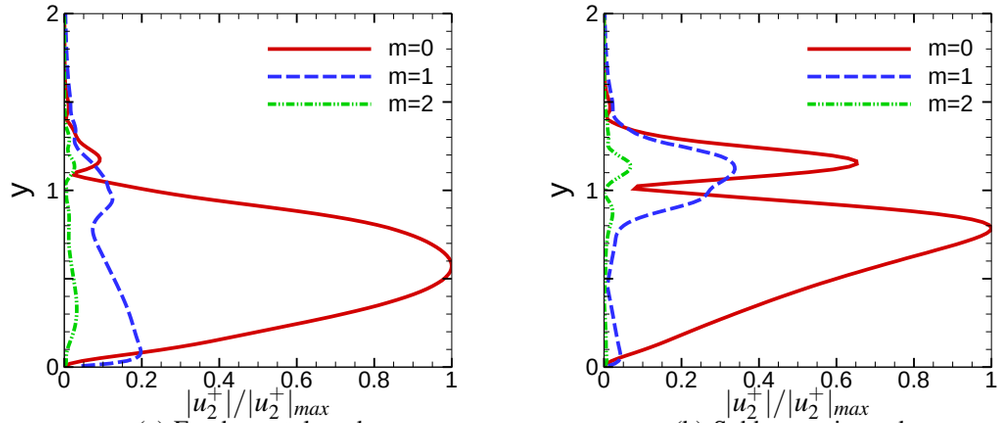

(a) Fundamental mode (b) Subharmonic mode

FIG. 10. Fourier analysis of the fundamental eigenfunctions on smooth wall at Mach 4.5 when the primary amplitude is 1.0. (a) $\beta_2 = 2.1$; (b)$\beta_2 = 3.5$.

is in good agreement with the measured data and DNS observations. It is worth noting that the distribution of (0,1) mode at $\beta_2 = 3.5$ moves up relative to the distribution at $\beta_2 = 2.1$ and the disturbance energy near the the boundary layer edge increases significantly.

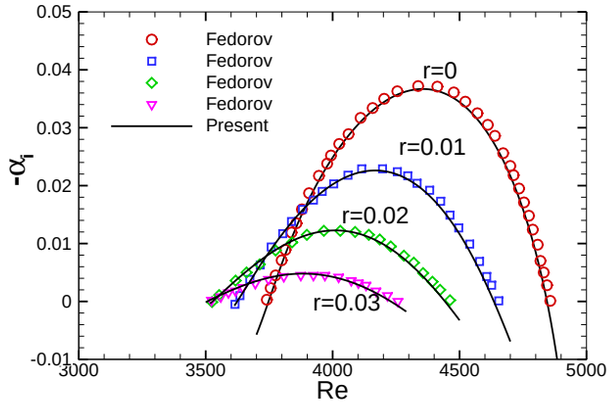

FIG. 11. Spatial growth rate of primary instability for Mack mode against Reynolds number *Re* with different pore radii *r*.

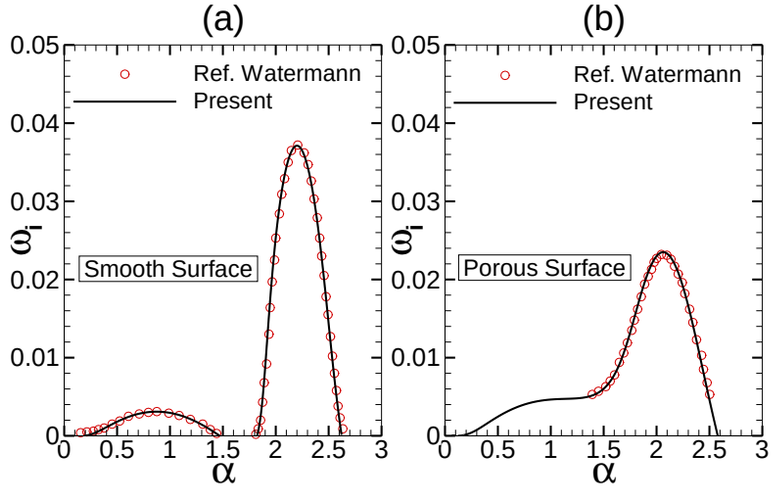

FIG. 12. Comparison of temporal primary growth rate versus wavenumber α between the present results and the DNS data. (a) smooth wall; (b) porous wall (r = 0.046875 and n=0.25).

B. Primary instability and secondary instability on porous surface

As known, the growth rate of the primary Mack mode is generally weakened by the porous surface thus delaying transition. Since the distribution of the corresponding disturbances is changed significantly with porosity, it is very important to get an accurate computation of changes to the primary instability due to porosity. The first validation case at Mach 6 comes from Fedorov et al.[2]. The Reynolds number varies from 3500 to 5000, and the dimensionless pore radius is in the range

of $0 \leq r \leq 0.3$. The porosity $n = 0.5$ and the reduced frequency $F = \omega \cdot Re = 2.8 \times 10^{-4}$. Fig. 11 displays the spatial growth rate of primary instability for Mack mode against Reynolds number Re with different pore radii r. Good agreement with Fedorov et al.'s results verify the correctness of the present linear stability calculations with the included porous model. In addition, Wartemann et al.[49] employed temporal DNS to simulate the instability properties over porous surface at Mach 6.0. The detailed flow conditions are listed in Table I, and the adiabatic wall condition results in a wall temperature of 1522.44K. Fig. 12(a) and (b) plot the present temporal primary instability calculations compared with DNS data of Wartemann, Lüdeke, and Sandham[49] over smooth and porous walls with $r = 0.046875$ and $n = 0.25$ respectively. This indicates that the present linear analysis with the porous surface model is correctly implemented and importantly demonstrates that the primary Mack mode is obviously weakened by the porous surface. Further validations with Wartemann et al.[49] DNS simulations are given in Fig. 13(a) and (b), respectively, showing the wall-normal disturbance over smooth and porous wall ($r = 0.046875$ and $n = 0.25$). As may be noted, the most significant variations of primary disturbance exist near the wall. According to the secondary instability analysis, the eigenfunctions of the fundamental mode mainly concentrate near the wall, meaning that the fundamental mode is probably affected by these change. We next undertake a series of secondary instability analyses for the porous surface to clarify this mechanism.

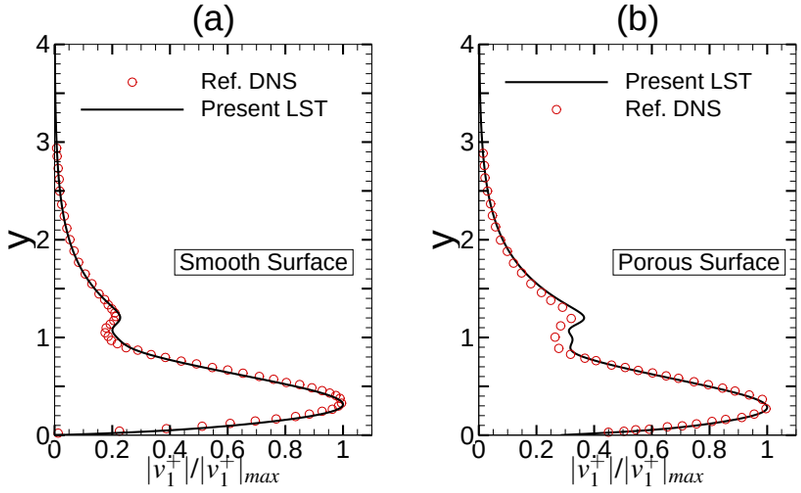

FIG. 13. Comparison of temporal primary eigenfunctions between the present results and the DNS data. (a) smooth wall; (b) porous wall (r = 0.046875 and n=0.25).

As mentioned above, at Mach 4.5, the smooth wall fundamental mode is weaker than the sub-

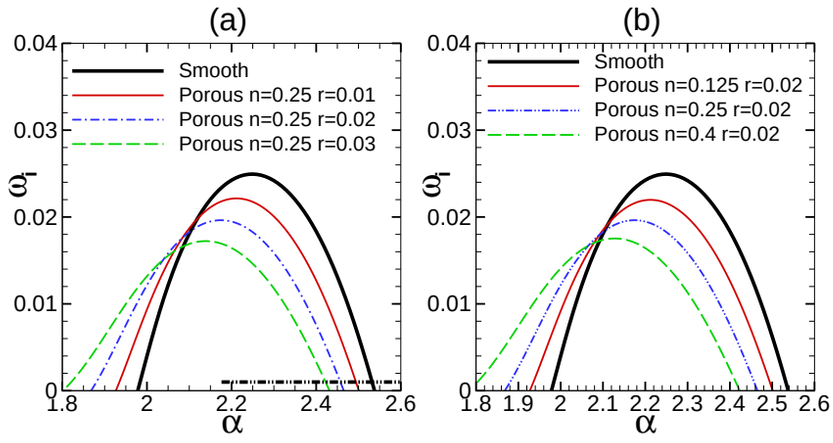

FIG. 14. Comparison of temporal primary growth rates against streamwise wavenumbers α at different pore radii r and porosity coefficients n. (a) $n = 0.25$ and $r = 0.01, 0.02, 0.03$; (b) $r = 0.02$ and $n = 0.125, 0.25, 0.4$.

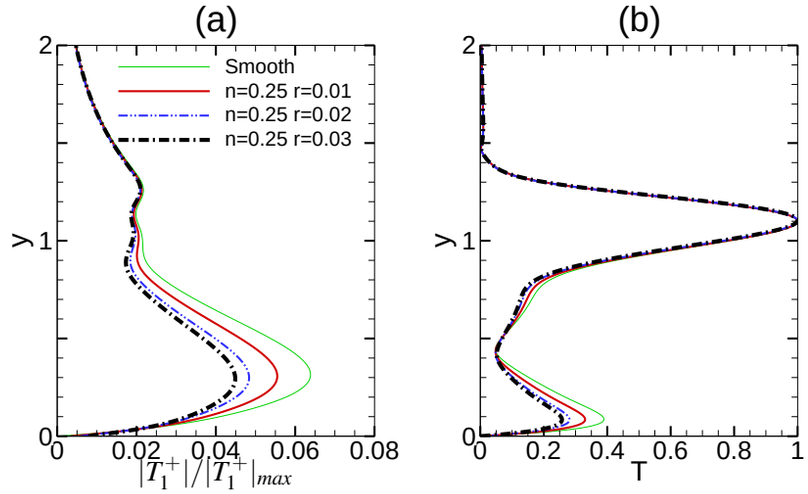

FIG. 15. Comparison of primary eigenfunctions with different pore radii. (a) normal disturbance $|v_1^+|$; (b) temperature disturbance $|T_1^+|/|T_1^+|_{max}$.

harmonic mode when the primary amplitude is small or medium, and stronger than the subharmonic mode when the primary amplitude is large enough. It should be acknowledged that when the primary amplitude is close to the saturated amplitude of the primary mode, it can be called large enough. Generally speaking, the saturated primary amplitude defined by the peak value of streamwise primary disturbance u_1^+ usually is of the order of $O(10^{-1})$. Correspondingly, the primary amplitude defined by the peak value of temperature disturbance T_1^+ has a saturated value of roughly $O(1)$. For comparison, various parameters of $r = 0.01, 0.02, 0.03$ and $n = 0.125, 0.25, 0.4$

are chosen to study the explicit rules of porous effects on secondary instability at Mach 4.5. Fig. 14 demonstrates the temporal growth rates of primary Mack mode disturbances with different porous parameters. The larger the pore radius or porosity coefficient, the more obvious it is that the primary mode is weakened. Note that the influence of porosity coefficient on the primary disturbances is similar to that of pore radius on the primary disturbances, so only the latter is studied hereafter. In order to construct the basic flow for secondary instability analysis, in a similar way with Ng and Erlebacher[32], the wavenumber α is chosen near the right-hand branch of the neutral curve of the primary Mack mode. For $r = 0.01, 0.02$ and 0.03, the corresponding streamwise wavenumbers α are determined as $2.42, 2.45$ and 2.48, respectively. With different pore radii, the corresponding primary disturbances are displayed in Fig.15. From the figure, it can be seen that the near-wall disturbances are changed significantly. The larger the pore radius or porosity coefficient, the more dramatic is the near wall variation.

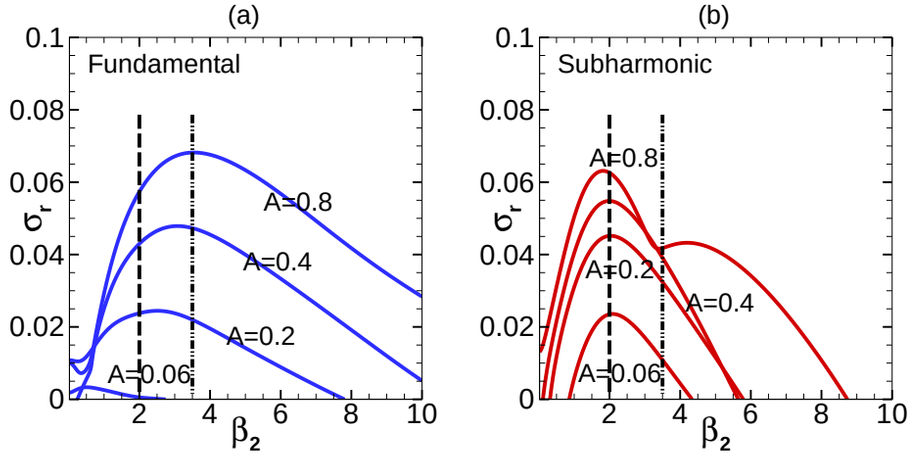

FIG. 16. Secondary instabilities of the 2D Mack mode primary disturbances at Mach 4.5 with various primary amplitudes on porous wall (r = 0.02 and n=0.25). (a) fundamental mode; (b) subharmonic mode.

Solving Eq.(10) with the boundary conditions given by Eq.(11), the secondary instability over the porous surface is investigated. Since the distribution of secondary instability results are very similar at various pore radii, only one group of results are selected for display and then only results where the differences are significant will be given special attention. With porosity parameters of $r = 0.02$ and $n = 0.25$, the temporal growth rates of fundamental mode and subharmonic mode versus spanwise wavenumber β_2 with various primary amplitudes are sketched in Fig. 16 (a) and (b), respectively. It can be seen that both the fundamental and subharmonic modes become more

unstable as the amplitude of the primary mode disturbance increases. However, the fundamental modes are more sensitive to the primary amplitude. Furthermore, the spanwise wavenumber corresponding to the maximum growth rate of subharmonic mode is about 2. When the primary amplitude is small, the subharmonic mode still dominates. But as the primary amplitude increases, the growth rate of the fundamental mode increases rapidly. Nevertheless, focusing on the spanwise wavenumber $\beta_2 = 2.0$ corresponding to the maximum growth rate of the subharmonic mode, it is worth mentioning that with the primary amplitude of Mack mode increasing, the fundamental mode will not surpass the subharmonic mode – which is totally different with the smooth wall results. While at a larger spanwise wavenumber β_2, it is obvious that the fundamental mode will be dominant when the primary amplitude is large enough.

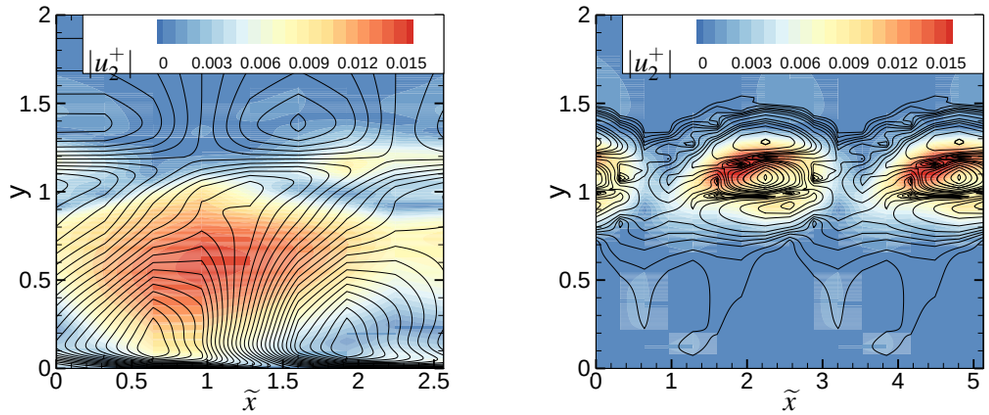

(a) Fundamental mode (b) Subharmonic mode

FIG. 17. Eigenfunctions of the secondary instability modes and the derivatives of the basic flow for secondary instability over porous surface ($r = 0.02$ and $n = 0.25$) at Mach 4.5 when the primary amplitude is 1.0 and $\beta_2 = 2.0$. (a) fundamental mode; (b) subharmonic mode.

On further analysis, when the amplitude of the primary Mack mode reaches 1, the eigenfunctions $|u_2^+|$ for the fundamental and subharmonic modes at $\beta_2 = 2.0$ are illustrated in Fig.17(a) and Fig.17(b), respectively. The disturbance energy of the fundamental mode is concentrated in the near-wall area, and the disturbance energy of subharmonic mode is mainly distributed near the boundary layer edge. Furthermore, the derivatives $\partial\widetilde{U}/\partial\widetilde{x}$ and the normal derivatives $\partial\widetilde{U}/\partial y$ are plotted in Fig.17 for comparison, which both play a crucial role in the production of the fundamental and subharmonic modes. Small differences in eigenfunctions overall appear in these figures compared with the smooth wall eigenfunctions. However, the porous wall with $r = 0.02$

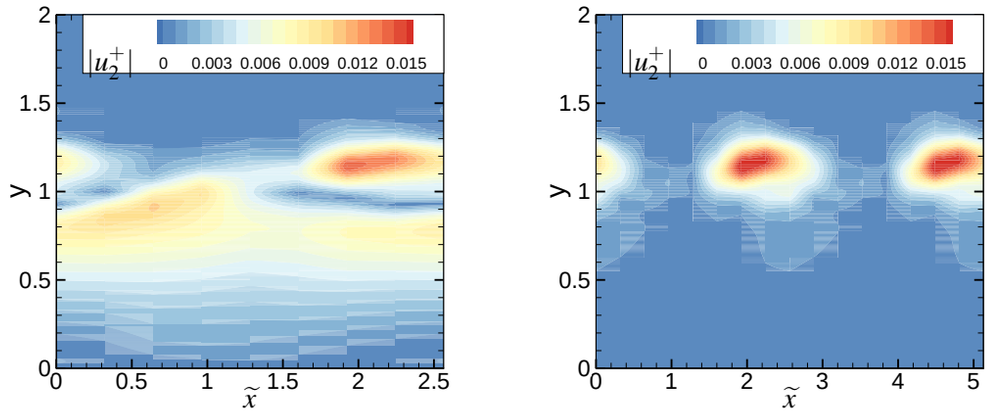

(a) Fundamental mode (b) Subharmonic mode

FIG. 18. Eigenfunctions of the secondary instability modes and the derivatives of the basic flow for secondary instability on porous wall ($r = 0.02$ and $n = 0.25$) at Mach 4.5 when the primary amplitude is 1.0 and $\beta_2 = 3.5$. (a) fundamental mode; (b) subharmonic mode.

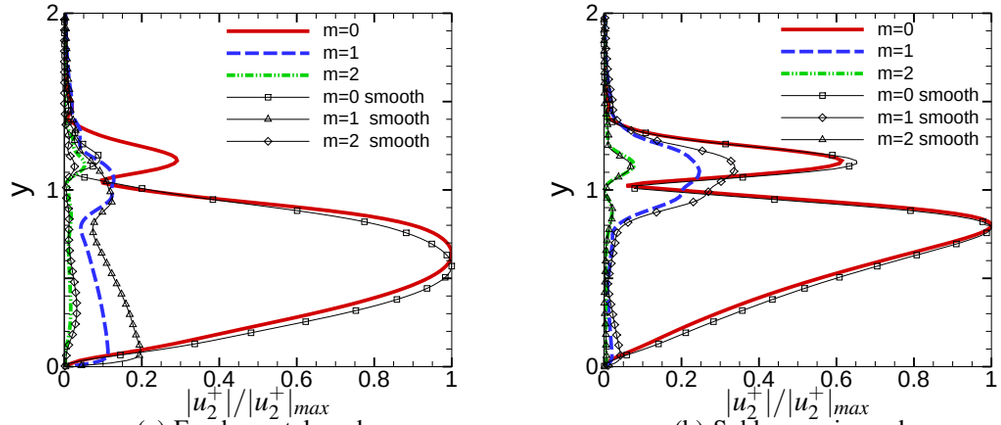

(a) Fundamental mode (b) Subharmonic mode

FIG. 19. Fourier analysis of the fundamental eigenfunctions on porous wall with $r = 0.02$ and $n = 0.25$ at Mach 4.5 when the primary amplitude is 1.0. (a) $\beta_2 = 2.0$; (b)$\beta_2 = 3.5$.

and $n = 0.25$ obviously decreases the modulus of the fundamental eigenfunction mode amplitude. Furthermore, when the amplitude of the primary Mack mode is 1, Fig.18(a) and (b) sketch the eigenfunctions $|u_2^+|$ for the fundamental and subharmonic modes at $\beta_2 = 3.5$, respectively. It can be seen that the eigenfunction distribution of the subharmonic mode and fundamental mode are mainly located near the edge of the boundary layer region. Compared with the eigenfunctions computed on the smooth wall at $\beta_2 = 3.5$, the modulus of the eigenfunctions on both fundamental mode and subharmonic mode is slightly weakened. The main reason for these changes is likely

to be due to the differences in the primary eigenfunction profile shape variation arising near the porous wall surface. Considering Fig. 15, it can be seen that relative changes in the primary disturbances arising from porous surface mainly occur near the wall. Due to these near wall variations of the primary disturbance structure, the modulus of the fundamental mode at $\beta_2 = 2.0$ is changed obviously compared with the values in Fig.8 and the fundamental mode is primarily concentrated within the boundary layer. Besides, the fundamental mode concentrated near the boundary layer edge for $\beta_2 = 3.5$, is slightly altered. Using Fourier analysis for the eigenfunctions at $\beta_2 = 2.0$ and $\beta_2 = 3.5$, the stationary (0, 1) mode always has the largest amplitude in the spectrum as shown in Fig.19. This property is unchanged, implying that stationary streaks dominate the fundamental resonances at the conditions discussed above.

Does the change of primary disturbance really have such a big impact? We next focus on assessing the contribution of the primary disturbance changes and the porous boundary conditions in the secondary instability analysis. In order to make it clear, Eq.(10) with homogeneous boundary conditions were solved. With the porous parameters of $r = 0.02$ and $n = 0.25$, the temporal growth rates of fundamental mode and subharmonic mode versus spanwise wavenumber β_2 with various primary amplitudes are sketched in Fig. 20 (a) and (b), respectively. It can be seen that the subharmonic modes hardly change, and the fundamental modes are slightly higher than that shown in Fig.16. Extracting the data at spanwise wavenumber $\beta_2 = 2.0$, corresponding to the maximum growth rate of the subharmonic mode, the explicit rules of the fundamental mode, the subharmonic mode and the detuned mode against primary amplitude A, with porous boundary conditions in Eq.(11) and homogeneous boundary conditions, are shown in Fig. 21(a) and (b), respectively. From the figure, it suggests that even though the homogeneous boundary conditions are chosen for secondary instability analysis, the fundamental mode, at $\beta_2 = 2.0$ with the porous parameters of $r = 0.02$ and $n = 0.25$, is still suppressed when the primary amplitude is large and becomes weaker than the subharmonic mode. Certainly, the porous boundary conditions can also affect the fundamental modes to some extent. Additionally, when the primary amplitude is 1.0, similar to the trend reflected by the growth rate, the eigenfunctions of the fundamental mode given by Eq.(10) with homogeneous boundary conditions as shown in Fig.22 at $\beta_2 = 2.0$ have larger values than the ones in Fig.17. As a result, it indicates that the changes in primary disturbances play a more critical role in the impact of secondary instability over the porous wall.

To investigate the effect of pore parameters, Eq.(10) with the boundary conditions in Eq.(11) were computed for the secondary instability. At spanwise wavenumber $\beta_2 = 2.0$, the explicit rules

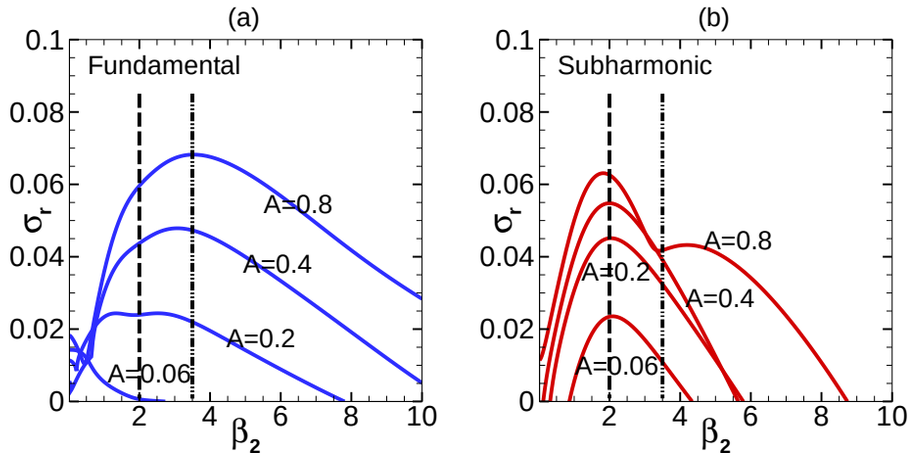

FIG. 20. Secondary instabilities of the 2D Mack mode primary disturbances at Mach 4.5 with various primary amplitudes on porous wall (r = 0.02 and n=0.25). (a) fundamental mode; (b) subharmonic mode.

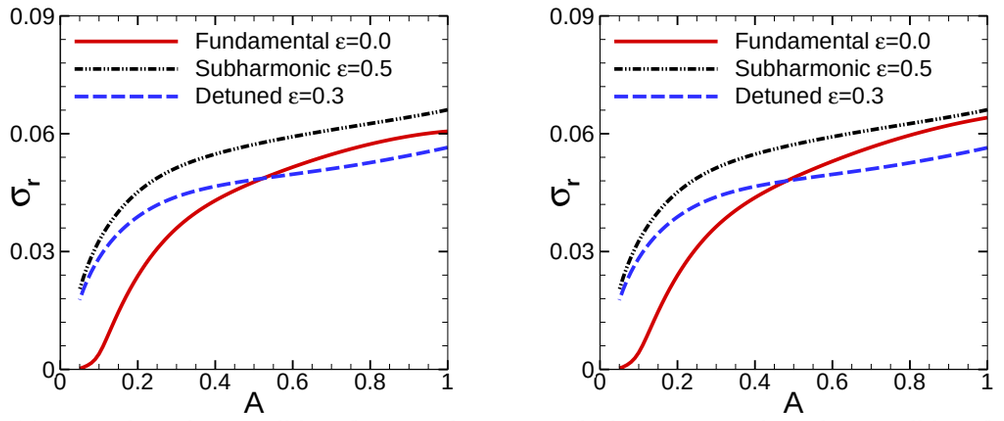

(a) porous boundary conditions for secondary instability

(b) homogeneous boundary conditions for secondary instability

FIG. 21. Temporal growth rates in secondary instability against primary amplitude A on porous surface with pore radius $r = 0.02$ at Mach 4.5 and $\beta_2 = 2.0$. (a) porous boundary conditions for secondary instability; (b) homogeneous boundary conditions for secondary instability.

of the fundamental mode, the subharmonic mode and the detuned mode against primary amplitude A, with $r = 0.01, 0.02$ and $r = 0.03$, are shown in Fig. 23(a) and (b), respectively. It can be seen that the larger the pore radius, it becomes evident that the fundamental mode is reduced when the primary amplitude is large, while the subharmonic mode hardly changes. At a larger spanwise wavenumber $\beta_2 = 3.5$, the explicit rules of the fundamental mode, the subharmonic mode and the

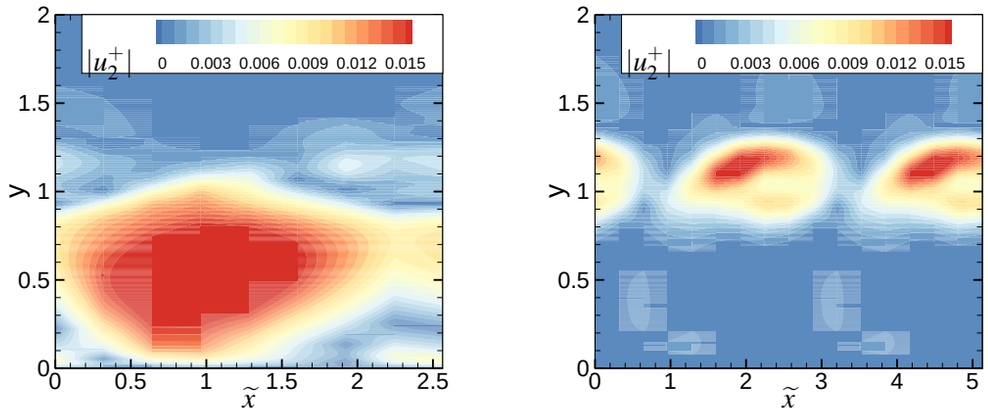

(a) Fundamental mode (b) Subharmonic mode

FIG. 22. Eigenfunctions of the secondary instability modes and the derivatives of the basic flow for secondary instability on porous wall with homogeneous boundary conditions at Mach 4.5 when the primary amplitude is 1.0 and $\beta_2 = 2.0$. (a) fundamental mode; (b) subharmonic mode.

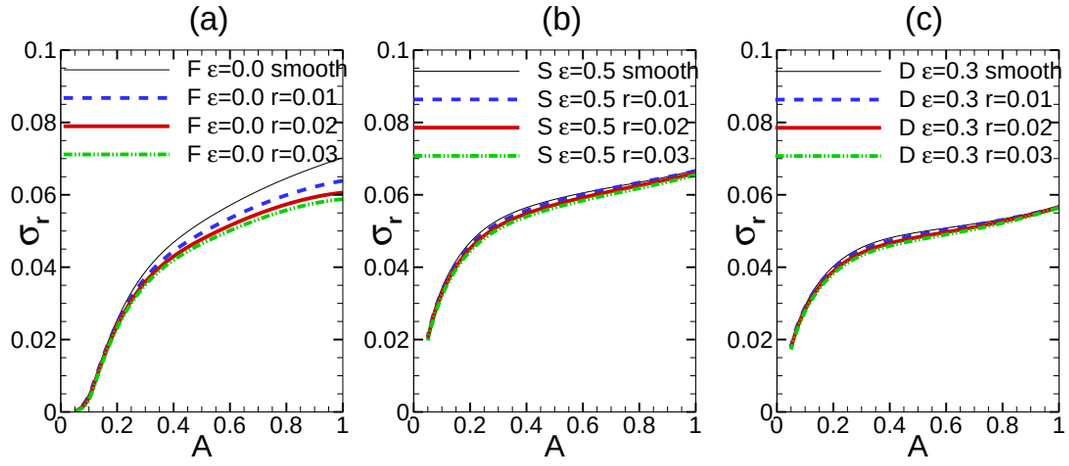

FIG. 23. Temporal growth rates in secondary instability against primary amplitude A on porous surface with various pore radii r at Mach 4.5 when $\beta_2 = 2.0$. (a) fundamental mode; (b) subharmonic mode; (c) detuned mode.

detuned mode against primary amplitude A, with $r = 0.01, 0.02, 0.03$, are plotted in Fig. 24(a), (b) and (c), respectively. As discussed above, when the spanwise wavenumber is large, the corresponding eigenfunctions in secondary instability move closer to the boundary layer edge. Because the primary disturbances are mainly changed near the wall due to the porous wall, the fundamental modes are influenced slightly. Therefore, at a larger spanwise wavenumber, the fundamental mode

is dominant. From the results in Fig. 24, the porous wall hardly affects the properties of secondary instability when the spanwise wavenumber is large. It is also important to note that the porosity coefficient has a similar effect on secondary instability with pore radius variations. The greater the porosity coefficient, the more stronger is suppression of the fundamental mode.

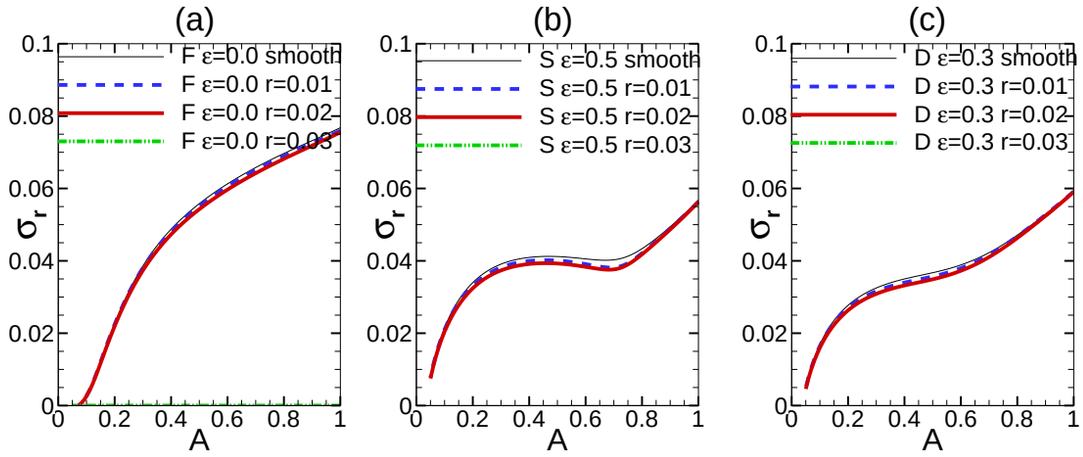

FIG. 24. Temporal growth rates in secondary instability against primary amplitude A on porous surface with various pore radii r at Mach 4.5 when $\beta_2 = 3.5$. (a) fundamental mode; (b) subharmonic mode; (c) detuned mode.

IV. CONCLUSIONS

This paper analyzed the secondary instability of Mack mode disturbances over porous surface in hypersonic boundary layers, using Fedorov et al.'s classical porous surface model. The secondary instability equations for a porous surface were derived based on Floquet theory. Contrasting results obtained on smooth wall and the porous wall at various conditions, the following conclusions are drawn:

(1). In hypersonic boundary layers, when the amplitude of the primary Mack mode is large, for almost all spanwise wavenumbers β_2, the fundamental modes always have a larger maximum growth rate than the subharmonic modes. The growth rates of the fundamental modes are proportional to the primary amplitude. This conclusion is reached for both smooth and porous walls. In other words, the primary amplitude plays a more crucial role in secondary instability, which is in agreement with the measured data of Chokani *et al.*[53]. Their experiment focused on the unstable Mack mode disturbances evolution, whereas our analysis has been based on a localised

analysis. However our key conclusions are similar to the experimental findings. With porous surfaces we find changes of primary disturbance shape play a more critical role in the secondary instability. On the smooth wall, the fundamental mode dominates the secondary instability when the primary amplitude is large and close to the saturated amplitude. Whereas since the porous surface significantly weakens the primary Mack mode, its amplitude is reduced and thus the presence of the dominant smooth wall fundamental mode was found to be completely absent. This conclusion proves that the present relation between secondary instability and primary amplitude of Mack mode disturbances is very important. Due to the decrease of the Mack mode amplitude in the presence of surface porosity, the subharmonic and fundamental resonances of the Mack mode observed on smooth surfaces can be significantly modified with appropriate porosity parameters.

(2). On the porous surface transition can be delayed, it occurs further downstream relative to the solid surface. The present analyses suggests that the eigenfunctions of fundamental modes are concentrated in the near-wall region and the eigenfunctions of subharmonic modes are mainly distributed near the edge of the boundary layer. Moreover, the mean shear is very important in the production of secondary instability modes. Fourier analysis indicates that over both smooth and porous surfaces, the stationary (0, 1) mode always has the largest amplitude in the spectrum of the fundamental modes.

(3). For the smooth wall, at the spanwise wavenumber β_2 corresponding to the maximum growth rate of the subharmonic mode, with increments of the primary disturbance amplitude the fundamental mode dominates when the primary amplitude is large i.e. ($O(1)$ defined by the peak value of primary temperature disturbances T_1^+). However, since the porous surface significantly affects the primary Mack mode disturbances near the wall, at the spanwise wavenumber corresponding to the maximum growth rate of the subharmonic mode, the fundamental mode is suppressed and does not surpass the subharmonic mode even though the primary amplitude is large. This conclusion holds even for small and medium spanwise wavenumbers. Furthermore, at a larger spanwise wavenumber the corresponding secondary instability eigenfunctions move towards the boundary layer edge. Since primary disturbances are mainly altered near the wall by the porous surface, the fundamental modes are only slightly influenced. Hence, at a larger spanwise wavenumber, the secondary instabilities for the porous wall hardly change relative to the smooth wall. At this condition, the fundamental mode will surpass the subharmonic mode and dominate the secondary instability when the primary amplitude is large.

(4). Furthermore, as the pore radius increases, the greater the reduction in the fundamental

mode growth occurs. The same rule applies to porosity coefficient. If appropriate porosity parameters are specified, the primary amplitude of the Mack mode can be weakened so that the fundamental mode may be suppressed. When the fundamental mode is weakened by the porous surface, the porosity is able to increase the relative role of the subharmonic resonance stages of the weakly-nonlinear development of the second Mack mode instability[53]. As a result, unlike the solid surface, there are no strongly preferred interaction modes of secondary instability over the porous surface[53]. It depends on the specific porosity parameters and flow conditions.

ACKNOWLEDGMENTS

This article was supported by the National Key Research and Development Program of China (Grant No. 2016YFA0401200) and the International Postdoctoral Exchange Fellowship Program (Grant No.20180018).

REFERENCES

[1]H. F. Fasel, A. Thumm, and H. Bestek, "Direct numerical simulation of transition in supersonic boundary layers: oblique breakdown," in *Fluids Engineering Conference* (Publ by ASME, 1993) pp. 77–92.

[2]A. V. Fedorov, N. D. Malmuth, A. Rasheed, and H. G. Hornung, "Stabilization of hypersonic boundary layers by porous coatings," AIAA Journal **39**, 605–610 (2001).

[3]T. Herbert, "Secondary instability of boundary layers," Annual Review of Fluid Mechanics **20**, 487–526 (1988).

[4]P. J. Schmid and D. S. Henningson, *Stability and transition in shear flows*, Vol. 142 (Springer Science & Business Media, 2012).

[5]P. S. Klebanoff, K. Tidstrom, and L. Sargent, "The three-dimensional nature of boundary-layer instability," Journal of Fluid Mechanics **12**, 1–34 (1962).

[6]Y. S. Kachanov, V. Kozlov, and V. Y. Levchenko, "Nonlinear development of a wave in a boundary layer," Fluid Dynamics **12**, 383–390 (1977).

[7]Y. S. Kachanov and V. Y. Levchenko, "The resonant interaction of disturbances at laminar-turbulent transition in a boundary layer," Journal of Fluid Mechanics **138**, 209–247 (1984).

[8]T. Corke and R. Mangano, "Resonant growth of three-dimensional modes in trnsitioning blasius boundary layers," Journal of Fluid Mechanics **209**, 93–150 (1989).

[9]F. Li, M. Choudhari, C.-L. Chang, and J. White, "Secondary instability of second mode disturbances in hypersonic boundary layers," NASA Tech. Rep. , NF1676L–13407 (2012).

[10]X. Wu, "Nonlinear theories for shear flow instabilities: Physical insights and practical implications," Annual Review of Fluid Mechanics **51**, 451–485 (2019).

[11]W. S. Saric and A. S. W. Thomas, "Experiments on the subharmonic route to turbulence in boundary layers," in *Turbulence and chaotic phenomena in fluids* (1984) pp. 117–122.

[12]Y. S. Kachanov, "Physical mechanisms of laminar-boundary-layer transition," Annu. Rev. Fluid Mech. **26**, 411–482 (1994).

[13]A. D. Kosinov and A. A. Maslov, "Development of artificially excited disturbances in supersonic boundary layer," in *Procedia IUTAM.* (Springer, 1985) pp. 601–606.

[14]A. D. Kosinov, A. A. Maslov, and S. G. Shevelkov, "Experiments on the stability of supersonic laminar boundary layers," J. Fluid Mech. **219**, 621–633 (1990).

[15]A. D. Kosinov, N. V. Semionov, and S. G. Shevelkov, "Investigation of supersonic boundary layer stability and transition using controlled disturbances," Methods of Aerophysical Research (ed. AM Kharitonov) **2**, 159–166 (1994).

[16]A. D. Kosinov, N. V. Semionov, S. G. Shevel'kov, and O. I. Zinin, "Experiments on the nonlinear instability of supersonic boundary layers," in *Nonlinear Instability of Nonparallel Flows* (Springer, 1994) pp. 196–205.

[17]A. D. Kosinov, A. A. Maslov, and N. V. Semionov, "An experimental study of generation of unstable disturbances on the leading edge of a plate at M= 2," J. Appl. Mech. Tech. Phys. **38**, 45–51 (1997).

[18]Y. G. Ermolaev, A. D. Kosinov, and N. V. Semionov, "Experimental investigation of laminar-turbulent transition process in supersonic boundary layer using controlled disturbances," in *Procedia IUTAM.* (Springer, 1996) pp. 17–26.

[19]G. Kolosov, A. Kosinov, Y. G. Yermolaev, and N. Semionov, "To nonlinear disturbance interactions in 3d supersonic boundary-layer," in *AIP Conference Proceedings*, Vol. 1770 (AIP Publishing LLC, 2016) p. 030052.

[20]A. D. Kosinov and A. Tumin, "Resonance interaction of wave trains in supersonic boundary layer," in *Procedia IUTAM.* (Springer, 1996) pp. 379–388.

[21]C. Mayer and H. Fasel, "Investigation of asymmetric subharmonic resonance in a supersonic

boundary layer at Mach 2 using DNS," in *AIAA Paper* (2008) pp. 2008–0591.

[22]A. Fezer and M. Kloker, "Spatial direct numerical simulation of transition phenomena in supersonic flat-plate boundary layers," in *Procedia IUTAM.* (Springer, 2000) pp. 415–420.

[23]A. D. Craik, "Non-linear resonant instability in boundary layers," J. Fluid Mech. **50**, 393–413 (1971).

[24]A. G. Volodin and M. B. ZelMan, "Three-wave resonance interaction of disturbances in a boundary layer," Fluid Dyn. **13**, 698–703 (1978).

[25]A. G. Volodin and M. B. Zelman, "The nature of differences in some forms of transition in the boundary layer," AIAA J. **19**, 950–952 (1981).

[26]F. Smith and P. Stewart, "The resonant-triad nonlinear interaction in boundary-layer transition," Journal of Fluid Mechanics **179**, 227–252 (1987).

[27]M. Zelman and I. Maslennikova, "Tollmien-schlichting-wave resonant mechanism for subharmonic-type transition," Journal of Fluid Mechanics **252**, 449–478 (1993).

[28]M. Goldstein and S. S. Lee, "Fully coupled resonant-triad interaction in an adverse-pressure-gradient boundary layer," Journal of Fluid Mechanics **245**, 523–551 (1992).

[29]J. Masad and A. Nayfeh, "Subharmonic instability of compressible boundary layers," Physics of Fluids A: Fluid Dynamics **2**, 1380–1392 (1990).

[30]J. Masad and A. Nayfeh, "Effects of suction and wall shaping on the fundamental parametric resonance in boundary layers," Physics of Fluids A: Fluid Dynamics **4**, 963–974 (1992).

[31]N. M. El-Hady, "Secondary instability of high-speed flows and the influence of wall cooling and suction," Physics of Fluids A: Fluid Dynamics **4**, 727–743 (1992).

[32]L. L. Ng and G. Erlebacher, "Secondary instabilities in compressible boundary layers," Physics of Fluids A: Fluid Dynamics **4**, 710–726 (1992).

[33]D. Bountin, A. Shiplyuk, and A. Maslov, "Evolution of nonlinear processes in a hypersonic boundary layer on a sharp cone," Journal of Fluid Mechanics **611**, 427–442 (2008).

[34]B. Wheaton, T. Juliano, D. Berridge, A. Chou, P. Gilbert, K. Casper, L. Steen, S. Schneider, and H. Johnson, "Instability and transition measurements in the Mach-6 quiet tunnel," in *39th AIAA Fluid Dynamics Conference* (2009) p. 3559.

[35]S. P. Schneider, "Developing mechanism-based methods for estimating hypersonic boundary-layer transition in flight: the role of quiet tunnels," Progress in Aerospace Sciences **72**, 17–29 (2015).

[36]B. C. Chynoweth, S. P. Schneider, C. Hader, H. Fasel, A. Batista, J. Kuehl, T. J. Juliano, and

B. M. Wheaton, "History and progress of boundary-layer transition on a Mach-6 flared cone," Journal of Spacecraft and Rockets **56**, 333–346 (2019).

[37]J. Sivasubramanian and H. Fasel, "Nonlinear stages of transition and breakdown in a boundary layer on a sharp cone at Mach 6," in *50th AIAA Aerospace Sciences Meeting including the New Horizons Forum and Aerospace Exposition* (2012) p. 87.

[38]J. Sivasubramanian and H. F. Fasel, "Numerical investigation of the development of three-dimensional wavepackets in a sharp cone boundary layer at Mach 6," Journal of Fluid Mechanics **756**, 600–649 (2014).

[39]X. Chen, Y. Zhu, and C. Lee, "Interactions between second mode and low-frequency waves in a hypersonic boundary layer," Journal of Fluid Mechanics **820**, 693–735 (2017).

[40]Q. Tang, Y. Zhu, X. Chen, and C. Lee, "Development of second-mode instability in a Mach 6 flat plate boundary layer with two-dimensional roughness," Physics of Fluids **27**, 064105 (2015).

[41]J. Sivasubramanian and H. F. Fasel, "Direct numerical simulation of transition in a sharp cone boundary layer at Mach 6: fundamental breakdown," Journal of Fluid Mechanics **768**, 175–218 (2015).

[42]C. Hader and H. F. Fasel, "Laminar-turbulent transition on a flared cone at Mach 6," in *46th AIAA Fluid Dynamics Conference* (2016) p. 3344.

[43]C. Hader and H. F. Fasel, "Fundamental resonance breakdown for a flared cone at Mach 6," in *55th AIAA Aerospace Sciences Meeting* (2017) p. 0765.

[44]C. Hader and H. F. Fasel, "Direct numerical simulations of hypersonic boundary-layer transition for a flared cone: fundamental breakdown," Journal of Fluid Mechanics **869**, 341–384 (2019).

[45]J. Liu and C. Zhang, "The fundamental secondary instability of the primary mack mode in hypersonic boundary layers on flat plates," Advances in Applied Mathematics and Mechanics **11**, 559–570 (2019).

[46]A. V. Fedorov, V. F. Kozlov, A. N. Shiplyuk, A. A. Maslov, and N. D. Malmuth, "Stability of hypersonic boundary layer on porous wall with regular microstructure," AIAA Journal **44**, 1866–1871 (2006).

[47]I. Egorov, A. Fedorov, and V. Soudakov, "Receptivity of a hypersonic boundary layer over a flat plate with a porous coating," Journal of Fluid Mechanics **601**, 165–187 (2008).

[48]S. Gaponov and B. Smorodsky, "Linear stability of supersonic boundary layer on porous surface," Recent Advances in Fluid Mechanics and Aerodynamics, Moscow , 68–73 (2009).

[49]V. Wartemann, H. Lüdeke, and N. Sandham, "Stability analysis of hypersonic boundary layer

flow over microporous surfaces," in *16th AIAA/DLR/DGLR International Space Planes and Hypersonic Systems and Technologies Conference* (2009) p. 7202.

[50]R. Zhao, T. Liu, C. Wen, J. Zhu, and L. Cheng, "Theoretical modeling and optimization of porous coating for hypersonic laminar flow control," AIAA Journal **56**, 2942–2946 (2018).

[51]R. Zhao, T. Liu, C.-y. Wen, J. Zhu, and L. Cheng, "Impedance-near-zero acoustic metasurface for hypersonic boundary-layer flow stabilization," Physical Review Applied **11**, 044015 (2019).

[52]X. Wang, "Stabilization of a hypersonic boundary layer using regular porous coating," in *2018 AIAA Aerospace Sciences Meeting* (2018) p. 2088.

[53]N. Chokani, D. A. Bountin, A. N. Shiplyuk, and A. A. Maslov, "Nonlinear aspects of hypersonic boundary-layer stability on a porous surface," AIAA Journal **43**, 149–155 (2005).

[54]C.-L. Chang, "The langley stability and transition analysis codes (lastrac): Lst, linear & nonlinear pse for 2d, axisymmetric, and infinite swept wing boundary layers," in *41st Aerospace Sciences Meeting and Exhibit* (2003) p. 974.

[55]C.-L. Chang, "Lastrac. 3d: Transition prediction in 3d boundary layers," in *34th AIAA Fluid Dynamics Conference and Exhibit* (2004) p. 2542.

[56]R. B. Lehoucq, D. C. Sorensen, and C. Yang, *ARPACK users' guide: solution of large-scale eigenvalue problems with implicitly restarted Arnoldi methods*, Vol. 6 (Siam, 1998).

[57]M. R. Malik, "Numerical methods for hypersonic boundary layer stability," Journal of Computational Physics **86**, 376–413 (1990).

[58]M. R. Malik, F. Li, M. M. Choudhari, and C.-L. Chang, "Secondary instability of crossflow vortices and swept-wing boundary-layer transition," Journal of Fluid Mechanics **399**, 85–115 (1999).

[59]M. Högberg and D. Henningson, "Secondary instability of cross-flow vortices in falkner–skan–cooke boundary layers," Journal of Fluid Mechanics **368**, 339–357 (1998).

[60]W. Koch, F. P. Bertolotti, A. Stolte, and S. Hein, "Nonlinear equilibrium solutions in a three-dimensional boundary layer and their secondary instability," Journal of Fluid Mechanics **406**, 131–174 (2000).

[61]Y. Zhang and J. Luo, "Application of arnoldi method to boundary layer instability," Chinese Physics B **24**, 124701 (2015).

[62]J. Liu, S. Zhang, and S. Fu, "Linear spatial instability analysis in 3d boundary layers using plane-marching 3d-lpse," Applied Mathematics and Mechanics **37**, 1013–1030 (2016).

[63]G. Xu, J. Chen, G. Liu, S. Dong, and S. Fu, "The secondary instabilities of stationary cross-flow

vortices in a mach 6 swept wing flow," Journal of Fluid Mechanics **873**, 914–941 (2019).

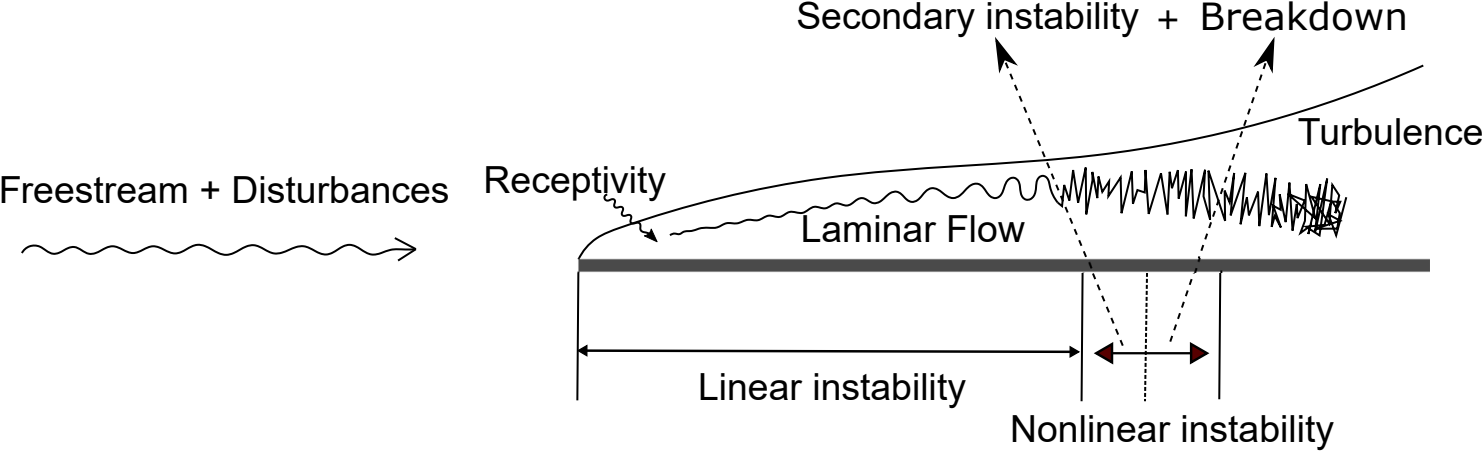
Secondary instability + Breakdown
Turbulence
Freestream + Disturbances
Receptivity
Laminar Flow
Linear instability
Nonlinear instability

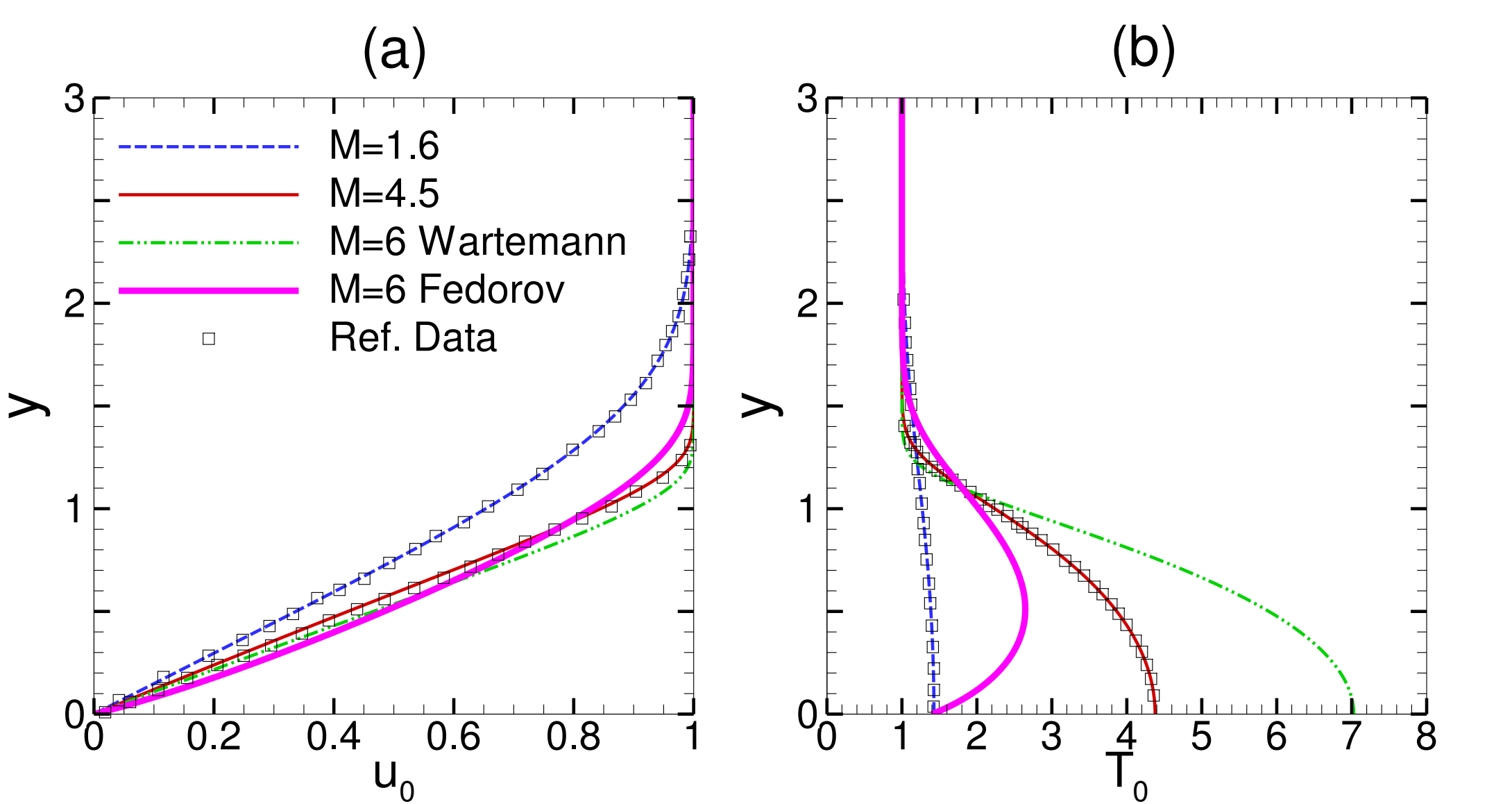
(a)
(b)
M=1.6
M=4.5
M=6 Wartemann
M=6 Fedorov
Ref. Data
y
u_0
T_0
0
0.2
0.4
0.6
0.8
1
2
3
4
5
6
7
8

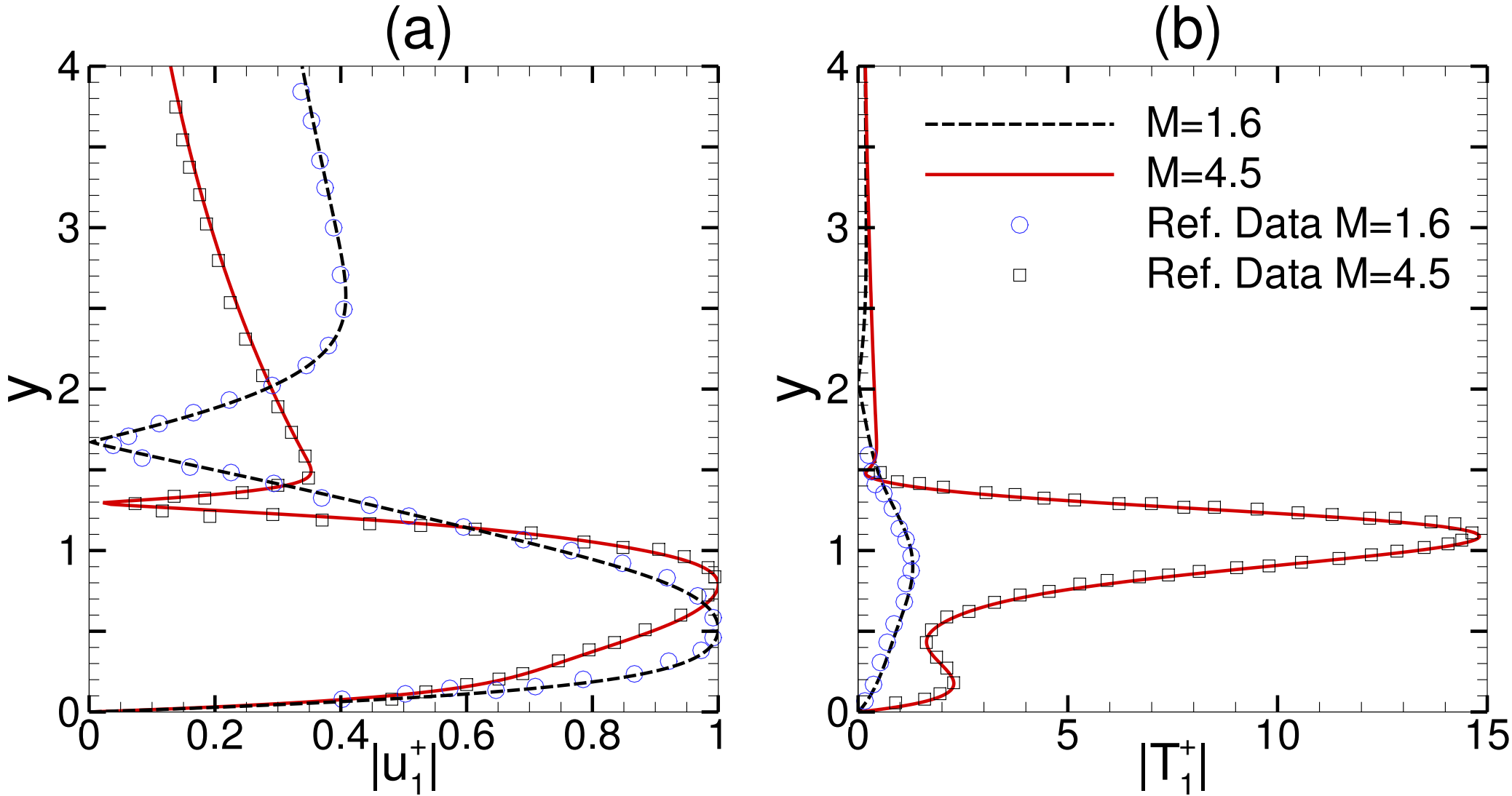
(a)
(b)
y
$|u_1^+|$
$|T_1^+|$
M=1.6
M=4.5
Ref. Data M=1.6
Ref. Data M=4.5
0
1
2
3
4
0.2
0.4
0.6
0.8
5
10
15

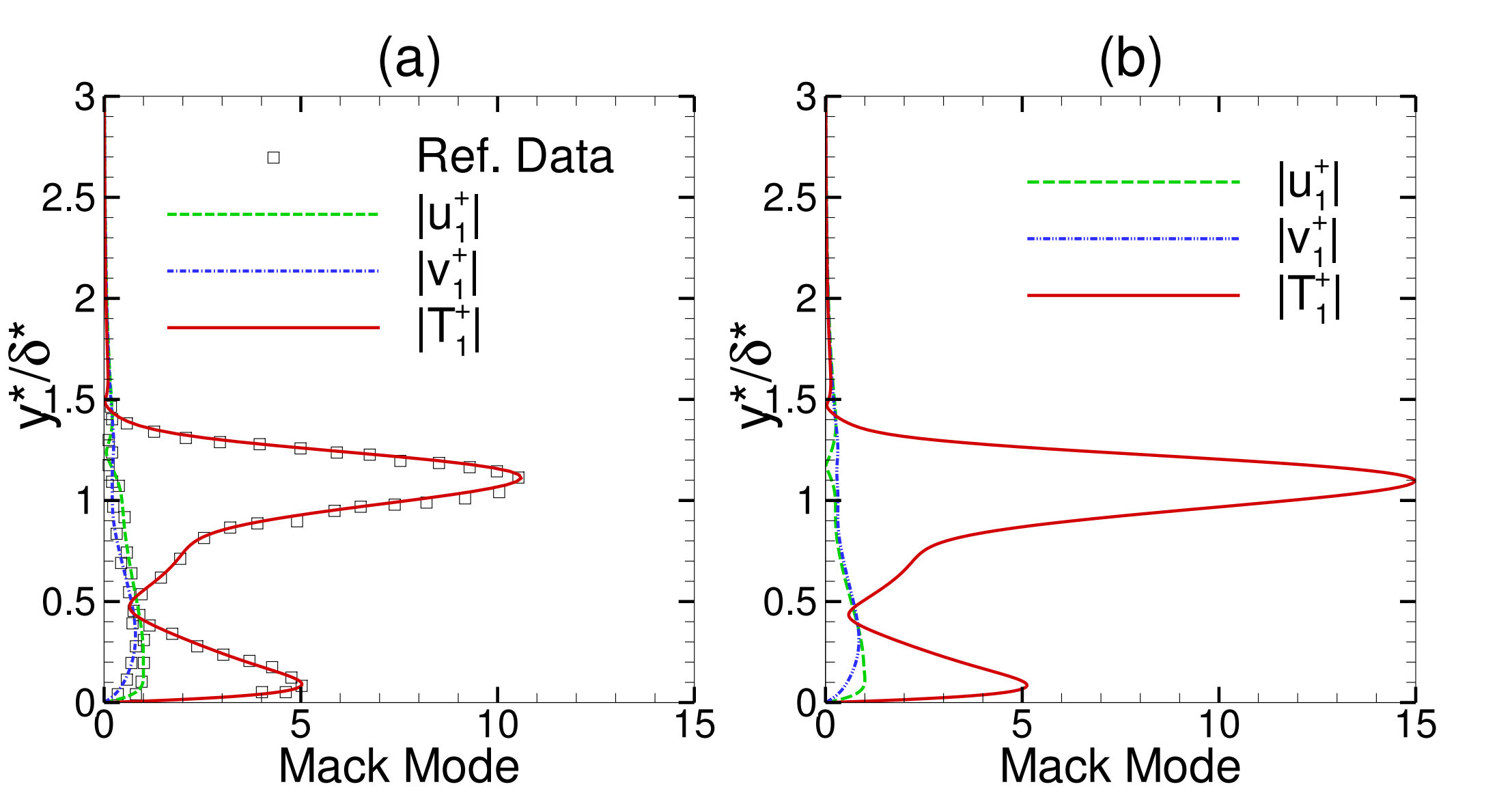
(a)
(b)
Ref. Data
$|u_1^+|$
$|v_1^+|$
$|T_1^+|$
y^*/δ^*
Mack Mode
0
0.5
1
1.5
2
2.5
3
5
10
15

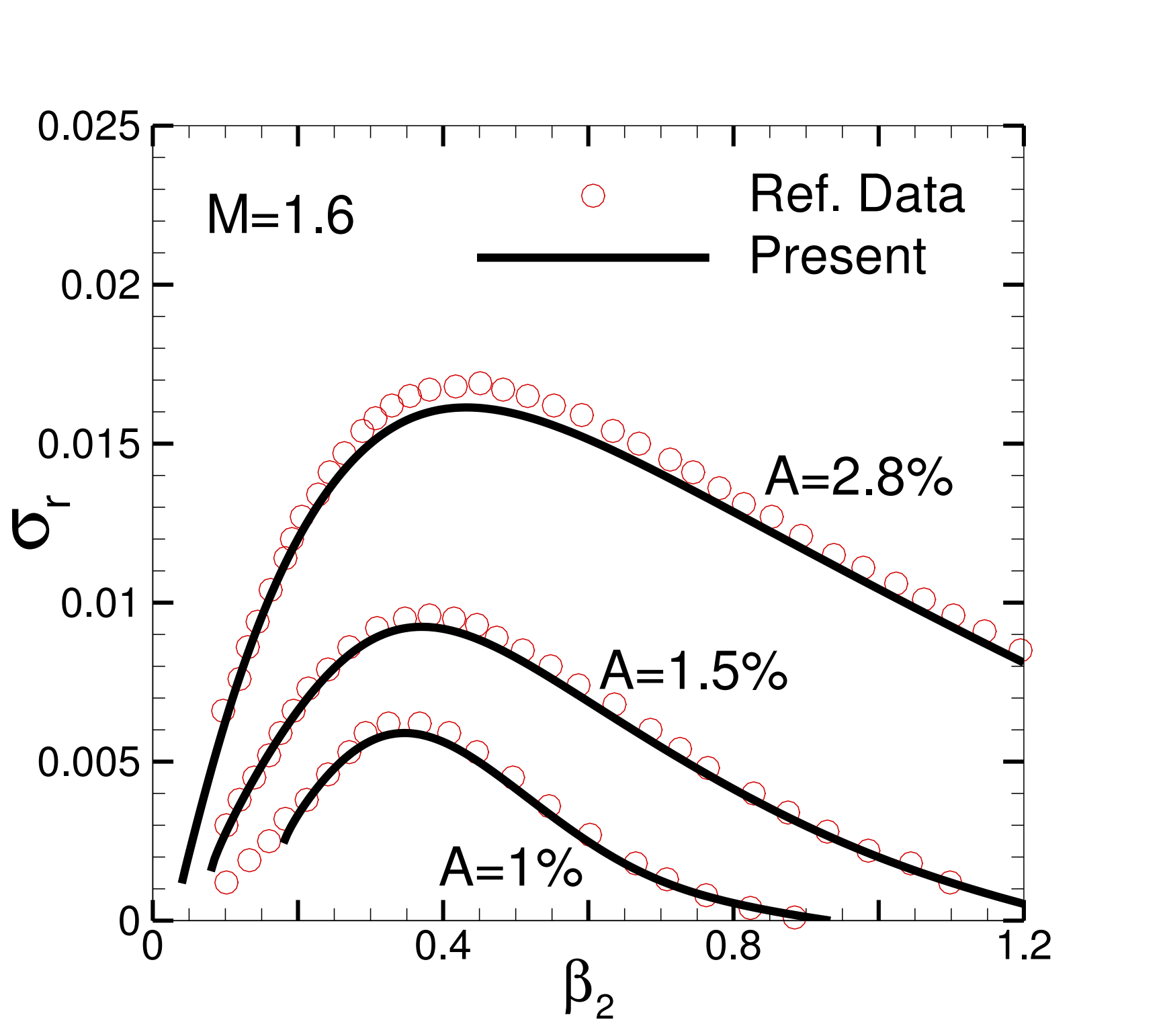
M=1.6
Ref. Data
Present
A=2.8%
A=1.5%
A=1%
σ_r
β_2
0.025
0.02
0.015
0.01
0.005
0
0
0.4
0.8
1.2

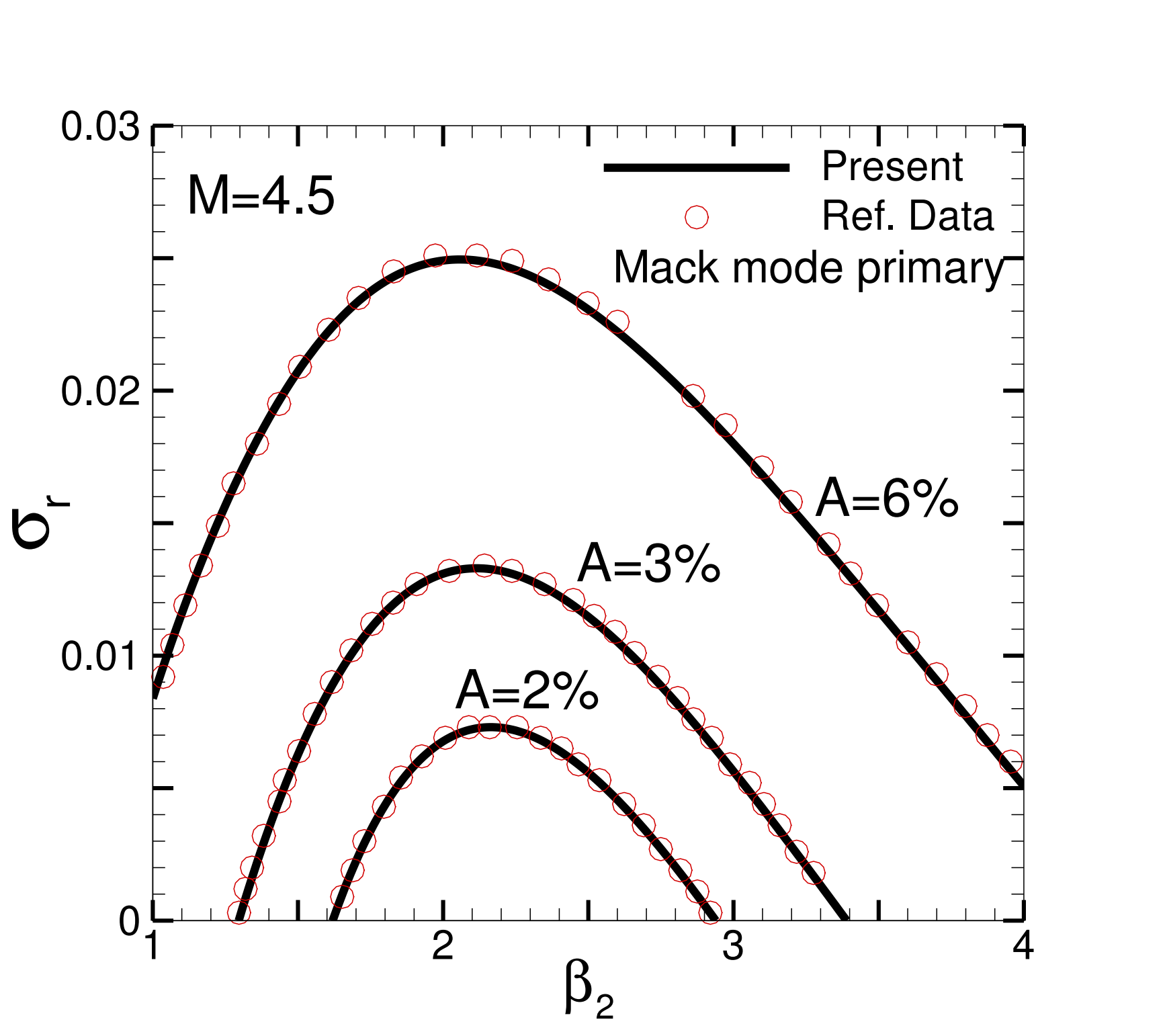
M=4.5
Present
Ref. Data
Mack mode primary
A=6%
A=3%
A=2%
σ_r
β_2
0.03
0.02
0.01
0
1
2
3
4

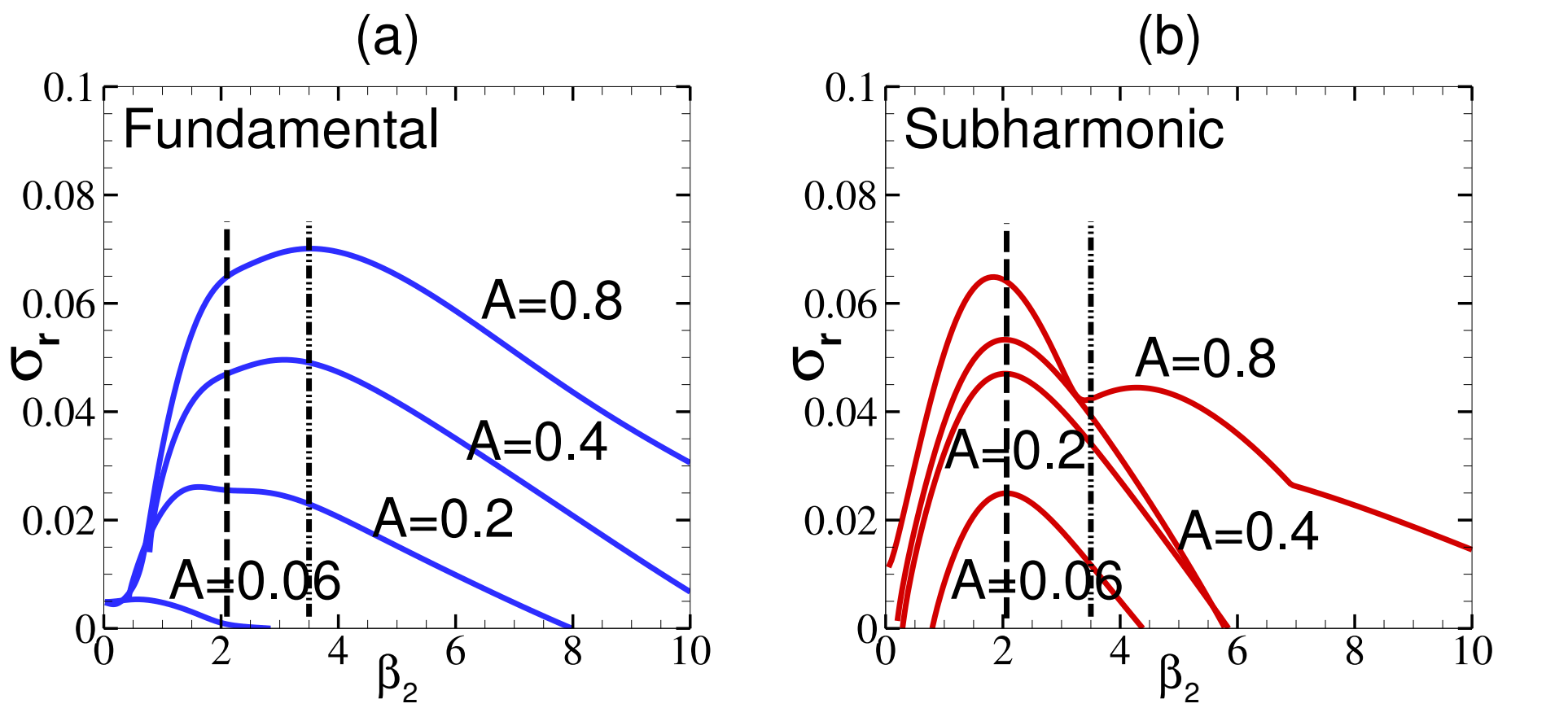
(a)
Fundamental
A=0.8
A=0.4
A=0.2
A=0.06
σ_r
β_2
0.1
0.08
0.06
0.04
0.02
0
0
2
4
6
8
10
(b)
Subharmonic
A=0.8
A=0.2
A=0.4
A=0.06
σ_r
β_2

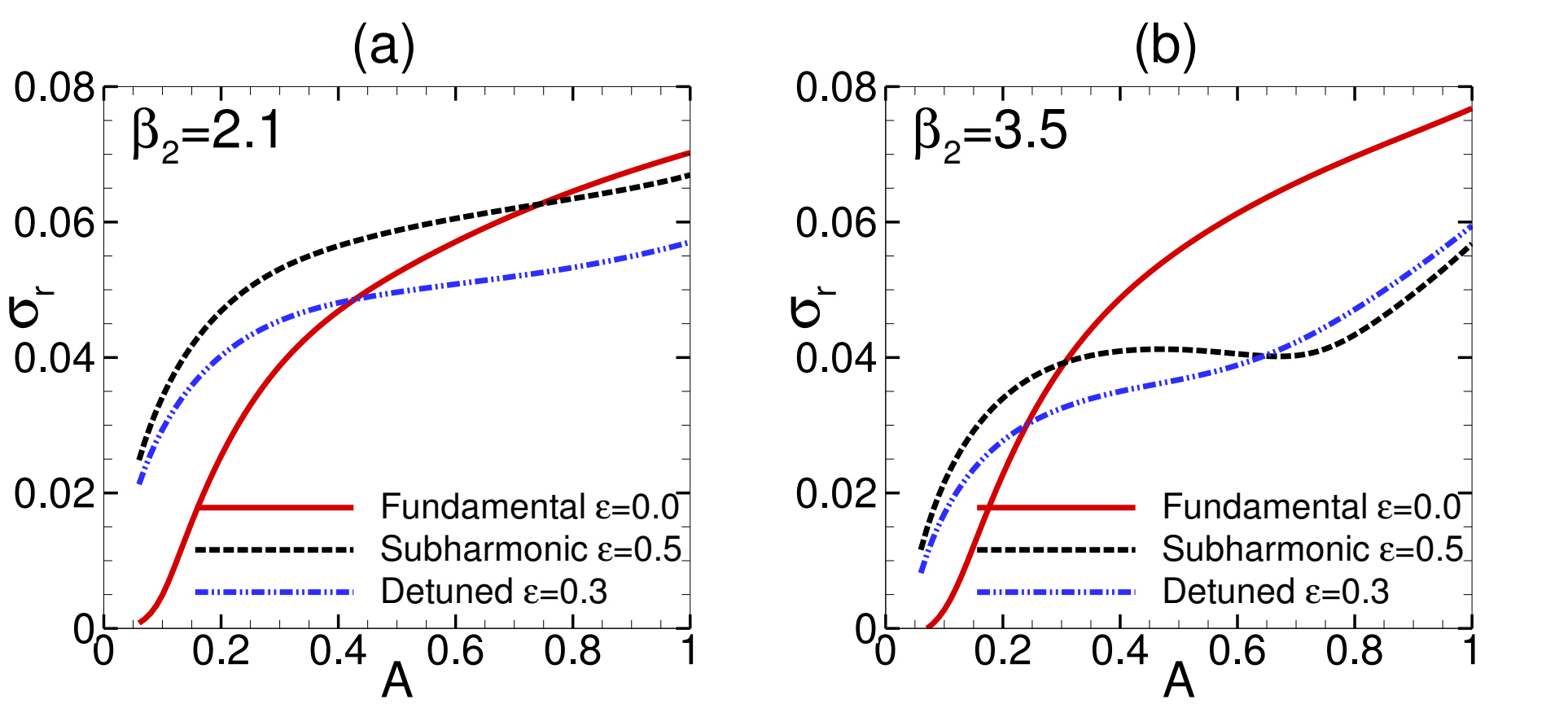
(a)
β2=2.1
σr
A
0.08
0.06
0.04
0.02
0
0.2
0.4
0.6
0.8
1
Fundamental ε=0.0
Subharmonic ε=0.5
Detuned ε=0.3
(b)
β2=3.5
σr
A
0.08
0.06
0.04
0.02
0
0.2
0.4
0.6
0.8
1
Fundamental ε=0.0
Subharmonic ε=0.5
Detuned ε=0.3

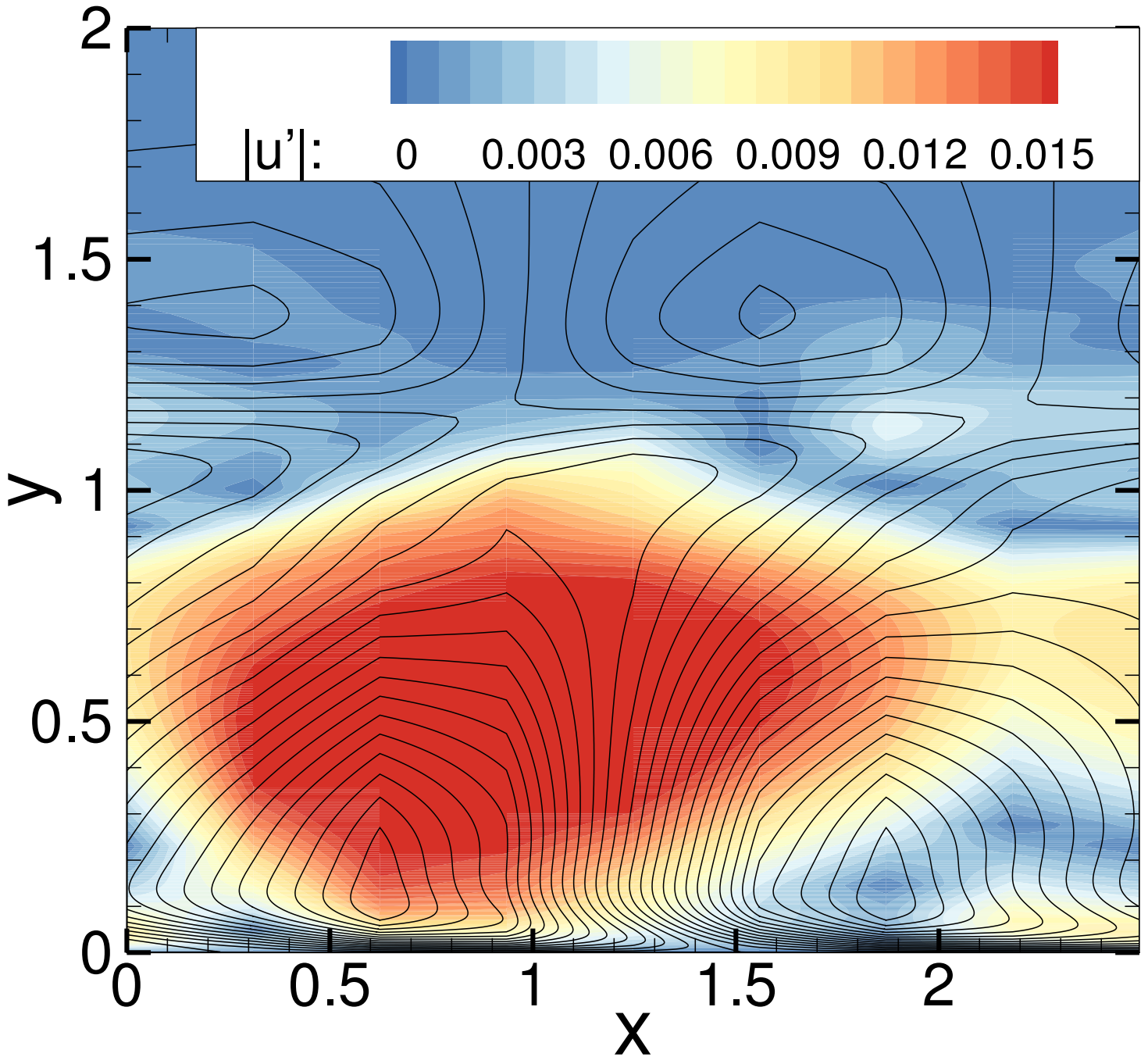
|u'|:
0
0.003
0.006
0.009
0.012
0.015
2
1.5
1
0.5
0
y
0
0.5
1
1.5
2
x

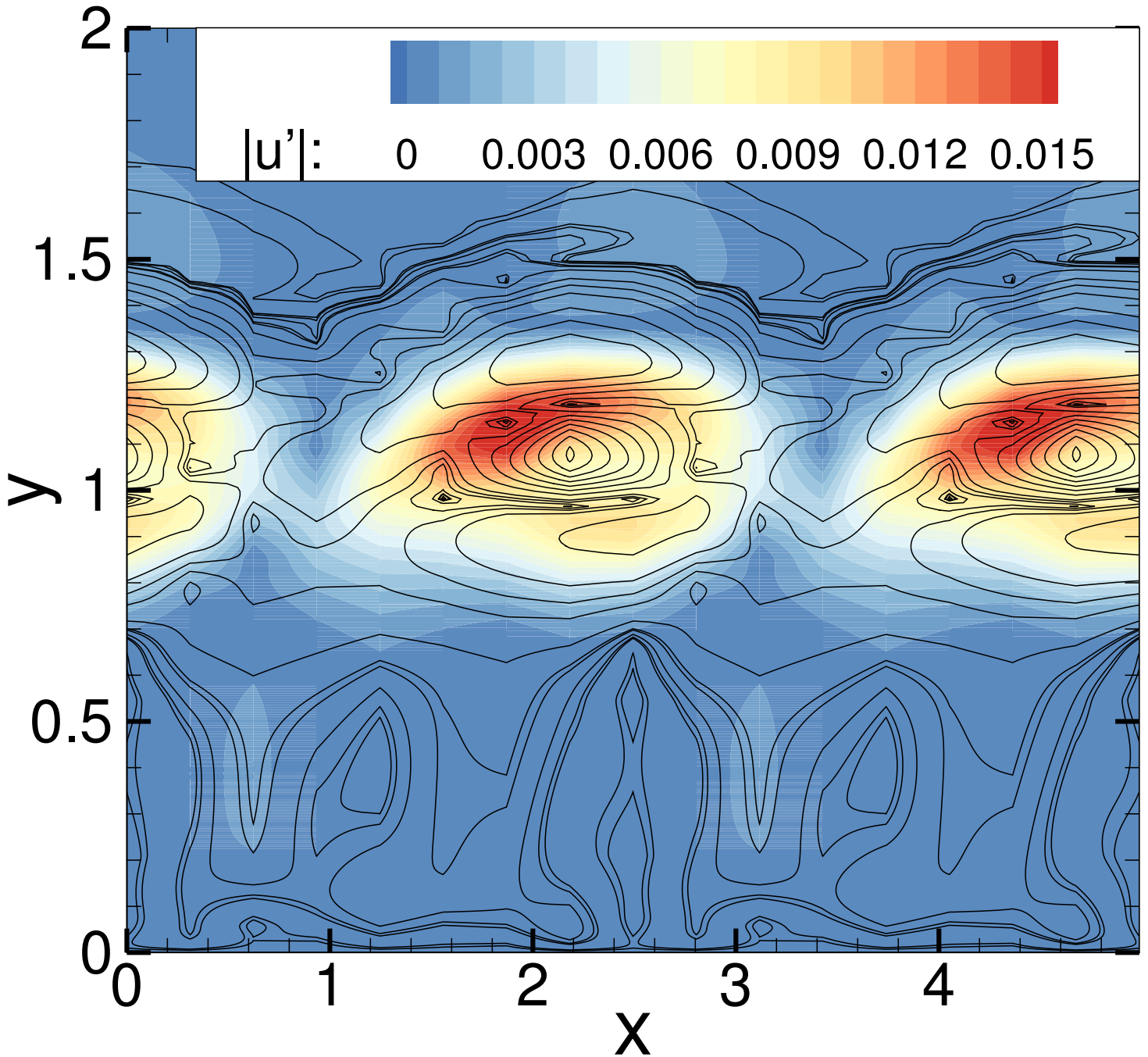
|u'|:
0
0.003
0.006
0.009
0.012
0.015
2
1.5
1
0.5
0
y
0
1
2
3
4
x

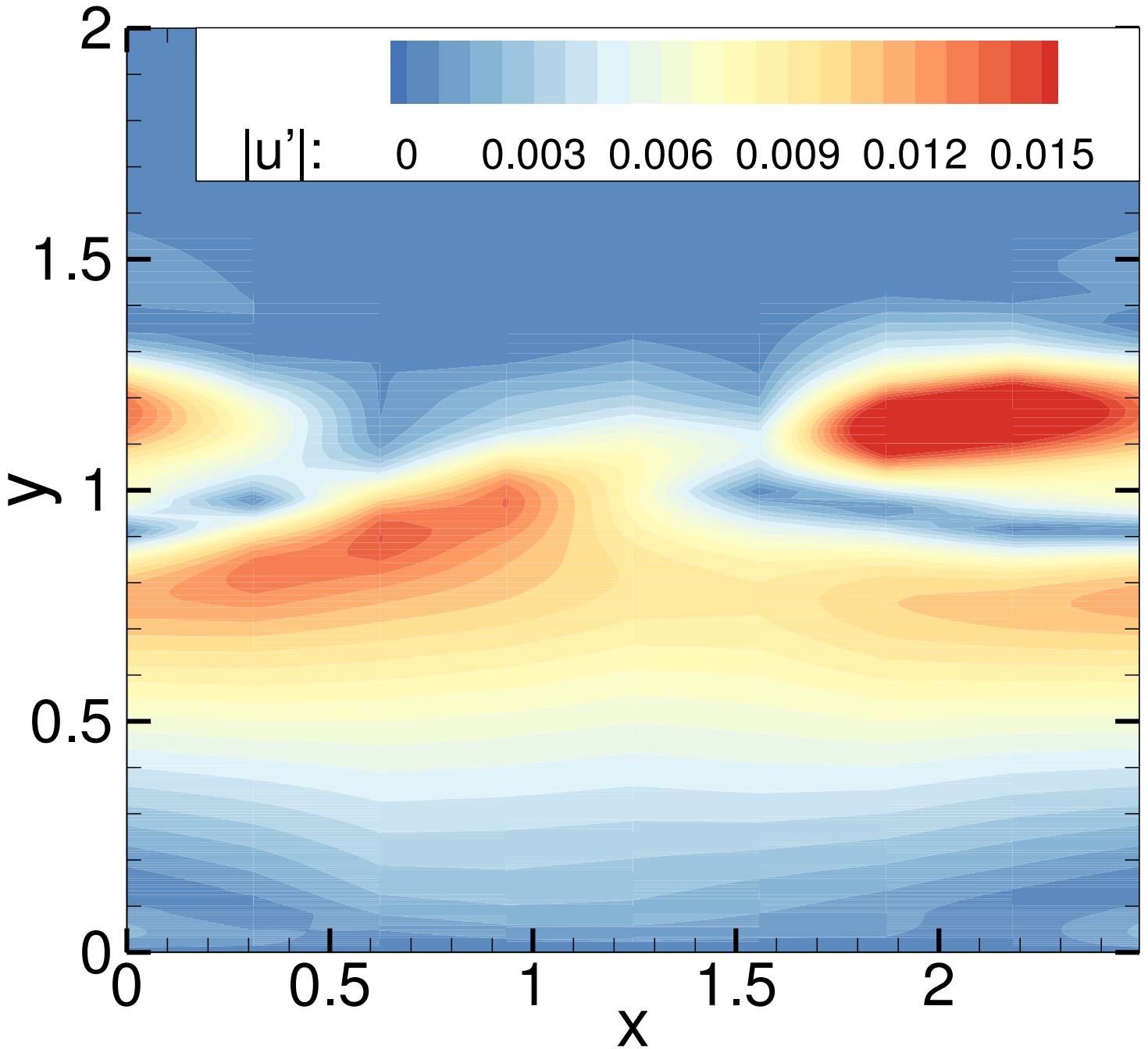
|u'|:
0
0.003
0.006
0.009
0.012
0.015
2
1.5
1
0.5
0
y
0
0.5
1
1.5
2
x

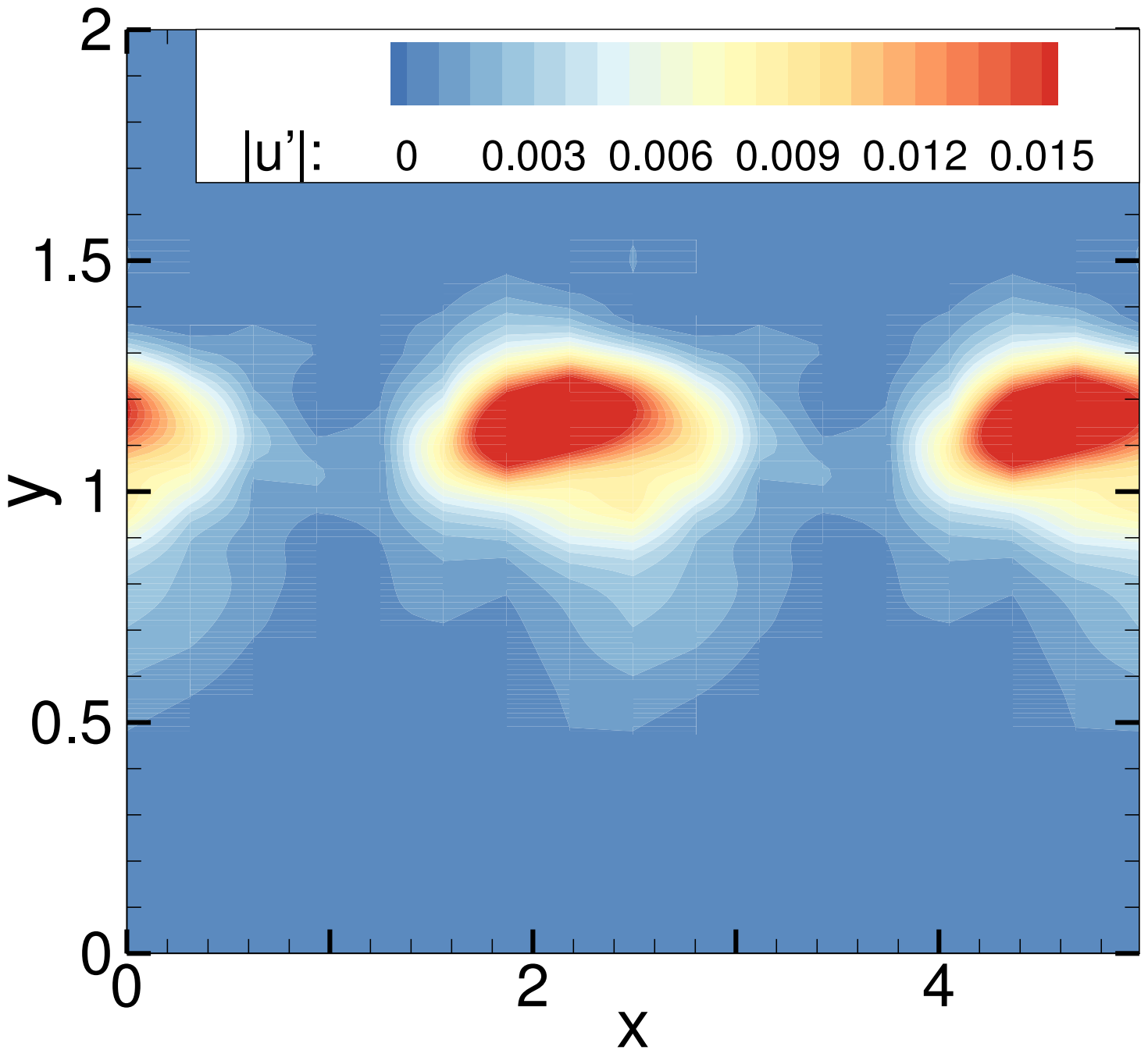
|u'|:
0
0.003
0.006
0.009
0.012
0.015
2
1.5
1
0.5
0
y
0
2
4
x

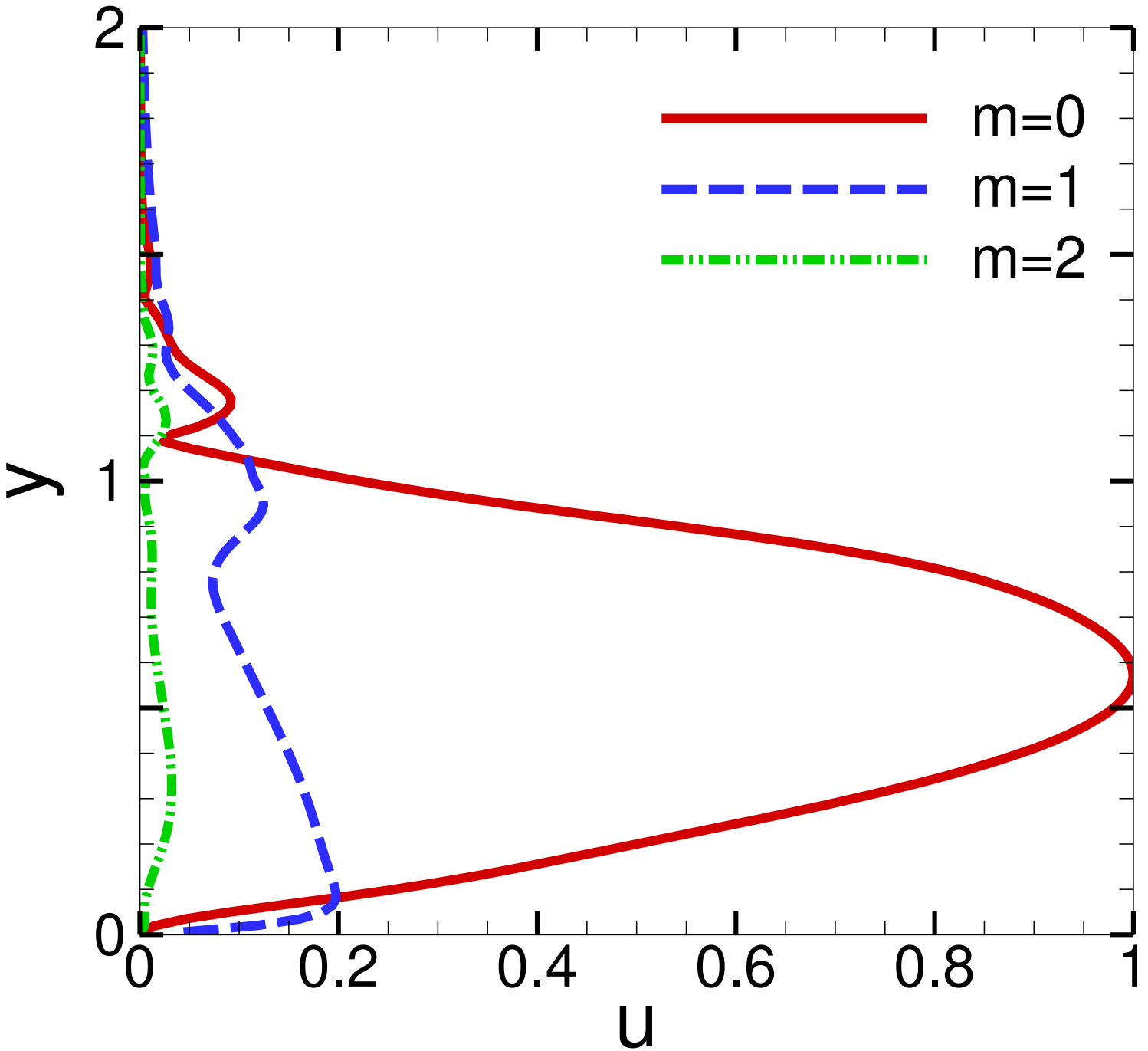
m=0
m=1
m=2
y
u
0
1
2
0
0.2
0.4
0.6
0.8
1

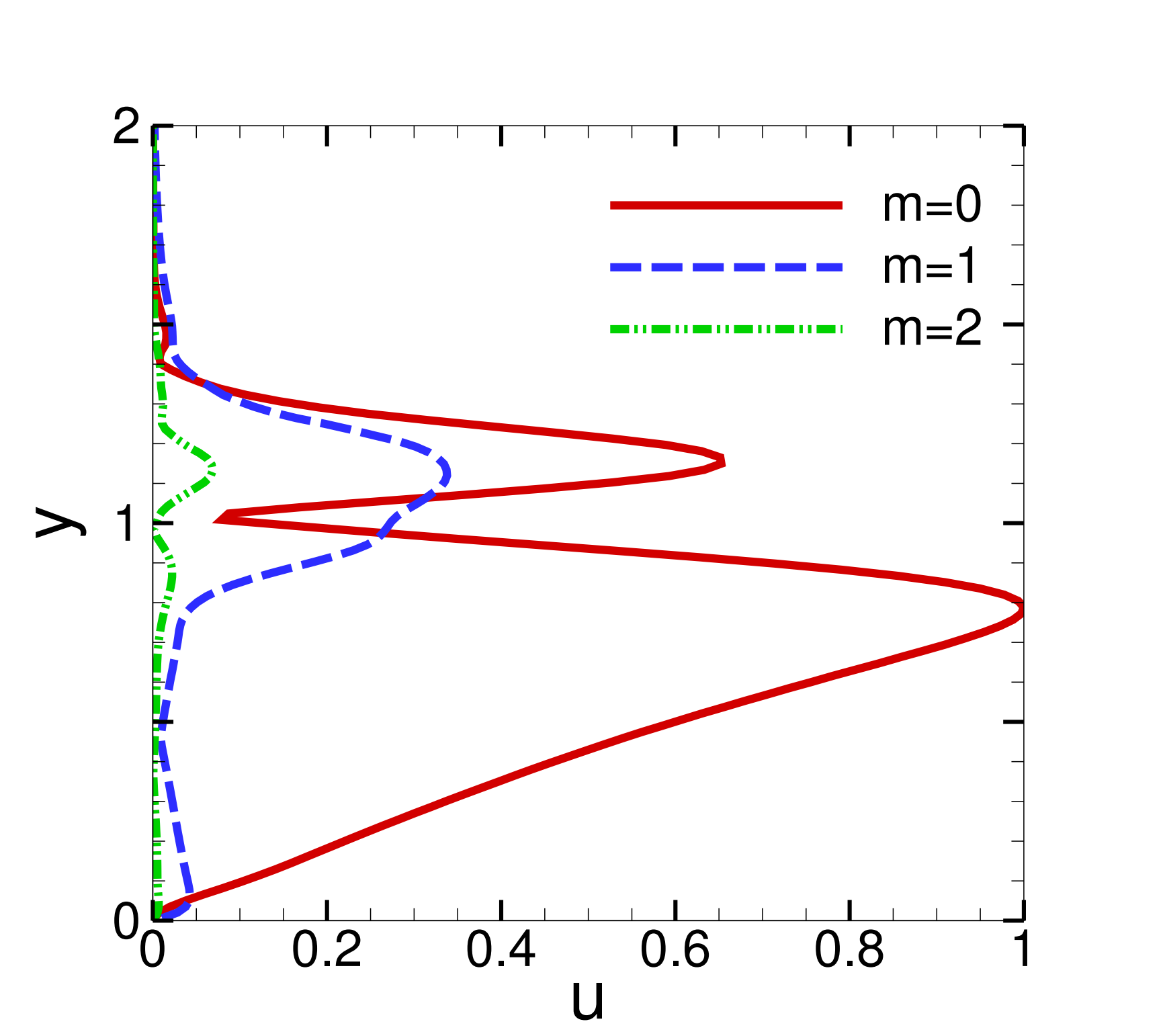
m=0
m=1
m=2
y
u
0
1
2
0
0.2
0.4
0.6
0.8
1

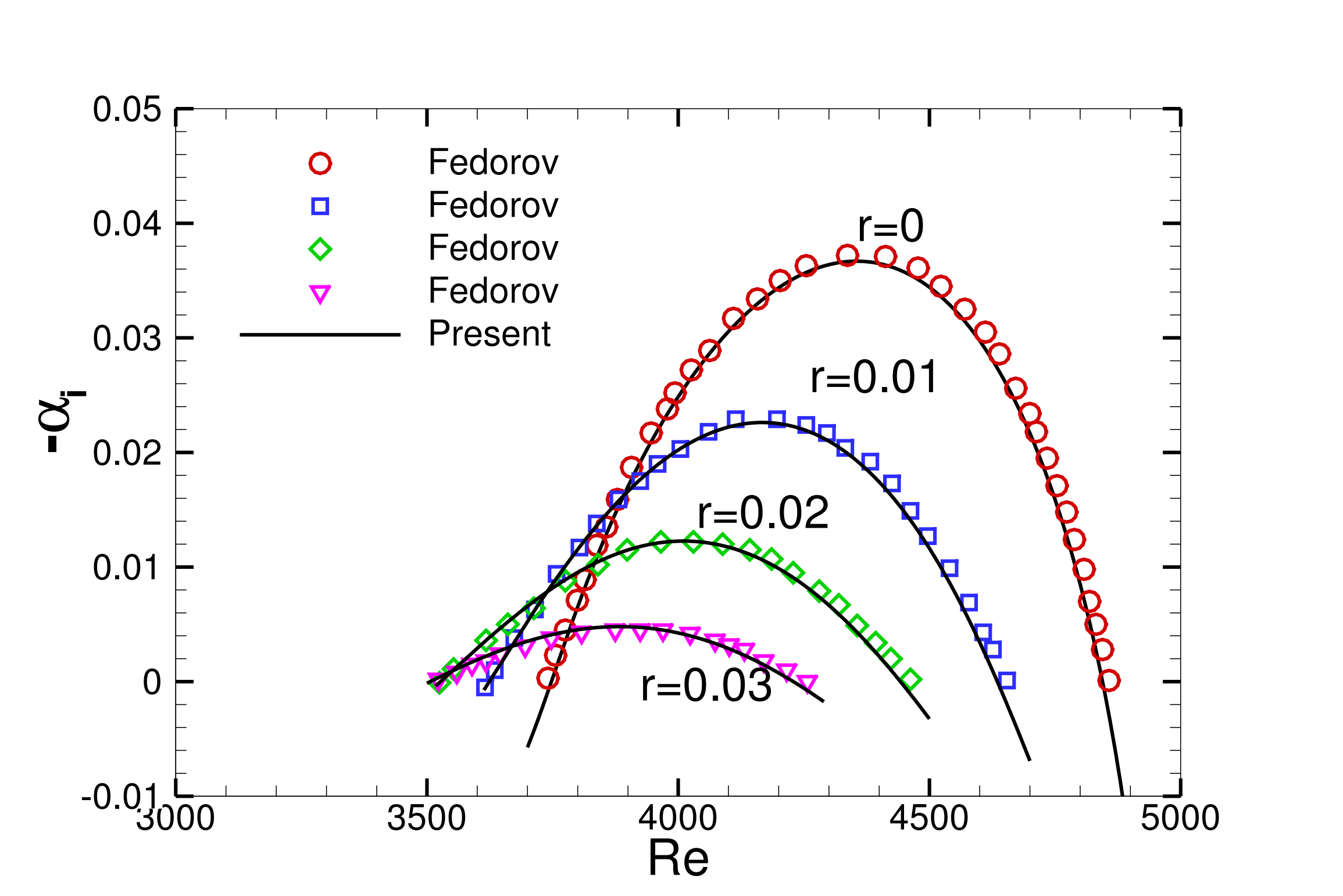
0.05
0.04
0.03
0.02
0.01
0
-0.01
-α_i
3000
3500
4000
4500
5000
Re
Fedorov
Fedorov
Fedorov
Fedorov
Present
r=0
r=0.01
r=0.02
r=0.03

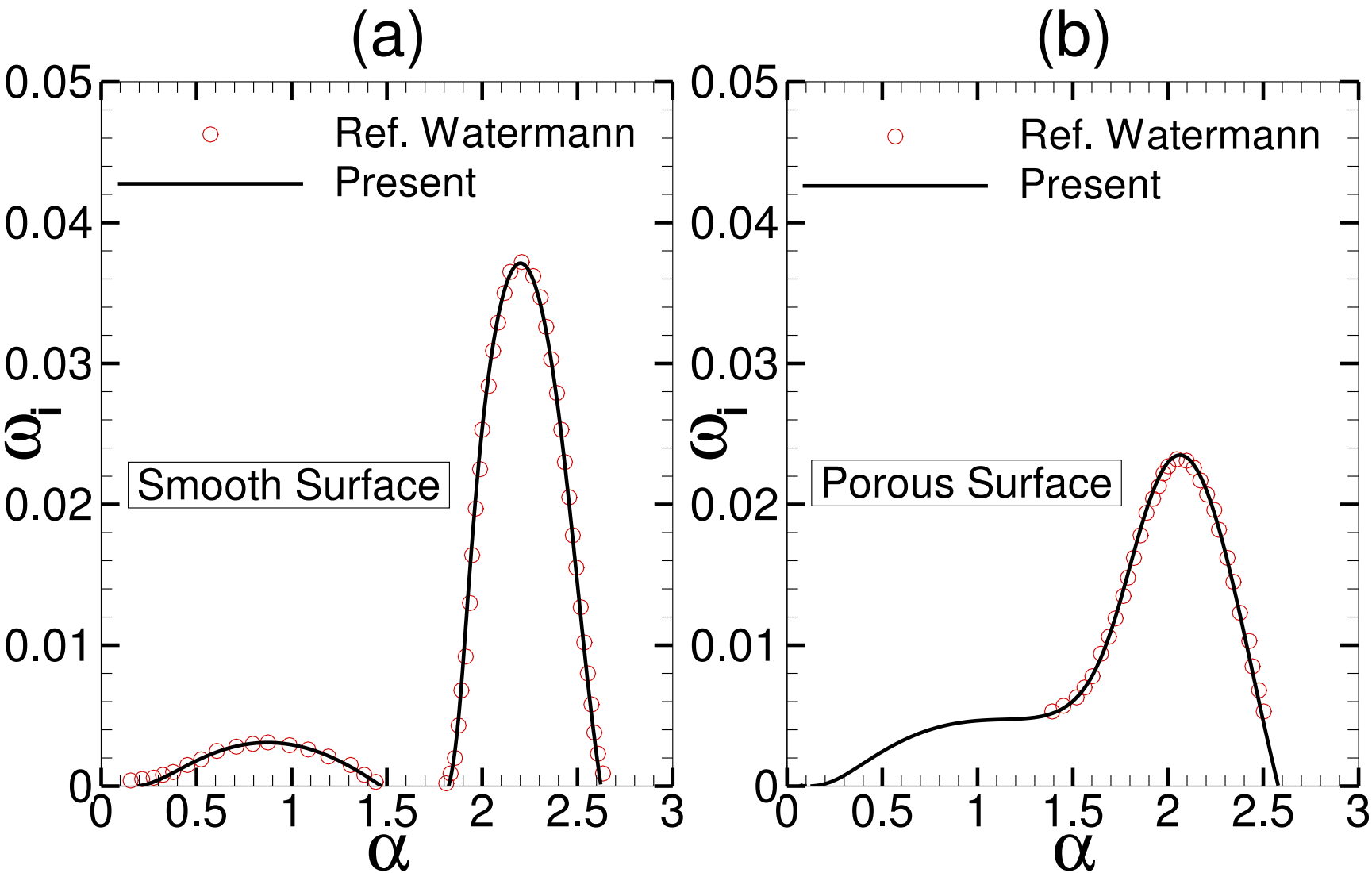
(a)
(b)
Ref. Watermann
Present
Smooth Surface
Porous Surface
ω_i
α
0.05
0.04
0.03
0.02
0.01
0
0.5
1
1.5
2
2.5
3

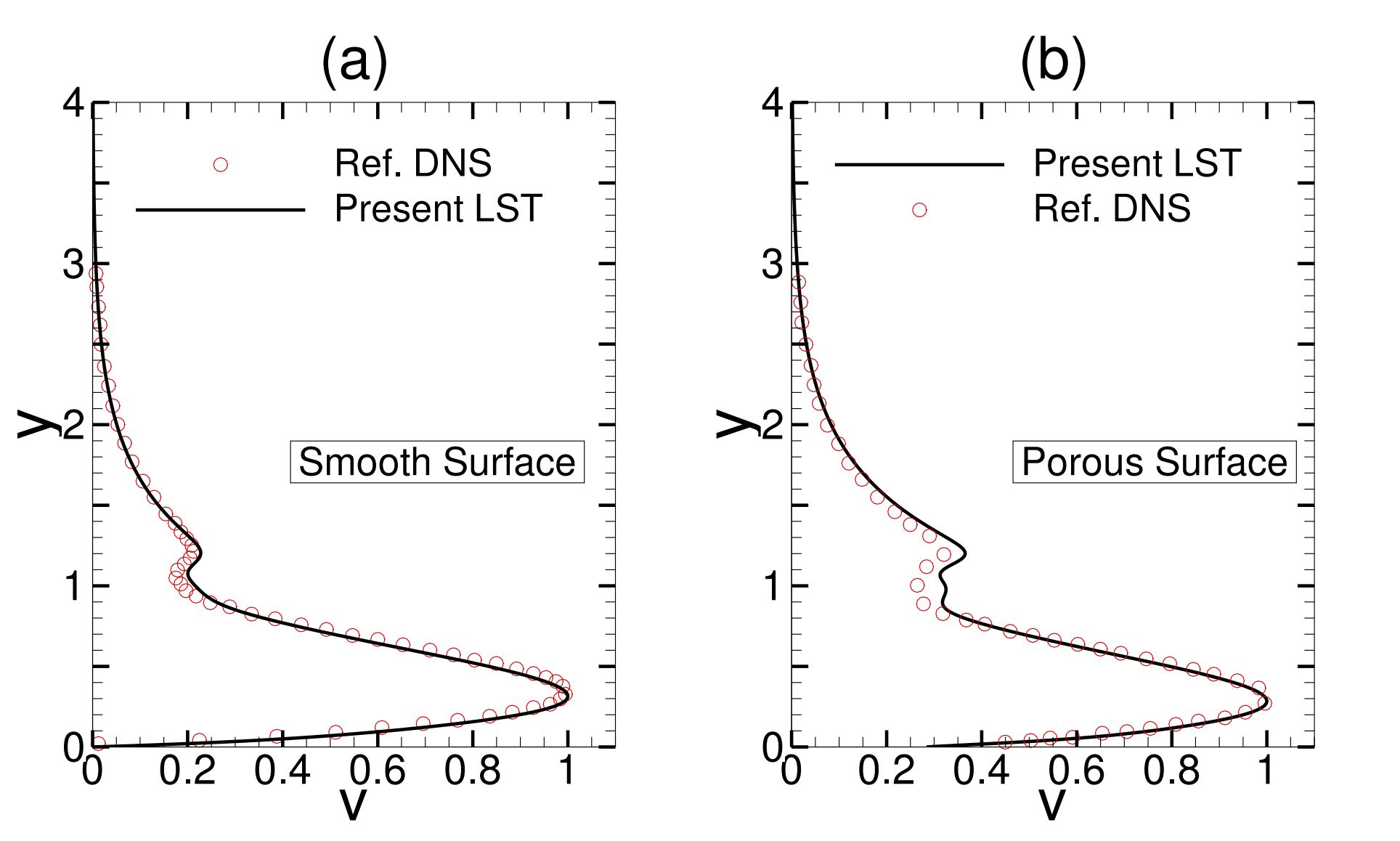
(a)
Ref. DNS
Present LST
Smooth Surface
y
v
0
1
2
3
4
0
0.2
0.4
0.6
0.8
1
(b)
Present LST
Ref. DNS
Porous Surface
y
v
0
1
2
3
4
0
0.2
0.4
0.6
0.8
1

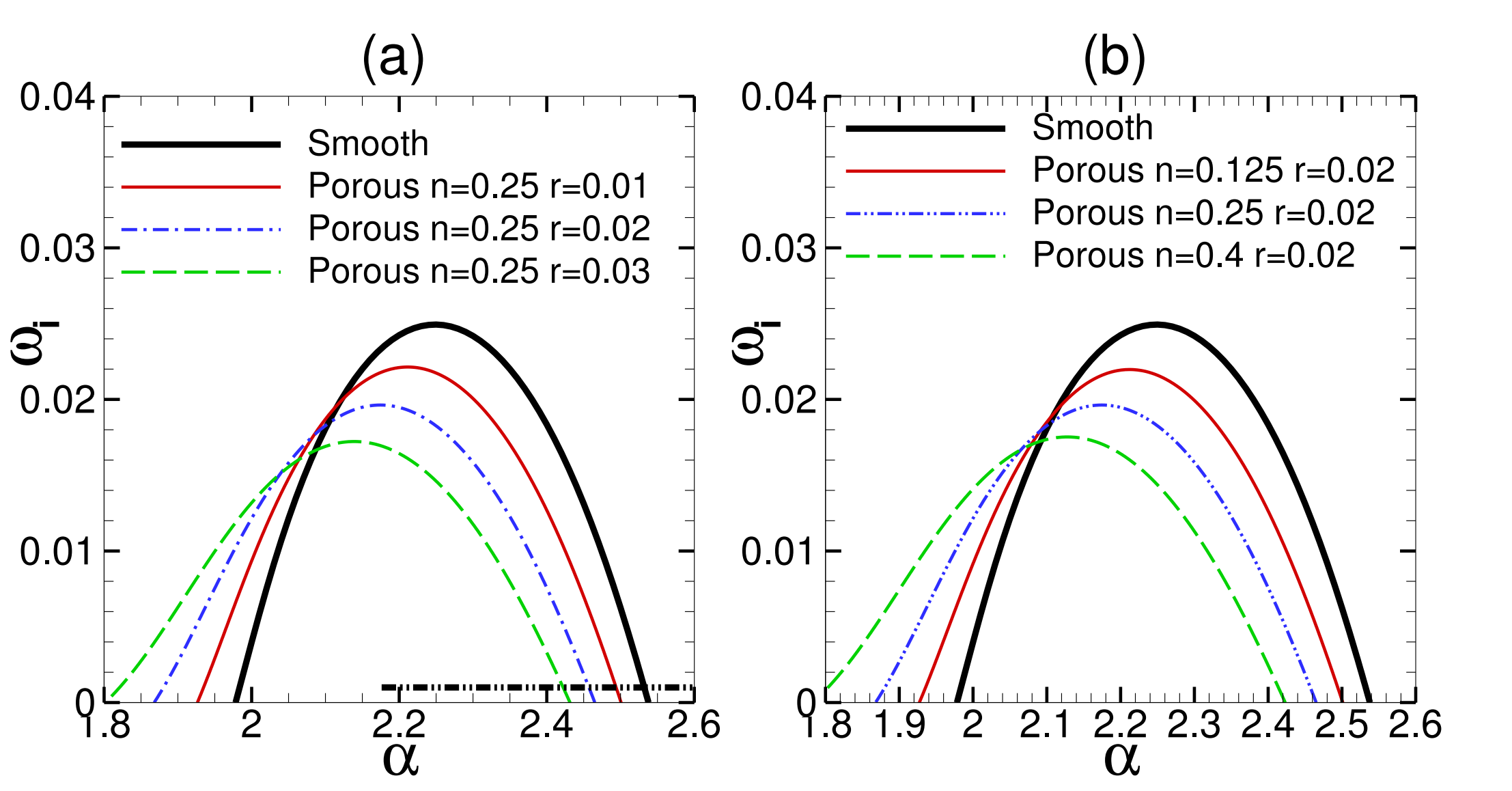
(a)
(b)
Smooth
Porous n=0.25 r=0.01
Porous n=0.25 r=0.02
Porous n=0.25 r=0.03
Porous n=0.125 r=0.02
Porous n=0.4 r=0.02
ω_i
α
0.04
0.03
0.02
0.01
0
1.8
1.9
2
2.1
2.2
2.3
2.4
2.5
2.6

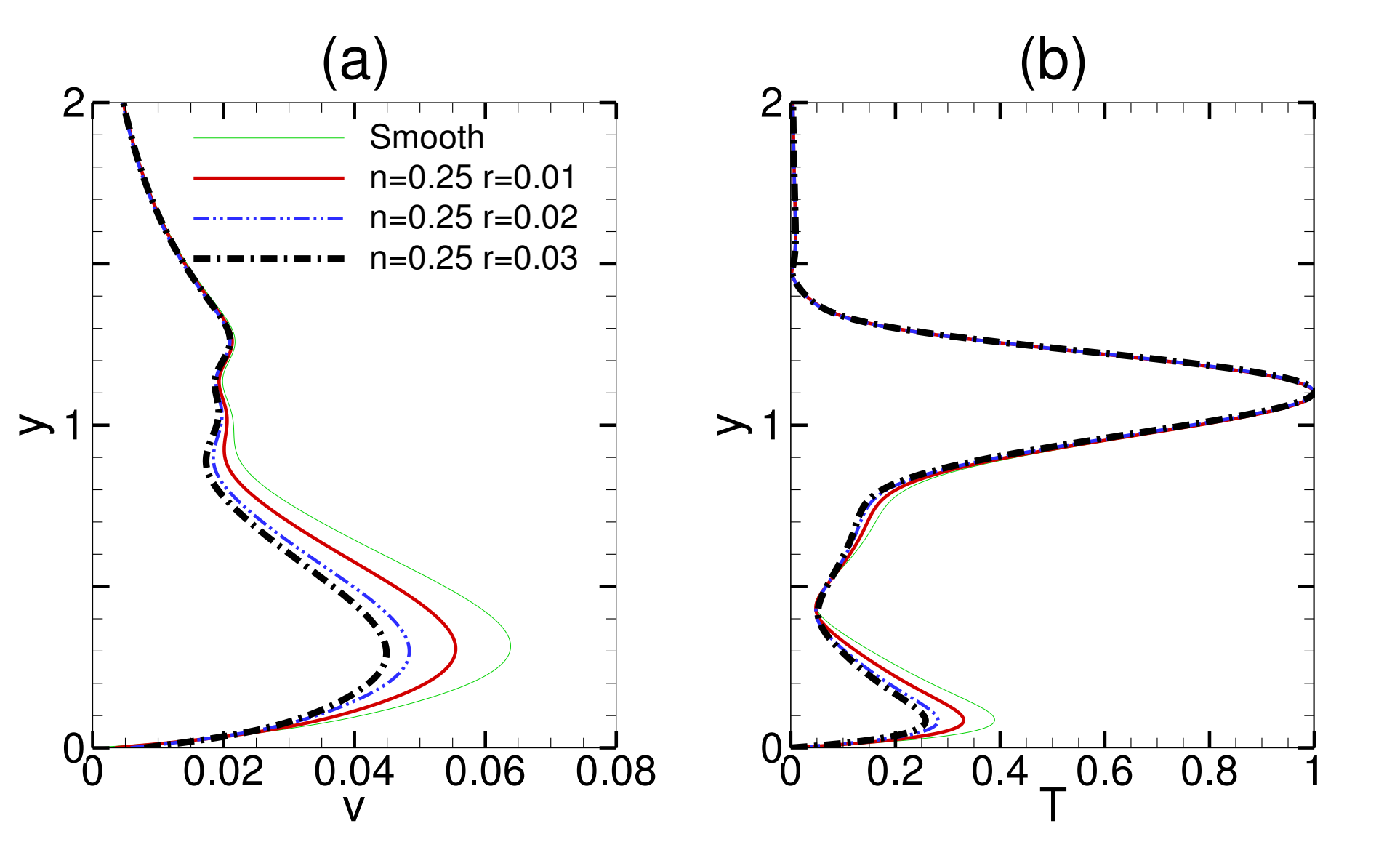
(a)
(b)
Smooth
n=0.25 r=0.01
n=0.25 r=0.02
n=0.25 r=0.03
y
v
T
0
1
2
0.02
0.04
0.06
0.08
0.2
0.4
0.6
0.8

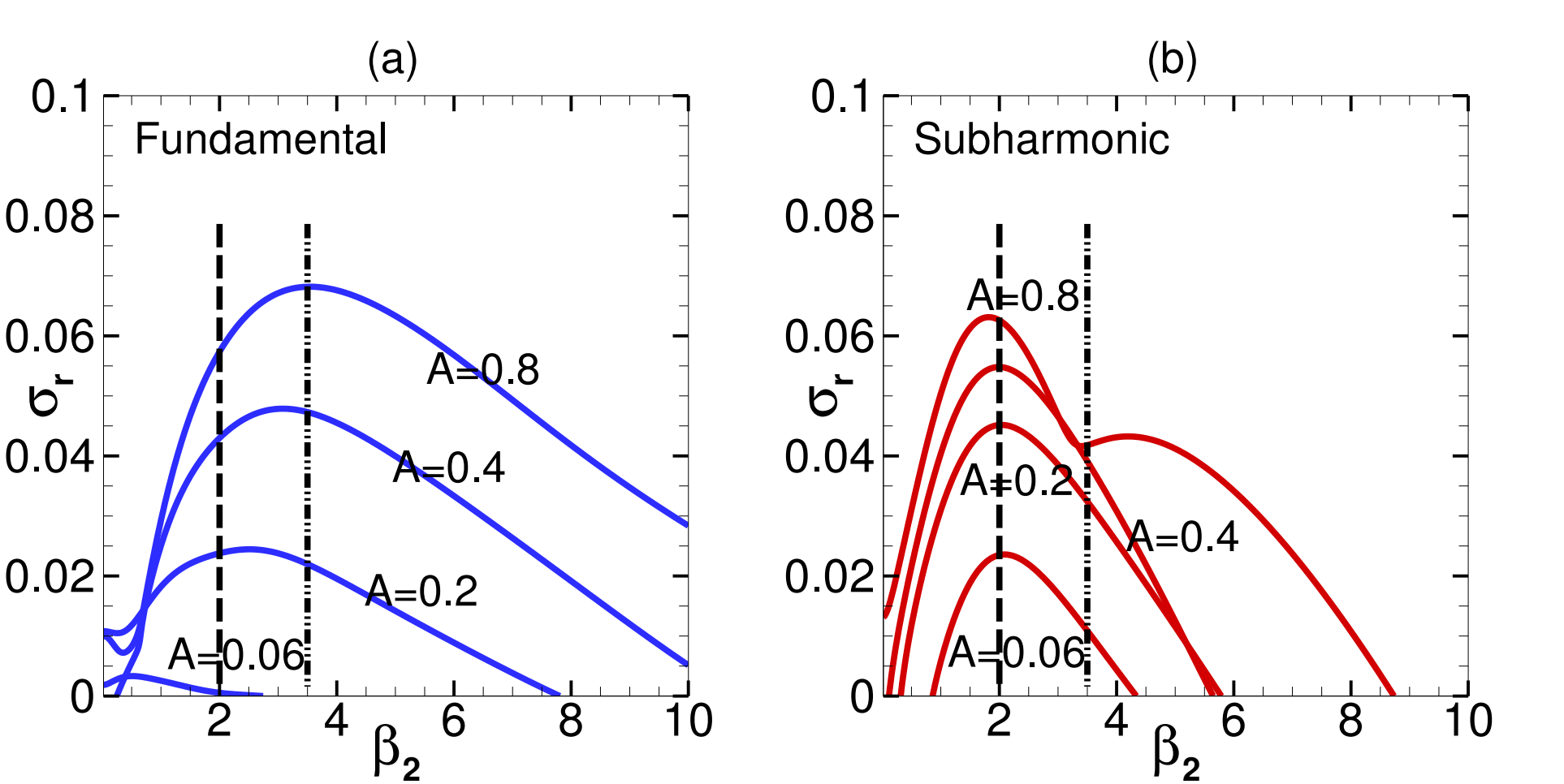
(a)
Fundamental
0.1
0.08
0.06
0.04
0.02
0
σ_r
A=0.8
A=0.4
A=0.2
A=0.06
2
4
6
8
10
β_2
(b)
Subharmonic
0.1
0.08
0.06
0.04
0.02
0
σ_r
A=0.8
A=0.2
A=0.4
A=0.06
2
4
6
8
10
β_2

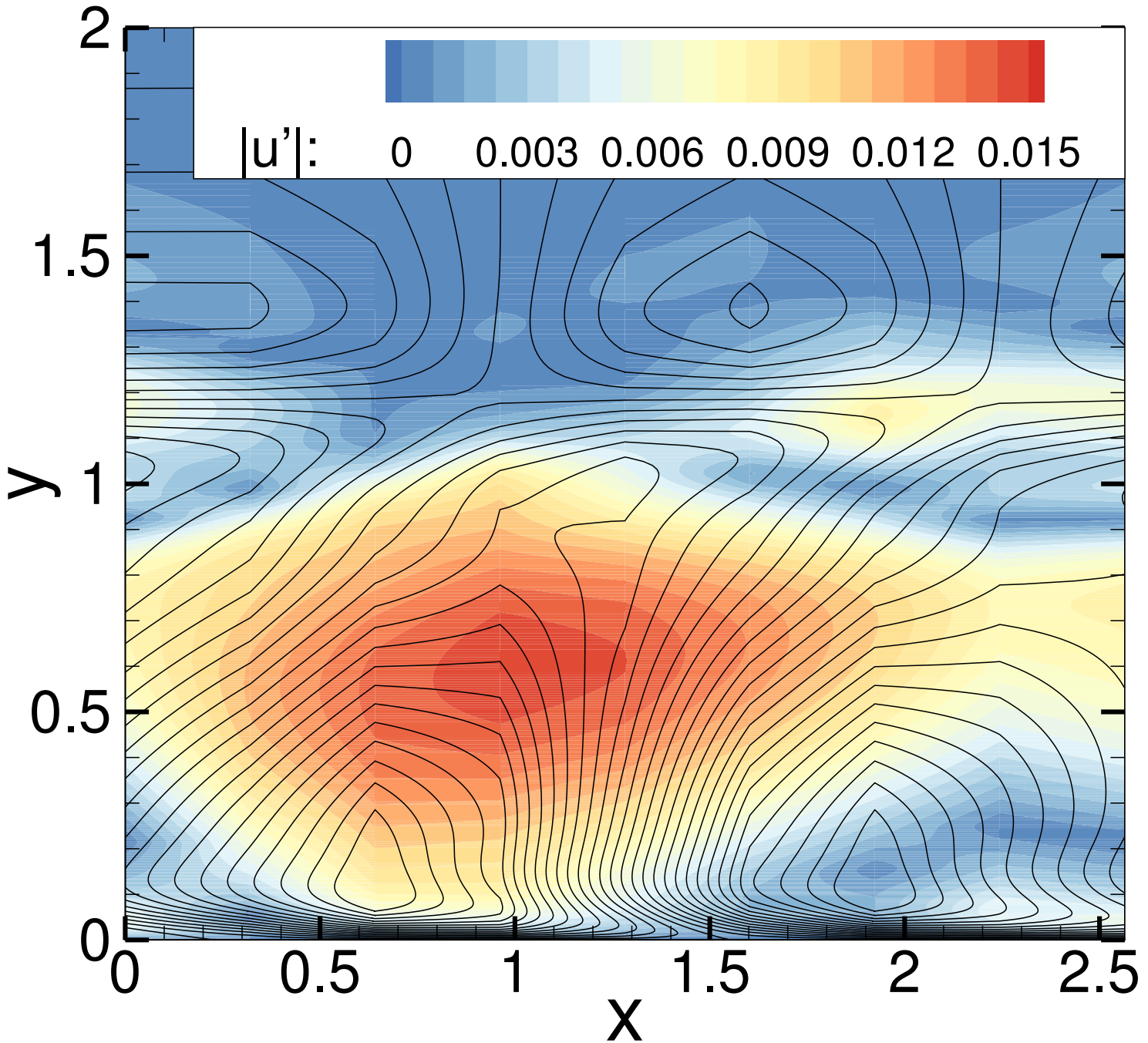
|u'|:
0
0.003
0.006
0.009
0.012
0.015
2
1.5
1
0.5
0
y
0
0.5
1
1.5
2
2.5
x

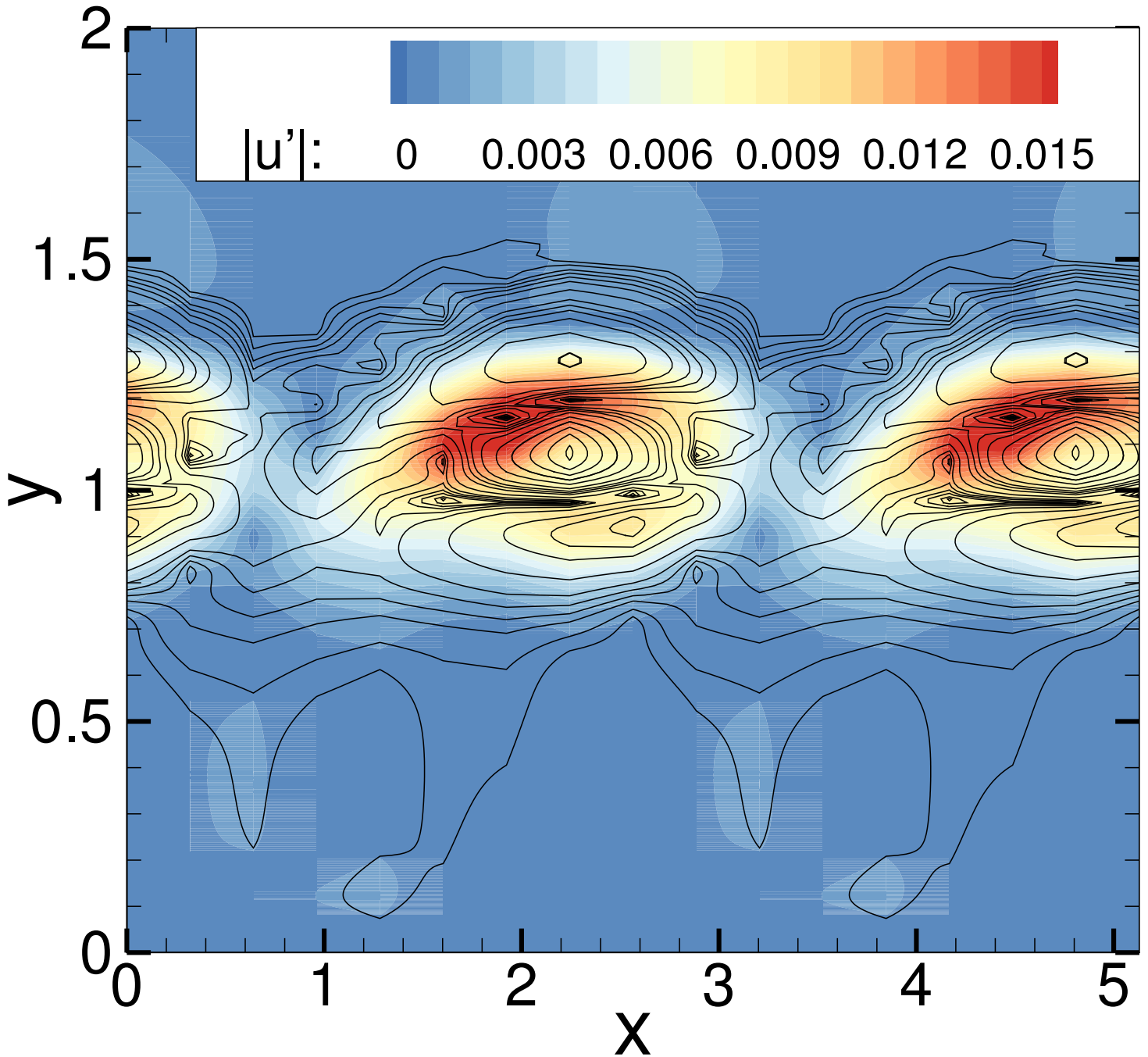
|u'|:
0
0.003
0.006
0.009
0.012
0.015
2
1.5
1
0.5
0
y
0
1
2
3
4
5
x

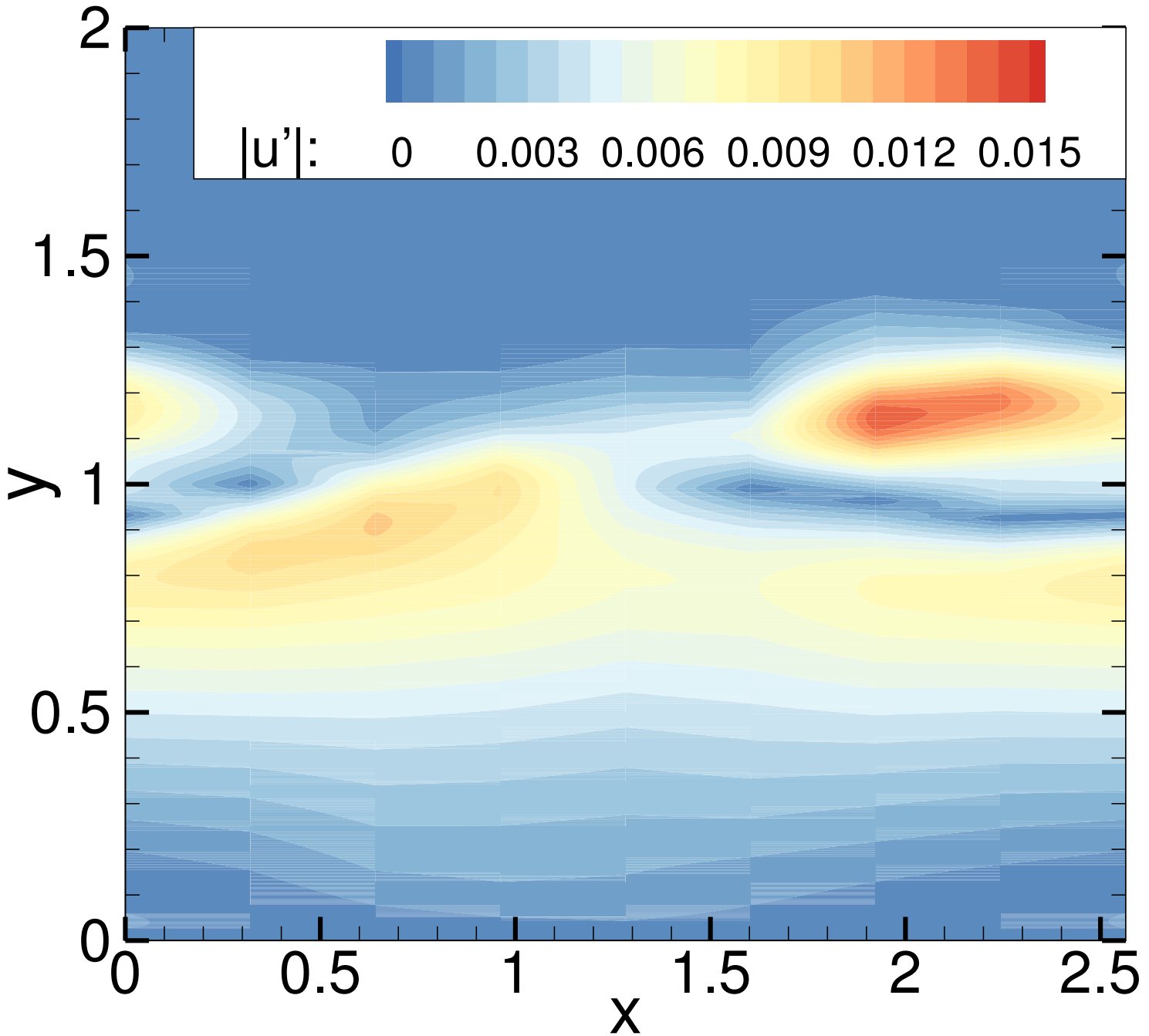
|u'|:
0
0.003
0.006
0.009
0.012
0.015
2
1.5
1
0.5
0
y
0
0.5
1
1.5
2
2.5
x

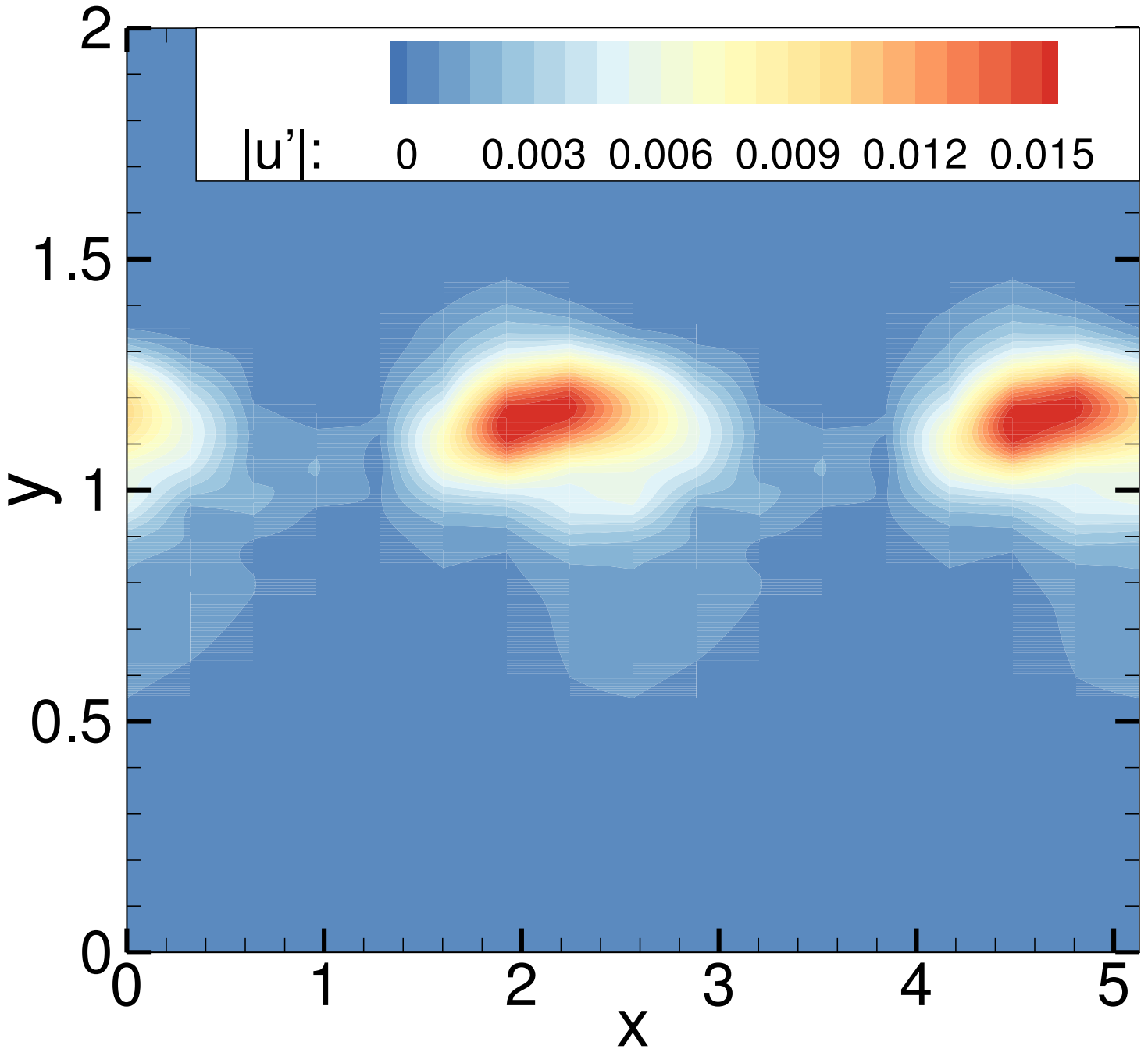
|u'|:
0
0.003
0.006
0.009
0.012
0.015
y
x
0
0.5
1
1.5
2
0
1
2
3
4
5

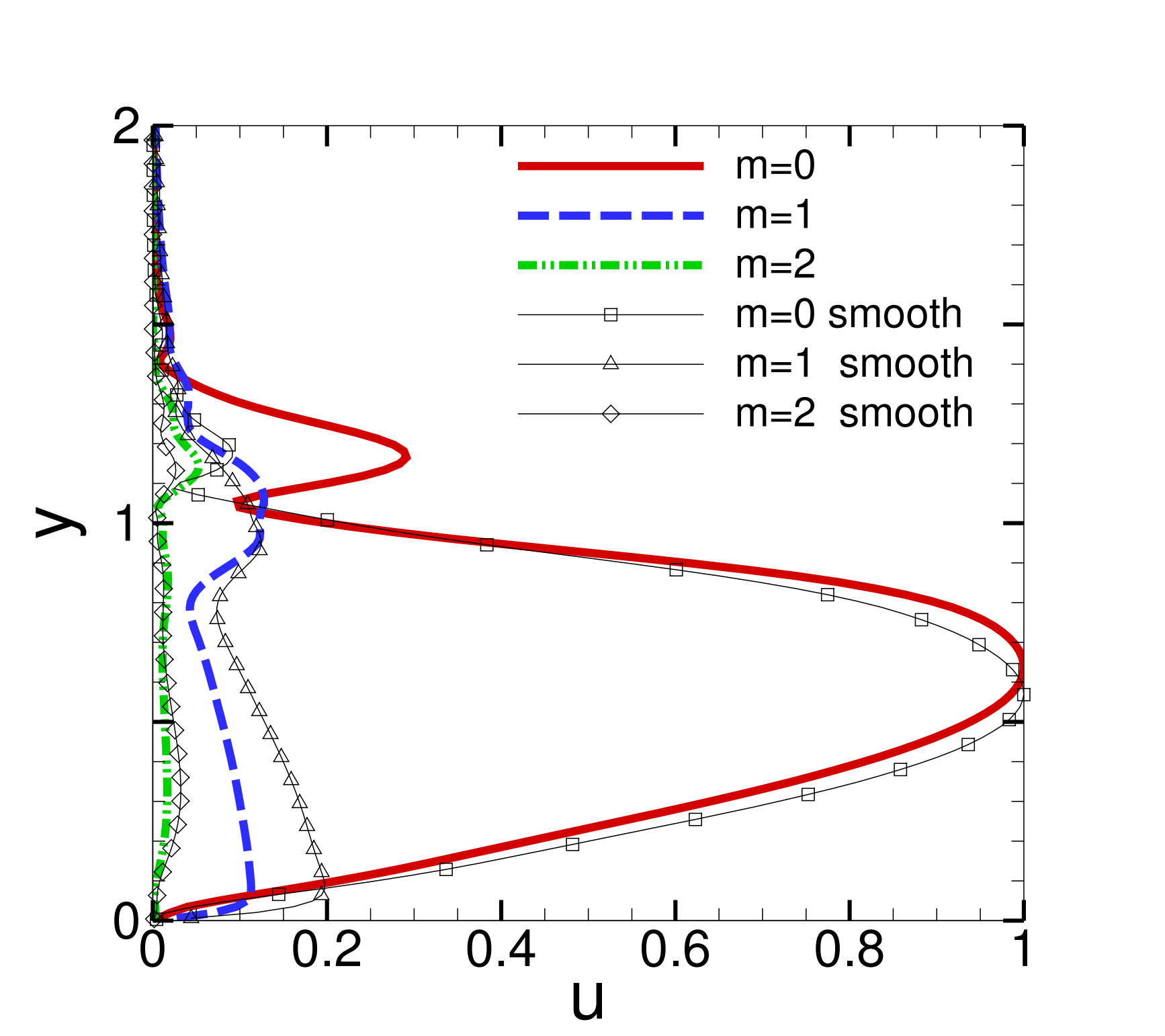
m=0
m=1
m=2
m=0 smooth
m=1 smooth
m=2 smooth
y
u
0
1
2
0
0.2
0.4
0.6
0.8
1

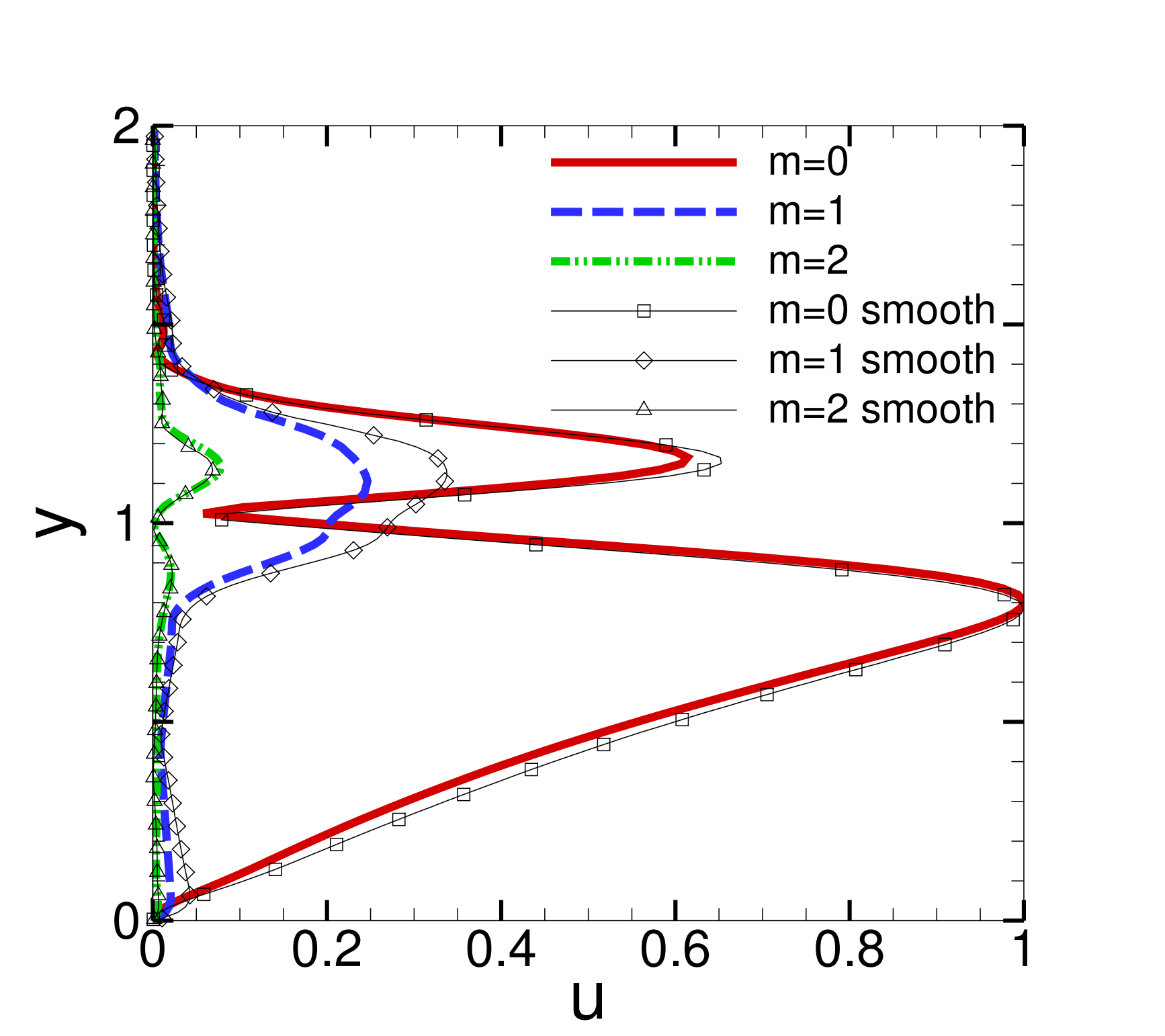
m=0
m=1
m=2
m=0 smooth
m=1 smooth
m=2 smooth
y
u
0
1
2
0
0.2
0.4
0.6
0.8
1

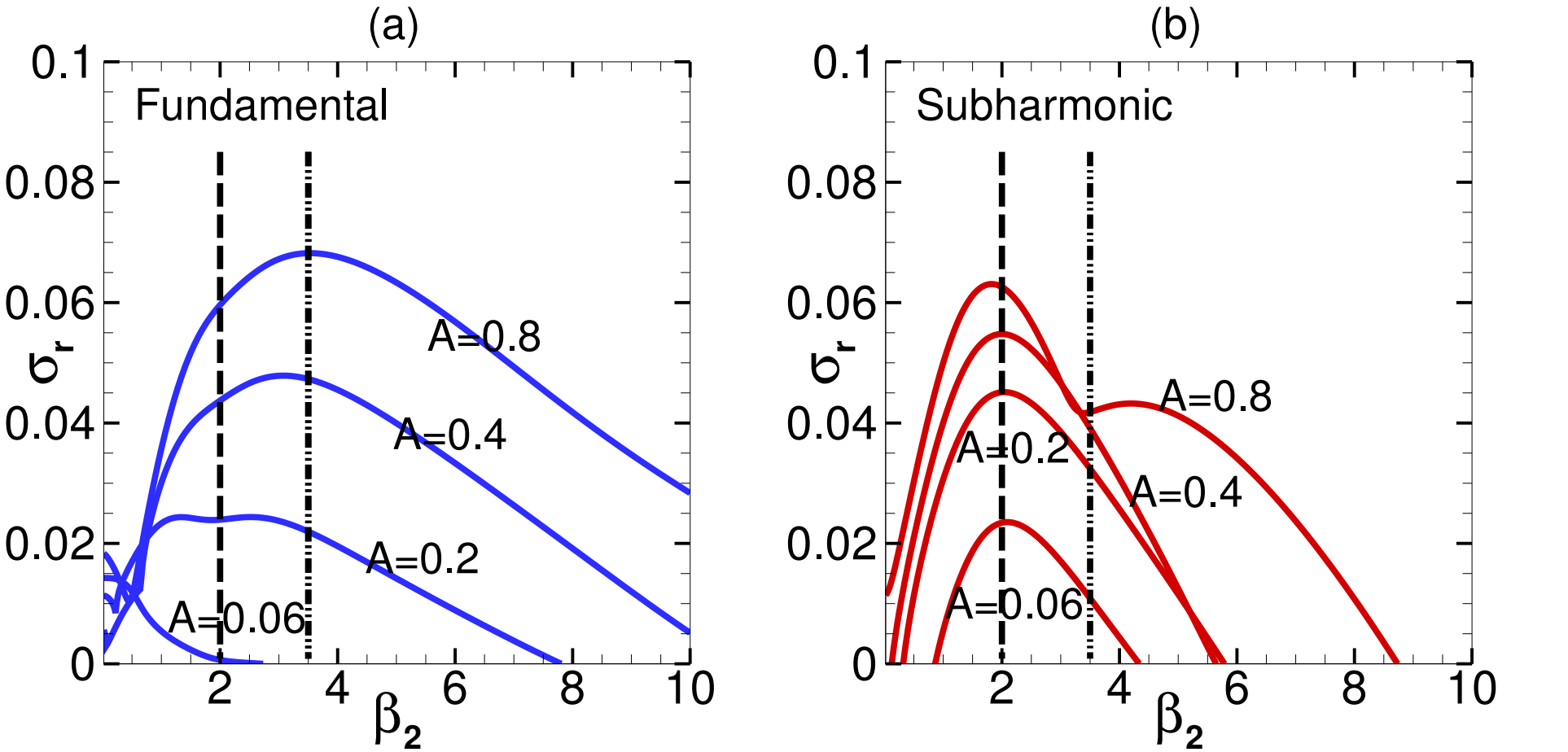
(a)
Fundamental
0.1
0.08
0.06
0.04
0.02
0
σ_r
A=0.8
A=0.4
A=0.2
A=0.06
2
4
6
8
10
β_2
(b)
Subharmonic
0.1
0.08
0.06
0.04
0.02
0
σ_r
A=0.8
A=0.2
A=0.4
A=0.06
2
4
6
8
10
β_2

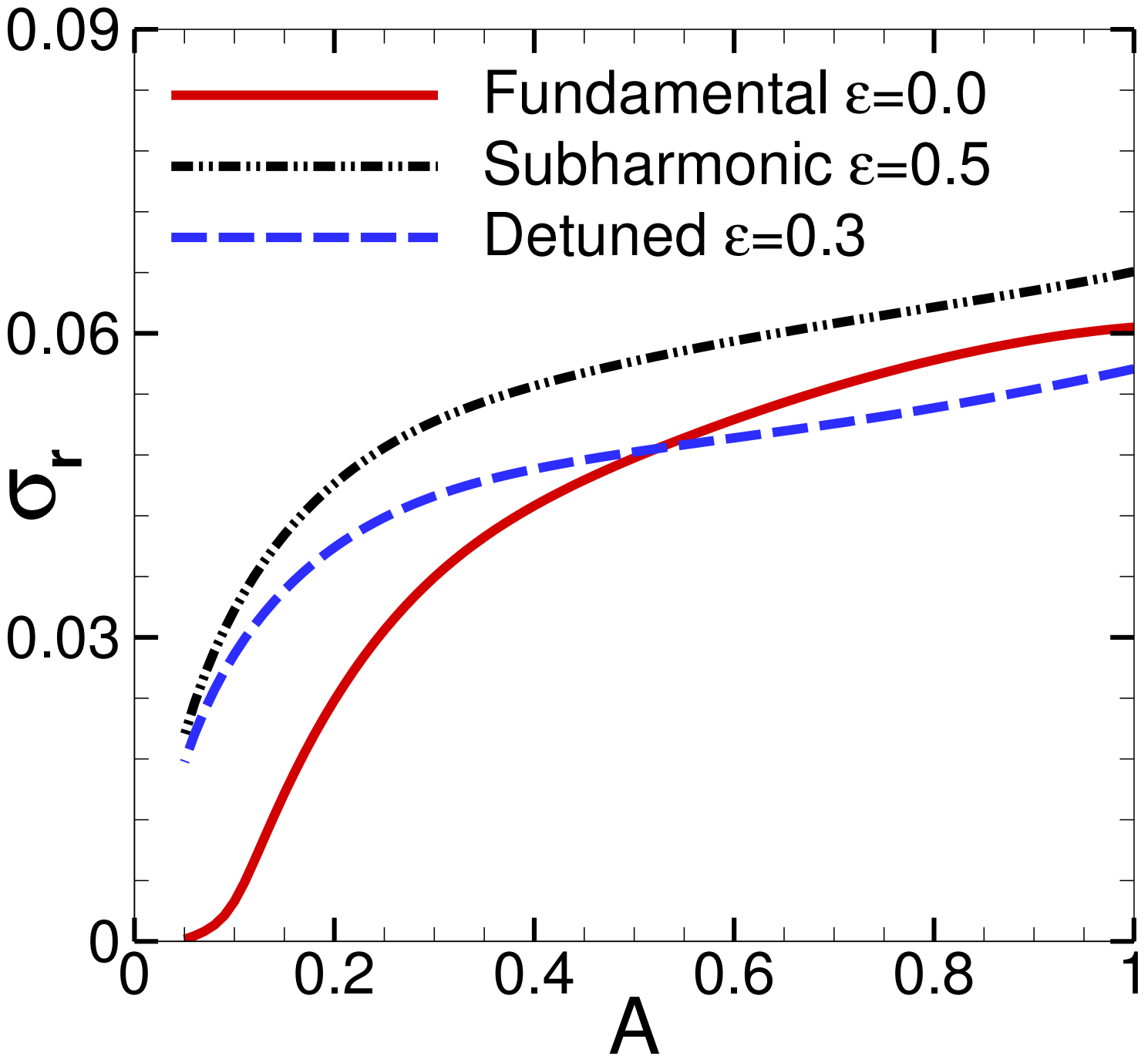
0.09
0.06
0.03
0
σ_r
Fundamental ε=0.0
Subharmonic ε=0.5
Detuned ε=0.3
0
0.2
0.4
0.6
0.8
1
A

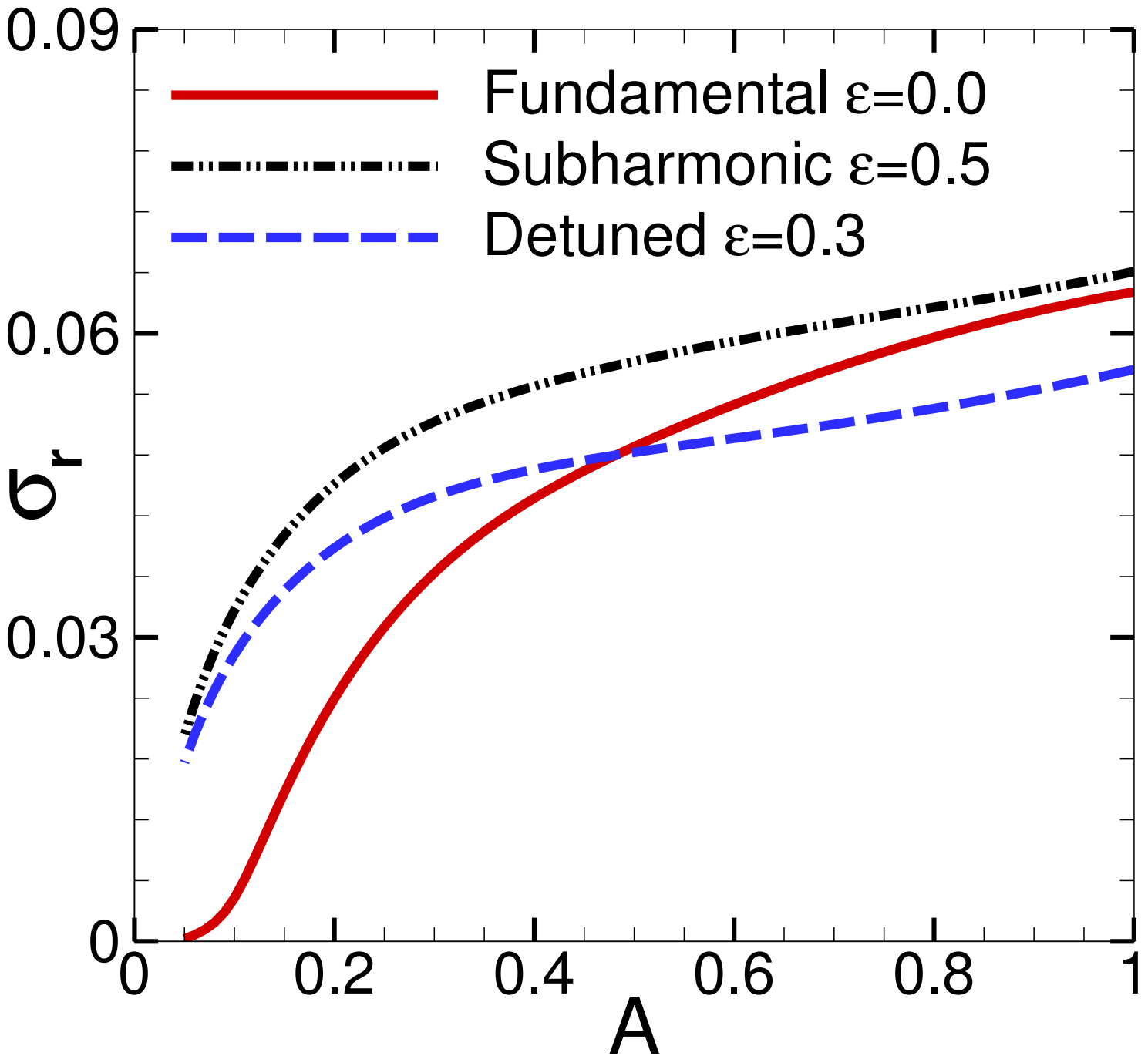
0.09
0.06
0.03
0
σ_r
0
0.2
0.4
0.6
0.8
1
A
Fundamental ε=0.0
Subharmonic ε=0.5
Detuned ε=0.3

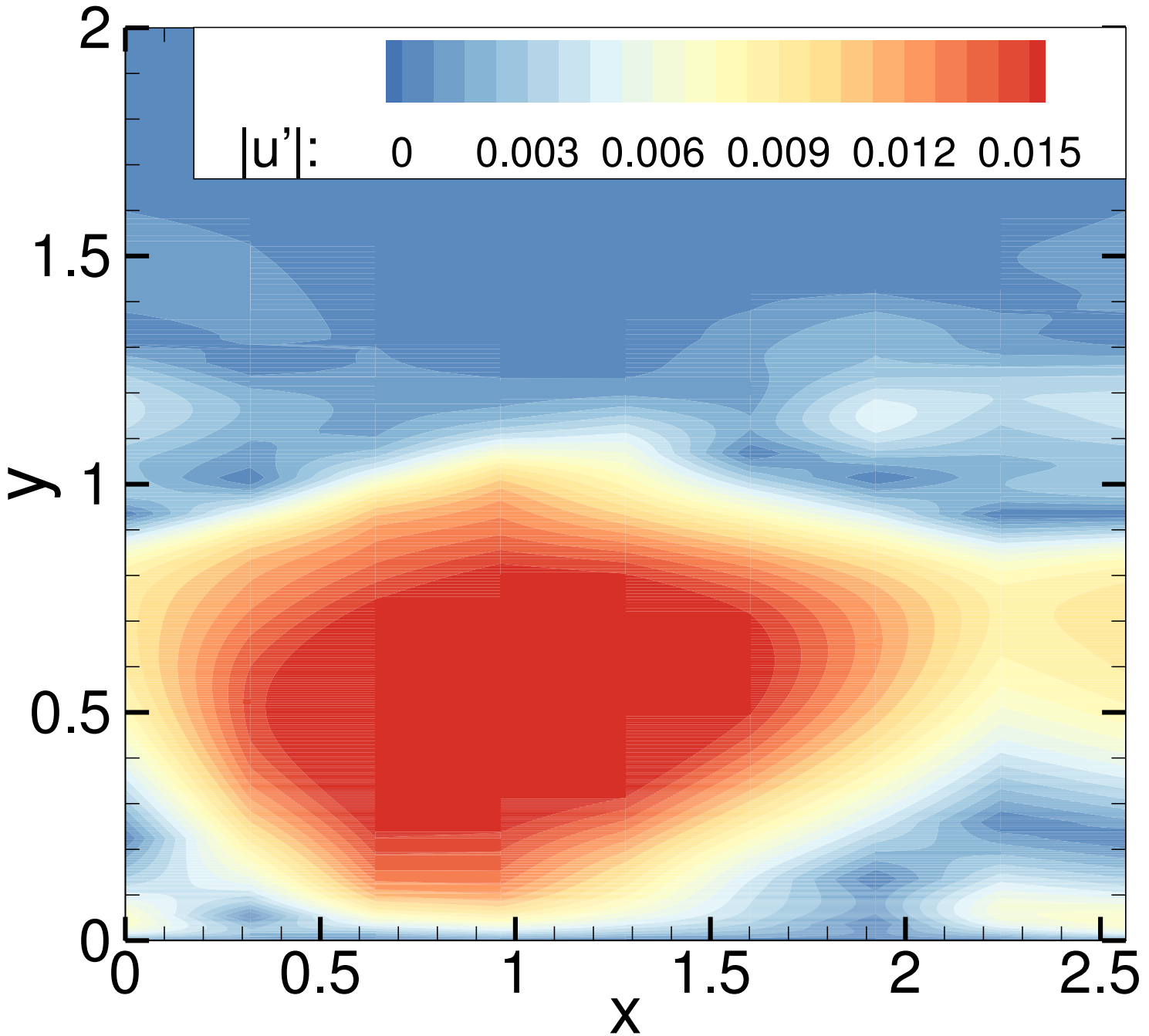
|u'|:
0
0.003
0.006
0.009
0.012
0.015
2
1.5
1
0.5
0
y
0
0.5
1
1.5
2
2.5
x

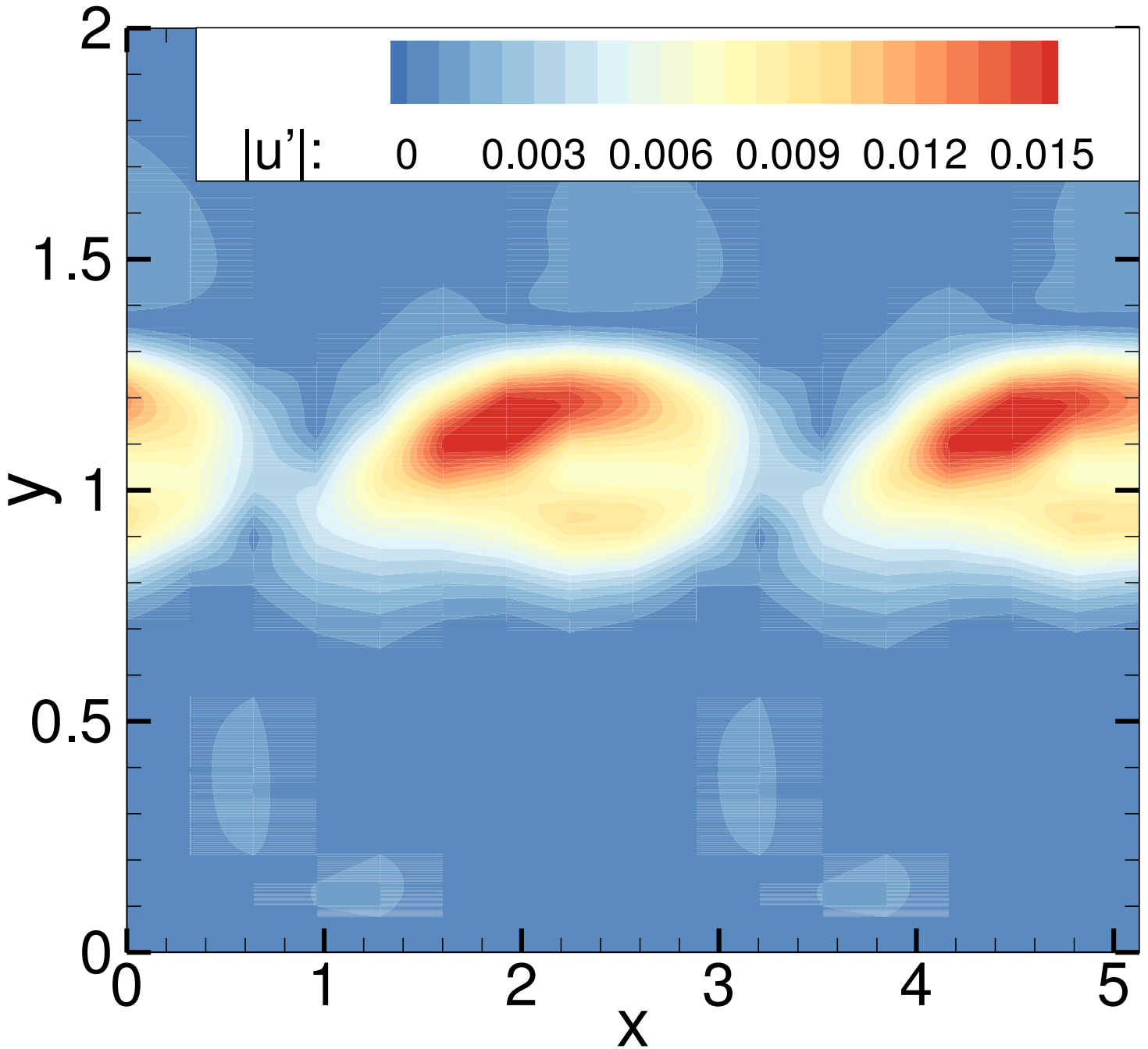
|u'|:
0
0.003
0.006
0.009
0.012
0.015
2
1.5
1
0.5
0
y
0
1
2
3
4
5
x

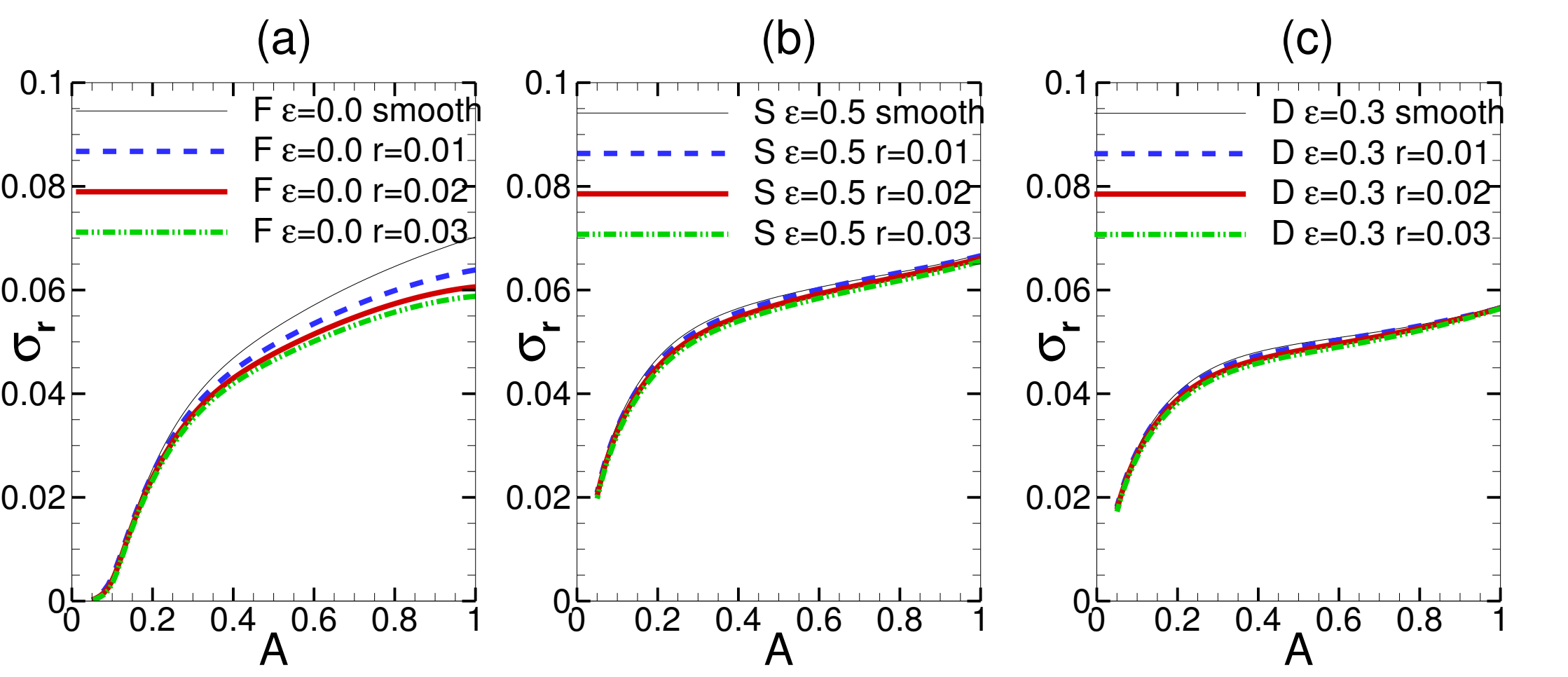
(a)
(b)
(c)
F ε=0.0 smooth
F ε=0.0 r=0.01
F ε=0.0 r=0.02
F ε=0.0 r=0.03
S ε=0.5 smooth
S ε=0.5 r=0.01
S ε=0.5 r=0.02
S ε=0.5 r=0.03
D ε=0.3 smooth
D ε=0.3 r=0.01
D ε=0.3 r=0.02
D ε=0.3 r=0.03
σr
A
0
0.02
0.04
0.06
0.08
0.1
0.2
0.4
0.6
0.8
1

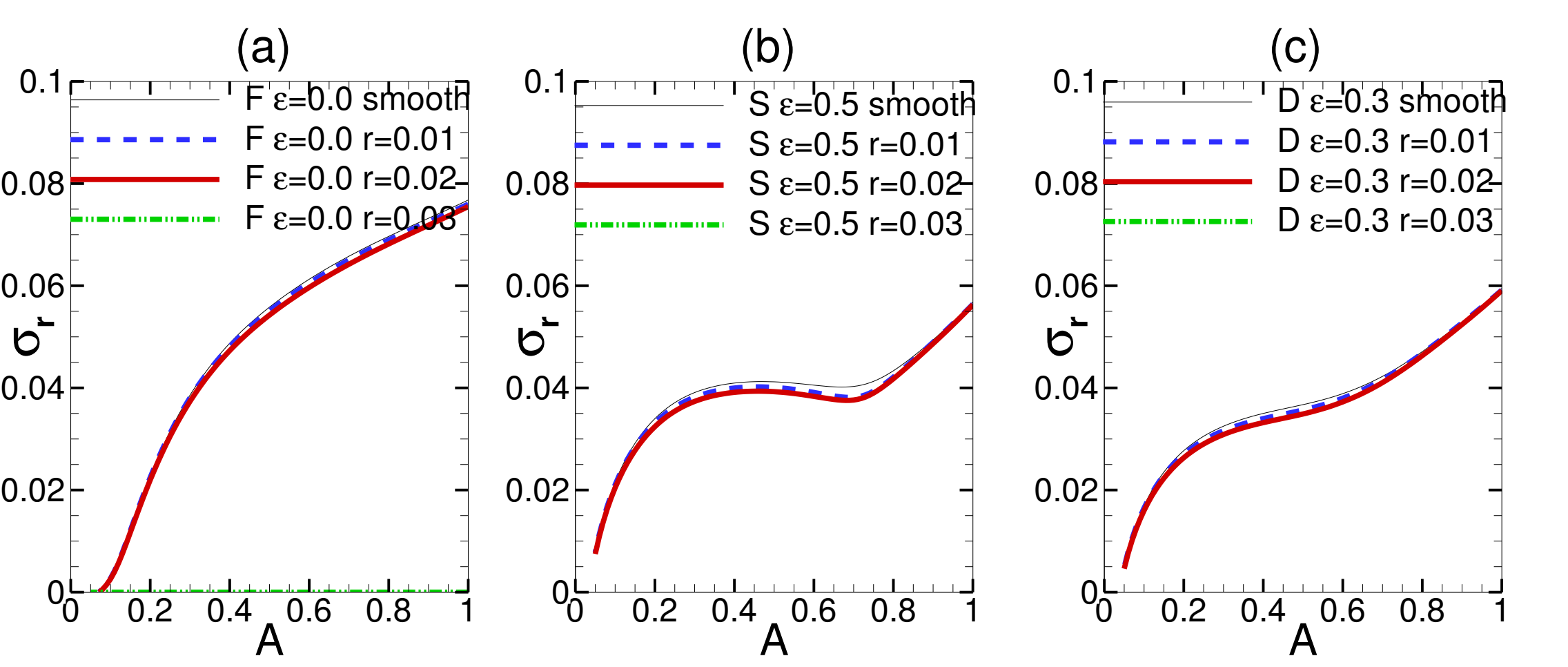
(a)
(b)
(c)
F ε=0.0 smooth
F ε=0.0 r=0.01
F ε=0.0 r=0.02
F ε=0.0 r=0.03
S ε=0.5 smooth
S ε=0.5 r=0.01
S ε=0.5 r=0.02
S ε=0.5 r=0.03
D ε=0.3 smooth
D ε=0.3 r=0.01
D ε=0.3 r=0.02
D ε=0.3 r=0.03
σr
A
0
0.02
0.04
0.06
0.08
0.1
0.2
0.4
0.6
0.8
1